

## Variable-Stiffness Tensegrity Modular Robots

Présentée le 26 mai 2021

Faculté des sciences et techniques de l'ingénieur  
Laboratoire de systèmes intelligents  
Programme doctoral en robotique, contrôle et systèmes intelligents

pour l'obtention du grade de Docteur ès Sciences

par

**Davide ZAPPETTI**

Acceptée sur proposition du jury

Prof. H. Shea, président du jury  
Prof. D. Floreano, directeur de thèse  
Prof. F. Iida, rapporteur  
Prof. J. Rieffel, rapporteur  
Prof. A. J. Ijspeert, rapporteur

---

---

A universal set of building rules seems to guide the design of organic structures  
from simple carbon compounds to complex cells and tissues

— By Donald E. Ingber on January 1, 1998

---

# Acknowledgments

I would like to express my deepest gratitude to all the people who made this journey possible. I would like to thank **Prof. Dario Floreano** for giving me the opportunity to carry out my PhD in his laboratory and to participate in many research-related activities, including participating in multiple conferences and events. which gave me great opportunities to meet people from the community and beyond. I would like to thank our administrative assistant **Michelle** for always finding solutions to my administrative issues and more. I am also thankful to **Corinne**, our doctoral school secretary, for always being there to help me. I would like to say a very special thanks to all the amazing collaborators I had the pleasure to work with. A special thank also to all the EPFL and abroad students that I had the pleasure to supervise and contributed to the accomplishments of this thesis. A big thanks to all the past and present **LIS members** for the moments we spent together and for supporting each other. A special thank also to all my friends in Lausanne and my parents **Anna** and **Claudio** who supported me during these years. At last but not least, my biggest thought goes to my beloved **Giulia**. You have been supporting me in every situation and it is thanks to you if I succeed in this PhD.

Lausanne, le 30 Mars 2021



# Abstract

The need for a new generation of robots able to safely locomote and manipulate beside or cooperatively with humans or in un-constructed environments has recently emerged as a priority of the robotics community. In the past two decades, this challenge has been tackled by the growing field of soft robotics mostly focusing on developing completely deformable soft robotic bodies that can freely deform along any direction and comply with any unexpected or excessive external force. However, intrinsic softness can be a limitation in situations that require exerting substantial forces, to withstand body-weights or to modulate forces applied to the environment.

Inspiration for a novel mechanically hybrid approach in robotics can come from a novel model for biological structures based on the concept of tensegrity. This model rejects the idea of the vertebrate musculoskeletal system as beams, columns, and levers, and acknowledges the bones as stiff under compression elements held and stabilized in their positions by the pull of tensile components such as muscles, tendons, ligaments, and fascia. Therefore, rather than a frame supporting an amorphous soft tissue mass, the whole vertebrate body is divided into several modules stabilized by these tension components and its stiffness can vary depending on the pre-stress (i.e. tone) and stiffness of its muscles. This structural organization allows biological organisms to be more mechanically adaptive, robust, and lightweight at the same time. They can exhibit high physical compliance, apply efficiently forces to the environment when needed, and, at the same time, withstand their bodyweight at different scales.

In the same way, modular tensegrity structures used in robotic applications can provide a lightweight and robust framework where integrating stiff under compression struts for bodyweight support; variable stiffness cables for applying directionally larger forces when required, and soft cables to absorb energy and allow compliance.

In this thesis, tensegrity modular structures are investigated as a new approach to develop soft robots with variable stiffness capabilities. This investigation led to a set of design strategies to manufacture and actuate tensegrity modules with programmable stiffness and deformation; to mechanically and electrically connect tensegrity modules to develop untethered applications, and to implement variable-stiffness capabilities in the modules for active and passive stiffness change. Finally, preliminary results and insights are presented on using heuristic algorithms as a design method to find task-optimal morphologies, stiffness, and control of modular tensegrity robots.

In this thesis modular tensegrity robots have been developed for performing locomotion and grasping tasks, however, the design methods presented can provide a guideline for designing robots for diverse applications where being lightweight, robust, and having variable-stiffness capabilities are of primary importance.

We believe that the work presented and discussed in this thesis answered a gap in the current literature and most importantly, will pave the way to future research on tensegrity robots for a great variety of tasks and robotic applications.

## Keywords

Tensegrity, soft robotics, variable-stiffness, modular robotics, evolutionary robotics

# Résumé

Le besoin d'une nouvelle génération de robots capables de locomotion et de manipulation en toute sécurité, à côté des humains ou en coopération avec eux, ainsi que dans des environnements non construits, est récemment apparu comme une priorité de la communauté robotique. Au cours des deux dernières décennies, ce défi a été relevé par le domaine en pleine expansion de la robotique moule, qui s'est principalement concentré sur le développement de corps robotiques souples complètement déformables, capables de se déformer librement dans n'importe quelle direction et de se soumettre à toute force extérieure inattendue ou excessive. Toutefois, la souplesse intrinsèque peut devenir un facteur limitant dans les situations qui exigent d'exercer des forces importantes, de supporter des poids corporels ou de moduler les forces appliquées à l'environnement.

L'inspiration pour une nouvelle approche mécaniquement hybride en robotique peut venir d'un nouveau modèle de structures biologiques basé sur le concept de tenségrité. Ce modèle rejette l'idée du système musculo-squelettique des vertébrés en tant que poutres, colonnes et leviers, et reconnaît les os comme des éléments rigides sous compression maintenus et stabilisés dans leur position par la traction de composants de traction tels que les muscles, les tendons, les ligaments et les fascias. Par conséquent, plutôt qu'un cadre supportant une masse de tissus mous amorphe, le corps entier du vertébré est divisé en plusieurs modules stabilisés par ces éléments de tension et sa rigidité peut varier en fonction de la précontrainte (c'est-à-dire du tonus) et de la raideur de ses muscles. Cette organisation structurelle permet aux organismes biologiques d'être à la fois plus adaptables, plus robustes et plus légers. Ils peuvent faire preuve d'une grande compliance physique, appliquer efficacement des forces à l'environnement lorsque cela est nécessaire et, en même temps, supporter leur poids corporel à différentes échelles.

De la même manière, les structures de tenségrité modulaires utilisées dans les applications robotiques peuvent fournir un cadre léger et robuste où l'on intègre des entretoises de compression rigides pour supporter le poids du corps, des câbles à rigidité variable pour appliquer des forces directionnelles plus importantes lorsque cela est nécessaire, et des câbles souples pour absorber l'énergie et permettre la compliance.

Dans cette thèse, j'ai étudié les structures modulaires de tenségrité comme une nouvelle approche pour développer des robots souples avec des capacités de rigidité variables. Cette recherche a conduit à un ensemble de stratégies de conception pour fabriquer et actionner des modules de tenségrité avec une rigidité et une déformation programmables ; pour connecter mécaniquement et électriquement les modules de tenségrité afin de développer des applications non attachées, et pour mettre en œuvre des capacités de rigidité variable dans les modules pour un changement de rigidité active et passive. Enfin, je présente des résultats et des aperçus préliminaires sur l'utilisation d'algorithmes heuristiques comme méthode de conception pour trouver des morphologies, une rigidité et un contrôle optimaux des tâches des robots à tenségrité modulaire.

Dans cette thèse, des robots à tenségrité modulaire ont été développés pour effectuer des tâches de locomotion et de préhension. Cependant, les méthodes de conception présentées peuvent servir de guide pour la conception de robots destinés à diverses applications où la légèreté, la robustesse et les capacités de rigidité variable sont primordiales.

Nous pensons que les travaux présentés et discutés dans cette thèse ont répondu à une lacune de la littérature actuelle et, plus important encore, qu'ils ouvriront la voie à de futures recherches sur les robots de tenségrité pour une grande variété de tâches et d'applications robotiques.

## Mots-clés





Tenségrité, robotique moule, rigidité variable, robotique modulaire, robotique évolutive



# Contents

<b>Acknowledgments.....</b>	<b>ix</b>
<b>Abstract .....</b>	<b>xi</b>
<b>Keywords .....</b>	<b>xi</b>
<b>Résumé .....</b>	<b>xii</b>
<b>Mots-clés.....</b>	<b>xii</b>
<b>List of Figures .....</b>	<b>xvii</b>
<b>Introduction .....</b>	<b>1</b>
From Rigid to Soft, to Variable-Stiffness.....	1
The bio-inspired tensegrity approach .....	2
<b>Chapter 1     State-of-the-art of Tensegrity robotics .....</b>	<b>6</b>
1.1     Tensegrity robots’ morphologies and actuation designs .....	6
1.2     Variable-stiffness tensegrity robots .....	9
1.3     Simulation of Tensegrity Robots .....	10
1.4     Control of tensegrity robots.....	10
1.5     Concluding Remarks.....	10
<b>Chapter 2     Modular design strategy and novel manufacturing technique.....</b>	<b>11</b>
2.1     A bio-inspired modular design strategy for tensegrity robots .....	11
2.1.1 Tensegrity Structures’ kit selection .....	12
2.2     Module Design and Manufacturing .....	13
2.2.1 Novel Manufacturing strategy .....	14
2.2.2 Connectivity.....	15
2.3     Tendon-Driven Actuation.....	16
2.4     A proof-of-concept Crawling Modular Tensegrity Robot .....	17
2.5     Discussion .....	18
<b>Chapter 3     A bio-inspired connection strategy for untethered soft modular tensegrity robots .....</b>	<b>19</b>
3.1     Introduction .....	19
3.2     Bio-inspired ball-joints connection strategy .....	20
3.3     Implementation of the junctions connection strategy .....	22

	3.3.1 Results .....	23
3.4	Soft modular untethered tensegrity robot demonstrators.....	25
3.5	Discussion .....	26
<b>Chapter 4</b>	<b>Design strategies for active stiffness-change of tensegrity modules .....</b>	<b>28</b>
4.1	Controllable active stiffness-change through activation of smart materials .....	28
	4.1.1 Methods .....	29
	4.1.2 Results .....	30
	4.1.3 Discussion .....	35
4.2	Controllable active stiffness-change with type-changing tensegrity structures .....	37
	4.2.1 Introduction.....	37
	4.2.2 Class-changing variable-stiffness strategy for tensegrity systems.....	38
	4.2.3 Hardware implementation .....	38
	4.2.4 Stiffness transition mechanism and tensegrity module's stiffness modes .....	41
	4.2.5 Model .....	41
	4.2.6 Results .....	42
	4.2.7 A continuous tensegrity spine manipulator.....	45
	4.2.8 Discussion .....	46
4.3	Concluding remarks .....	47
<b>Chapter 5</b>	<b>Dual-stiffness design strategy for passive stiffness change of tensegrity structures.....</b>	<b>49</b>
5.1	Introduction and design strategy.....	49
5.2	Buckling strut design and its characterization .....	50
	5.2.1 Parametric study to design stiffness and buckling load.....	52
5.3	Dual-stiffness tensegrity module design and characterization .....	53
5.4	Dual-stiffness tensegrity robot demonstrators.....	55
	5.4.1 Dual-stiffness Tensegrity drone quadcopter .....	55
	5.4.2 The wheeled rover demonstrator .....	56
5.5	Discussion .....	58
<b>Chapter 6</b>	<b>Heuristic algorithms to design task-optimal morphology, stiffness, and control of modular tensegrity robots. 59</b>	
6.1	Introduction .....	59
6.2	Co-evolution of body and brain of the tensegrity modular robots with programmed stiffness .....	60
	6.2.1 Results .....	61
6.3	Co-evolution of body, brain, and stiffness of tensegrity modular robots .....	63
	6.3.1 Method .....	63
	6.3.2 The sim-to-real problem.....	63
	6.3.3 Results .....	65
6.4	Discussion .....	67

<b>Chapter 7</b>	<b>Conclusions.....</b>	<b>69</b>
7.1	Summary .....	69
7.2	Future work and possible research directions .....	70
7.3	Opportunities.....	72
<b>Chapter 8</b>	<b>Annex A – Supporting information on LMPA-based VSC and VSTS manufacturing.....</b>	<b>73</b>
	 Manufacturing and characterization of variable-stiffness cables (VSCs).....	73
	 3-strut Variable-stiffness tensegrity structure (VSTS) .....	74
	 Underactuated VSTS joint .....	74
	 Kinematic experiments.....	74
	<b>References .....</b>	<b>75</b>
	<b>Curriculum Vitae .....</b>	<b>85</b>

# List of Figures

Figure 1 – Examples of industrial rigid robots (a) and completely soft robots (b). .....	1
Figure 2 – The bio-tensegrity model. ....	2
Figure 3. Examples of different polyhedral tensegrity structures used as robotic morphologies.....	6
Figure 4. Examples of different actuation technologies for tensegrity robots.....	7
Figure 5. Examples of different actuation strategies for tensegrity robots. ....	7
Figure 6. Examples of tensegrity robots inspired by biological structures. ....	8
Figure 7. Examples of modular tensegrity robots in literature. ....	9
Figure 8. Examples of variable-stiffness tensegrity structures in literature. ....	9
Figure 9 – The cytoskeleton of a cell and a tensegrity structure model.....	11
Figure 10 - Overview of conceptual tensegrity toolkit modules and assembled tensegrity robots. ....	13
Figure 11. The icosahedron tensegrity module. ....	13
Figure 12. The novel flat manufacturing technique. ....	14
Figure 13. Stiffness programmability of the tensegrity modules. ....	15
Figure 14. The latching-based connection system. ....	16
Figure 15. The tendon-driven actuation system for a tensegrity module with controlled compression. .....	17
Figure 16. A proof-of-concept modular tensegrity locomoting robot.....	18
Figure 17. The Adherens Junctions in multi-cellular biological systems. ....	20
Figure 18. Bio-inspired junction connector for soft modular tensegrity robots.....	21
Figure 19. The two modules morphology tensegrity kit. ....	22
Figure 20. Experimental results of experiments 1-8. ....	24
Figure 21. Experimental results of experiments 9-10. ....	25
Figure 22. The modular tensegrity kit and the two soft untethered robotic demonstrators.....	27
Figure 23. Overview of the active stiffness-change strategy based on LMPA Variable-stiffness cables. .....	29
Figure 24. 3-strut tensegrity structure cables analyses.....	30
Figure 25. Variable-stiffness results in compression and bending of an individual 3-strut module....	32
Figure 26. Variable-stiffness results in compression and bending of a two 3-strut modules beam....	33
Figure 27. A 3-strut VSTS module with the ability to self-deploy and lock its shape in both deployed and undeployed states. ....	34
Figure 28. Underactuated VSTS joint module and its shape deformations.....	35
Figure 29. Schematic representation of a type-changing variable-stiffness tensegrity structure and its bio-inspiration from a vertebrate spine. ....	38
Figure 30. Tensegrity type-changing module design.....	40

Figure 31. Type-changing tensegrity module stiffness characterization. ....	42
Figure 32. Type-changing tensegrity module parameters study. ....	43
Figure 33. Type-changing tensegrity module workspace characterization. ....	45
Figure 34. A tensegrity spine manipulator designed with an adapted type-changing tensegrity module composed of five vertebrae. ....	46
Figure 35. Variable stiffness tensegrity manipulator stiffness modes. ....	47
Figure 36. Examples of a rigid tensegrity module and a dual-stiffness tensegrity module. ....	50
Figure 37. Dual-stiffness strut design and model. ....	51
Figure 38. Dual-stiffness strut characterization. ....	51
Figure 39. The programmability of the dual-stiffness behavior. ....	52
Figure 40. Dual-stiffness tensegrity module design. ....	53
Figure 41. Dual-stiffness module characterization. ....	54
Figure 42. Dual-stiffness module characterization. ....	54
Figure 43. Four modules dual-stiffness frame. ....	55
Figure 44. Dual-stiffness Tensegrity drone quadcopter design. ....	55
Figure 45. Dual-stiffness tensegrity drone characterization. ....	56
Figure 46. Dual-stiffness wheeled rover design. ....	57
Figure 47. Dual-stiffness wheeled rover characterization. ....	57
Figure 48. Module actuation control parameters. ....	60
Figure 49. Co-evolution results with two different modules' stiffness. ....	62
Figure 50. The actuation system of the module. ....	64
Figure 51. The ANN model prediction of actuated cable lengths. ....	65
Figure 52. Evolutionary runs feature spaces results. The red circles highlight the best unique solution per run. ....	66
Figure 53. Simulated and real robot trajectory comparison. ....	67
Figure 54. A sequence of images of an evolved robot locomotion in hardware. ....	67
Figure 55. VSCs manufacturing steps. ....	73



# Introduction

Recently, the need for a new generation of robots able to leave structured environments and factory floors emerged as a priority of the robotics community. Traditionally, rigid-bodied robots used today in manufacturing are built of rigid links and joints to perform tasks rapidly and reliably. However, they are heavy, requiring high energy to accelerate, hold positions and quickly stop when necessary. Moreover, rigid robots are unsafe for interaction with human beings and cluttered environments due to high inertia and inability to absorb energy at impacts. To overcome these limitations, researchers started to develop robots and machines increasingly softer, lighter, and mechanically adaptive approaching the mechanical compliance, density, and versatility of materials and organisms found in nature. Thanks to this new approach, in the last decades, the field of robotics further expanded into the domains of healthcare, cooperative human assistance, and field and space exploration [1] [2] [3] [4].

## From Rigid to Soft, to Variable-Stiffness

Conventional rigid robots are built with materials of 3–10 orders of magnitude more rigid and 3-20 times heavier than the materials in natural organisms [5] [6]. This substantial mismatch in weight and mechanical compliance is a big reason why rigid robots are often biologically incompatible and even dangerous for human interaction and rarely exhibit energy efficiency, agility, and mechanical adaptability of natural organisms [7].

To overcome rigid robots' limitations, in the early days of soft robotics, roboticists focused on developing robot bodies made exclusively of soft materials [8] [9] with rigidity and weight similar to the ones exhibited by natural organisms.

Soft robots bodies can undergo large deformations, comply with object surfaces, absorb the energy of impacts exhibiting physical robustness. All qualities that can lead to having safe human-robot interaction at potentially low cost and energy efficiency.

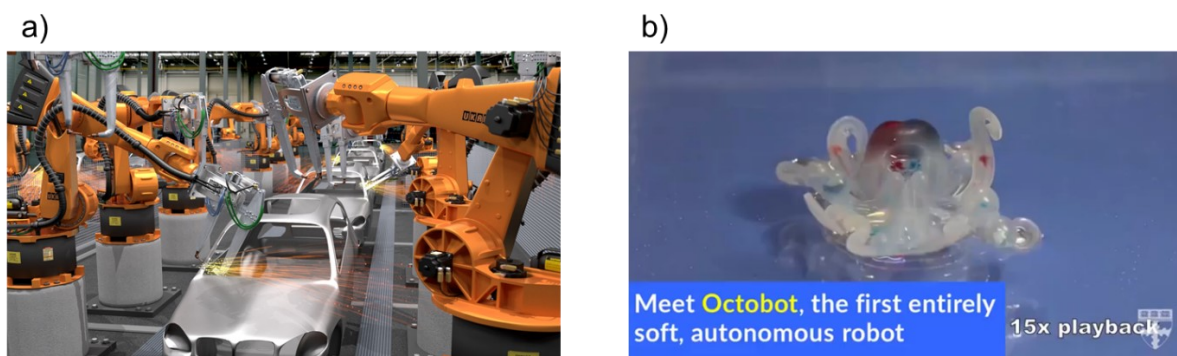


Figure 1 – Examples of industrial rigid robots (a) and completely soft robots (b).

However, being completely soft has drawbacks, too. Completely soft bodies cannot apply strong forces to the environment and they typically require stiffness tuning to increase forces transmitted during actuation to perform a task [5]. Nature gives us examples of soft animals and living structures able to change the rigidity of selected body parts, such as octopus's tentacles, the elephant trunk, humans' tongue, and lips.

Moreover, completely soft robots cannot sustain efficiently bodyweights cause of their lack of rigidity. Soft animals in nature tend to be small or live in an environment where a surrounding medium helps them to support their bodies (e.g. in

water or underground) like earth-worms or squids, and jellyfishes. While, larger terrestrial animals, comparable with the human scale, typically have bodies made of different materials including skeletons composed of stiff bones to support their body weight in a more energy-efficient way [6].

These biological pieces of evidence suggest that a core challenge of soft robotics research is to develop an integrated approach, where rigid structures and soft structures are merged with variable-stiffness technologies in a new generation of lightweight, compliant, and mechanically adaptive robots. Such robots should be able to exhibit physical robustness and compliance for safe human-robot interaction and, at the same time, to apply efficiently forces to the environment when needed, and withstand their bodyweight at different scales. Such an integrated approach can potentially increase soft robot applications in all types of tasks and environments.

## The bio-inspired tensegrity approach

Inspiration for a novel approach in designing soft robots can come from nature itself and specifically from how natural organisms and biological structures are modeled.

Over the years, given the limitations that the Hookean and Newtonian model had in describing kinematics and dynamics of biological structures [8], S. Levin [9] and others [10] have proposed a new model for biological structures based on the concept of tensegrity. The term “tensegrity” has been coined by architect R. Buckminster Fuller to describe a structure that maintains its mechanical integrity throughout the pre-stretching of some elements constantly in tension (called “cables” in red in Figure 2) connected in a network with other elements constantly under compression (called “struts” in green in Fig. 2) [10].

This model rejects the idea of the vertebrate musculoskeletal system as beams, columns, and levers, and acknowledges the bones as stiff under compression elements held and stabilized in their positions by the pull of tensile components such as muscles, tendons, ligaments, and fascia. Therefore, rather than a frame supporting an amorphous soft tissue mass, the whole vertebrate body is stabilized by these tension components and its stiffness can vary depending on the pre-stress (i.e. tone) and stiffness of its muscles [9] [12].

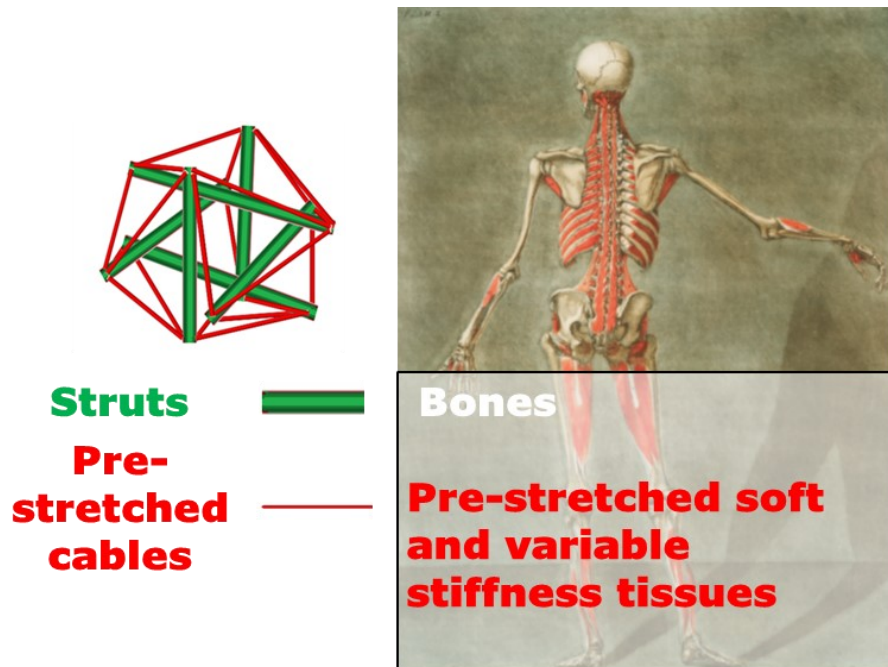


Figure 2 – The bio-tensegrity model.

(a) Example of tensegrity structures and their components. (b) A graphical representation of the human muscle skeleton system (Credits: Rawpiel\_Ltd by Arnauld-Eloi Gautier-Dagoty).

This structural organization allows biological organisms to be mechanically adaptive. They can exhibit high physical robustness and compliance, apply efficiently forces to the environment when needed, and, at the same time, withstand their bodyweight at different scales. In the same way, tensegrity structures used in robotic applications can provide a lightweight and robust framework where integrating stiff under compression struts for bodyweight support; variable stiffness cables for applying directionally larger forces when required, and soft cables to absorb energy and allow compliance.

Moreover, tensegrity structures show other mechanical advantages typical of biological structures. When a load is applied to a tensegrity, it is distributed in the whole structure, with the tension elements always remaining in tension and the compression elements always remaining in compression, therefore, each structural element can be optimized for only one type of stress and be lighter. Extensive research in civil engineering has proved that the tensegrity paradigm offers minimum mass-to stiffness solutions for a variety of load conditions [11] [12]. This feature allows tensegrity structures and biological organisms to withstand large forces and be lightweight at the same time [9] [14].

### **Modularity**

Tensegrity structures are observed in nature at different scales, showing often a modular organization [13]. For example, at the macroscopic level, muscles are organized in modular groups and fasciae [14], and the spine in a chain of vertebrae suspended in a network of muscles and tendons [9]. At the microscopic level, cells are modeled as self-stabilized tensegrity modules that, when assembled, compose tissues and macrostructures [10]. It has been suggested that also at the nanoscale, some proteins and basic molecules maintain integrity with a tensegrity structure serving as basic modules to assemble different biological components [10].

The modularity gives an important advantage to biological tissues: robustness. In modular tensegrities systems, individual tensegrity components can be disrupted without compromising overall system integrity [9] [10]. For instance, if accidentally a tensile component in the human body is severed (e.g. the Achilles tendon), form control in the ankle module is lost but other joints and parts of the leg and body don't lose their integrity and can still function redistributing loads [15]. In the same way, modularity can be beneficial in designing tensegrity robots with failure-robust bodies.

Moreover, modularity can limit the inherent complexity in manufacturing and assembling self-stabilizing tensegrity structures, since the production of identical simple unit modules can lead to standardized manufacturing and assembling processes.

Furthermore, modularity can help to overcome a historical limitation in designing tensegrity robots: the form-finding problem. Different statically self-stabilized tensegrity structures can be defined according to the number of struts and cables, their network configuration (e.g. struts and cables positions in the three-dimensional space), and cables' pre-stretch [11]. These variables are generally determined through analytical, numerical, or heuristic form-finding methods [16]. However, tensegrity networks with task-optimal morphologies, specific mechanical properties, integrated actuation, and variable stiffness components, represent a more complex and with more variables form-finding problem to solve. Therefore, rather than investigate how to form-find tensegrity structures, a modular approach gives the possibility to use existing known simple shape tensegrities as building blocks for constructing target robotic bodies and gives us the possibility to focus on how to functionalize these structures for robotic applications. These modules can be passive, for transmitting forces across the assembly, or active, including an actuation mechanism to actuate the assembly or a variable stiffness mechanism to change its mechanical properties.

In conclusion, modular tensegrity structures can provide a lightweight and robust framework where integrating stiff under compression struts for bodyweight support; variable stiffness cables for applying directionally larger forces when required, and soft cables to absorb energy and allow compliance. All these advantages are not only beneficial for biological structures and biological organisms but, as well, can be exploited in a new design approach for developing soft robots for a great variety of tasks and robotic applications.

## **Thesis Outline**

In this thesis, we investigated tensegrity modular structures as a new approach to develop soft robots with variable stiffness capabilities.

This investigation led to a set of design strategies to manufacture and actuate tensegrity modules with programmable stiffness and deformation (*Chapter 2*); to connect mechanically and electrically tensegrity modules without hindering deformability (*Chapter 3*), and to implement variable-stiffness capabilities in the modules for active (*Chapter 4*) and passive (*Chapter 5*) stiffness change. Finally, in *Chapter 6*, we present preliminary results and insights on using heuristic algorithms to design task-optimal morphologies, stiffness, and control of modular tensegrity robots.

## **Chapter 1. The state of the art of tensegrity robotics**

In the first chapter, we review and discuss the state of the art of tensegrity robotics. Moreover, we individuate current limitations for developing modular variable-stiffness tensegrity robots with task-optimal morphology, stiffness, and control.

## **Chapter 2. Manufacturing and Actuation strategy for modular tensegrity robots**

In the second chapter, we introduce a novel manufacturing strategy to facilitate the realization of tensegrity structures using planar manufacturing techniques, such as 3D printing. We used this strategy to develop icosahedron tensegrity modules with programmable stiffness that can deform in a three-dimensional space.

We also describe a modular actuation strategy to actively control the deformation of the tensegrity modules along specific direction axes. We developed icosahedron tensegrity modules with pre-programmed linear actuation allowing them to have contraction movement along a predetermined axis. Finally, we demonstrated how these 1DOF actuated modules can be assembled into multi-DOF actuated robotic structures, such as a modular crawling robot biomimicking peristaltic locomotion.

The main contributions of Chapter 2 are:

- A novel planar manufacturing technique for tensegrity structures with programmable stiffness
- A modular actuation strategy for modular tensegrity structures
- The demonstration of a proof-of-concept crawling robot with the novel actuated tensegrity modules

## **Chapter 3. A bio-inspired connection strategy for untethered soft modular tensegrity robots**

In the third chapter, we present a new bio-inspired inter-module connection strategy that connects tensegrity modules mechanically and electrically. We show that our strategy allows connected modules to retain stiffness in the same order of magnitude as individual modules while providing low electrical resistance for passing energy and communication signals among modules. We demonstrate the connection strategy with two proofs-of-concept untethered soft modular tensegrity robots: a gripper and a crawler.

The main contributions of Chapter 3 are:

- A novel bio-inspired connection strategy for deformable modular tensegrity robots
- Design and manufacturing of a soft modular robotic kit to assemble reconfigurable untethered modular tensegrity robots
- The demonstration of two proofs-of-concept untethered modular tensegrity robots: a soft locomoting crawling robot and a soft robotic gripper

## **Chapter 4. Design strategies for active stiffness-change of tensegrity modules:**

In chapter four we introduce two novel design strategies to implement active stiffness-change capability into tensegrity modules. The chapter is divided into two parts, in the first part, we present a novel design approach to develop variable-stiffness tensegrity structures (VSTSs) that relies on the use of variable-stiffness cables (VSCs). We show the capabilities of the proposed VSTS in three validation scenarios with different tensegrity structures: 1) a two-modules tensegrity beam with tuneable load-bearing capability, 2) a tensegrity module that can self-deploy and lock its shape in both deployed and undeformed states, and 3) an actuated tensegrity module with underactuated shape deformations.

In the second part, we describe a novel variable-stiffness design strategy based on type-changing tensegrity structures. We investigate the strategy on a proof-of-concept tensegrity module which uses an active mechanism to add or remove a ball-joint constraint among its rigid components, allowing transition among different tensegrity types and stiffness modes. We demonstrate the variable-stiffness strategy by developing a variable-stiffness robotic spine that can operate in different stiffness modes.

The main contributions of Chapter 4 are:

- A novel smart-materials cable-based design strategy for developing tensegrity modules with active stiffness change capability
- Demonstration of three novel abilities exhibited by tensegrity modules with active-stiffness control of their cables
- A novel variable-stiffness design strategy based on type-changing tensegrity modules
- The demonstration of a proof-of-concept robotic variable-stiffness spine based on type-changing tensegrity modules

### **Chapter 5. Dual-stiffness design strategy for passive stiffness change of tensegrity structures.**

In chapter five we introduce a novel design strategy to develop modular tensegrity structures able to passively change-stiffness during collisions. We named such structures *dual-stiffness tensegrity structures*. The dual-stiffness allows tensegrity modular robots to be rigid during navigation and to soften during collisions to absorb energy, and avoid damage. Simulations and real experiments on a single module and two robotic demonstrators are performed to validate the dual-stiffness concept. The two demonstrators are a quadcopter drone composed of four connected modules and a wheeled rover composed of two connected modules.

The main contributions of Chapter 5 are:

- A novel dual-stiffness strut-based design strategy for developing passive variable-stiffness tensegrity modules and structures
- The demonstration of two proof-of-concept robots with passive stiffness-change capability: a wheeled rover and a quadcopter drone

### **Chapter 6. Heuristic algorithms to design task-optimal morphology, stiffness, and control of modular tensegrity robots.**

In this chapter, we present results and insights on the use of heuristic algorithms to design task-optimal morphology, stiffness, and control of modular tensegrity robots. The chapter is divided into two parts.

In the first part of the chapter, we demonstrate the feasibility of using a heuristic algorithm to design soft tensegrity modular robots with open-loop controllers. The method consists of using the modular tensegrity hardware platform presented in chapter 2, coupled with an evolutionary and simulation software platform. Moreover, we demonstrate the importance of including the cables' stiffness as a design parameter of the optimization.

In the second part of the chapter, we present preliminary results on how to perform the sim-to-real transfer of modular tensegrity robots evolved with the presented design method. Moreover, we show the first transferred to reality modular tensegrity robot.

The main contributions of Chapter 6 are:

- The development of an evolutionary platform to design soft modular tensegrity robots
- The demonstration of the importance of stiffness optimization in modular tensegrity robots
- The demonstration in the hardware of a proof-of-concept novel locomotion strategy of a tensegrity modular robot designed by co-evolving morphology, stiffness, and control

# Chapter 1 State-of-the-art of Tensegrity robotics

In this chapter, the tensegrity robots design methods in the literature are presented and discussed. The analyses include design strategies to implement modularity and variable stiffness. Moreover, an overview of existing methods to simulate and control tensegrity robots is presented. Finally, concluding remarks on the state of the art are discussed.

## 1.1 Tensegrity robots' morphologies and actuation designs

The concept of developing biologically inspired soft robots using tensegrity structures has been firstly suggested in 2008 with preliminary work in simulation by Rieffel et al. [17] and by Paul in hardware [18]. Since then, new technologies emerged to physically build such robots. However, some limitations, such as the complexity in manufacturing and designing actuated tensegrity structures, have led to simple intuitive morphologies and actuators placement.

In terms of morphology, most tensegrity robots present in literature follow two trends: tensegrities with polyhedral morphology (i.e. tensegrity structures resembling polyhedral convex solids) [19] (Fig 2a-b), or tensegrities with morphologies inspired by the artistic representation of biological structures. Only a few cases of modular tensegrity robots exist inspired by the artistic representation of the vertebral spine.

### Polyhedral tensegrity robots

The robots of this category are usually developed by functionalizing with intuitively placed actuators polyhedral tensegrity structures. The chosen structures are usually known to be self-stabilizing and their mechanical properties are well investigated in the literature. Eventually, a control algorithm is then designed for such structures to perform a certain task, mainly locomotion. The most popular morphology is the icosahedron tensegrity structure [20]. Other types of polyhedral tensegrity include dodecahedrons [21], prisms [18], and others similar to those [22, 23] [24] [25]. In the literature, these structures have been functionalized with several types of actuators, often servomotors [26] and including smart materials [27] [28] [29], and pneumatic soft actuators [21] [30].

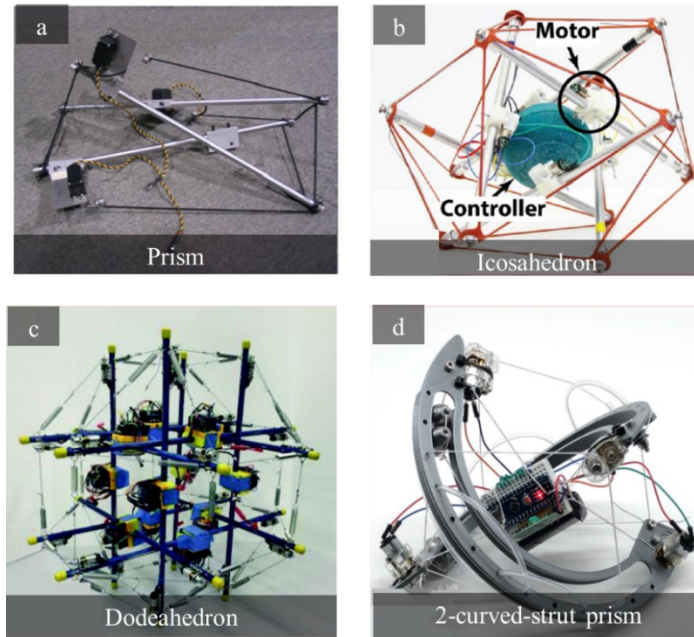


Figure 3. Examples of different polyhedral tensegrity structures used as robotic morphologies.

(a) Example of a tensegrity robot with prism morphology [17], (b) example of a tensegrity robot with icosahedron morphology [20], (c) example of a tensegrity robot with dodecahedron morphology [38], (d) example of tensegrity robot with rounded-struts-prism morphology [21].

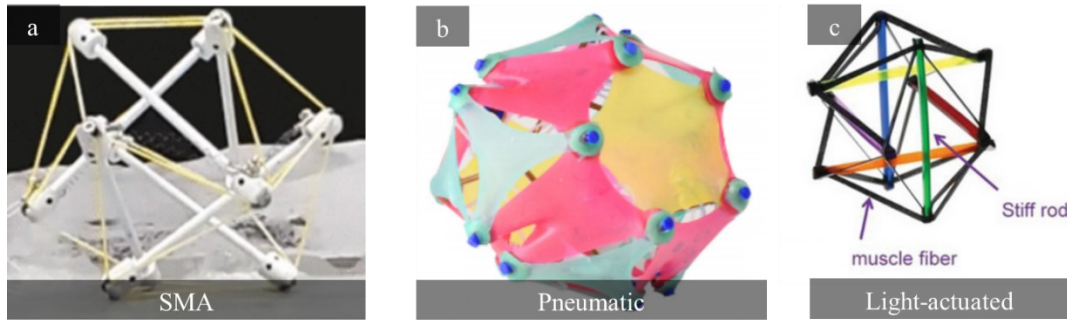


Figure 4. Examples of different actuation technologies for tensegrity robots.

(a) Example of a SMA actuated tensegrity robot [26], (b) example of pneumatically actuated tensegrity robot [20], (c) example of light-actuated tensegrity robot [27].

Such robots are developed for diverse mode of locomotion, such as: rolling [31] [32] [33] [34] [35] [36], crawling/vibration [37] [38] [39] [40] [41] [40], hopping [42] [43], and flying [44]. The most advanced polyhedral tensegrity robots have been developed by NASA AMES in collaboration with the BEST Lab resulting in icosahedral tensegrity robots, such as the SUPER-ball and ReCTer, which can roll, even on rough terrains and on slopes, with an optimized control of the six embedded tendon-driven actuators (Figure 5A) [32] [26].

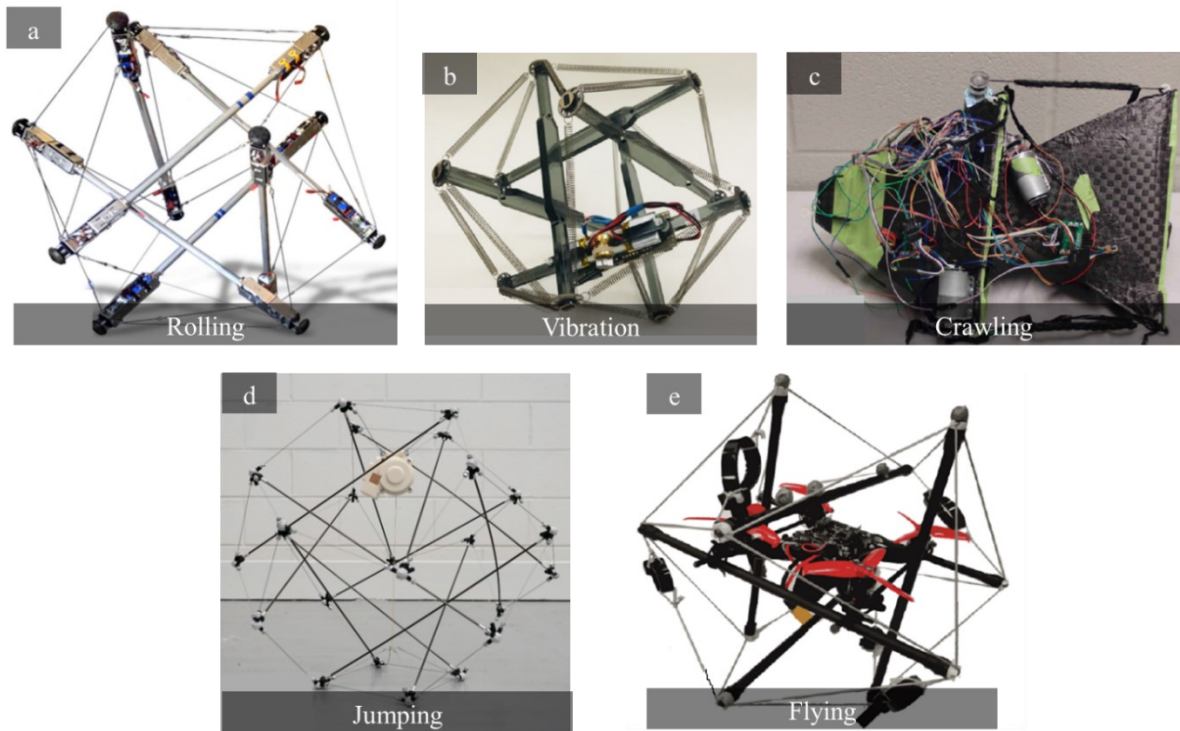


Figure 5. Examples of different actuation strategies for tensegrity robots.

(a) Example of rolling tensegrity robot [31], (b) example of locomotion by vibration of a tensegrity robot [37], (c) example of crawling tensegrity robot [38], (d) example of a jumping tensegrity robot [41], (e) example of a flying tensegrity robot [43].

### Bio-inspired tensegrity robots

The robots of this category are usually developed by functionalizing with actuators bio-mimicking artistic tensegrity structures or intuitive morphologies resembling biological structures. The most utilized artistic works used as inspiration are bio-

tensegrity models of the human musculoskeletal system designed by T. Flemons. Most advanced three-dimensional investigations include a quadruped with passive legs [45]; elbow [46] and shoulder joints [47], tensegrity hand [48], foot mechanism [49] and tensegrity arms [50] (Figure 6d). In particular, the tensegrity arm has a shoulder and elbow developed in a modular fashion. It can actuate four active degrees of freedom to create a relatively large workspace. However, the tensegrity structure is customized for a specific limb shape and function and cannot be modified (e.g. adding wrists and hands for manipulation) without changing the self-stabilized structure and re-design the whole tensegrity system. Moreover, none of the examples in literature make use of variable-stiffness, one of the main features of the biological structures they are inspired from.

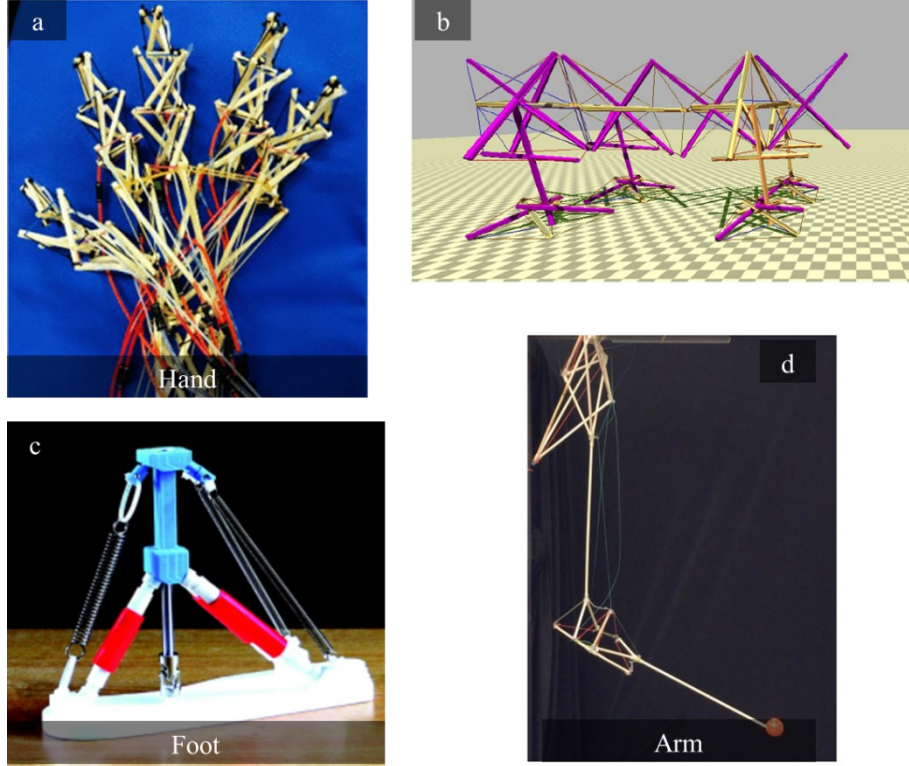


Figure 6. Examples of tensegrity robots inspired by biological structures.

(a) Example of a tensegrity robotic hand [47], (b) example of tensegrity quadruped [44], (c) example of tensegrity robotic foot [48], (d) example of a tensegrity robotic arm [18].

### Modular tensegrity robots

Modular tensegrity systems have been often investigated for developing passive tensegrity structures such as toys [51], and metamaterials [52] [53] [54] [55] [56]. Some more advanced applications are deployable rigid modular tensegrity structures in active architecture [35] [36]. However, not many examples exist in robotics literature. Most of the examples are in simulation and on optimizing controllers for spine-like bio-inspired tensegrity structures for locomotion [45] [57] [58] [59] [60] [61]. Only recently a novel 3D printing design method allowed the development of modular chain-like tensegrity structures used as soft robotics legs [62]. However, the developed hardware does not have embedded actuators and relies on external actuation and power. Moreover, none of the examples in literature make use of variable-stiffness, one of the main features of the biological structures they are inspired from.

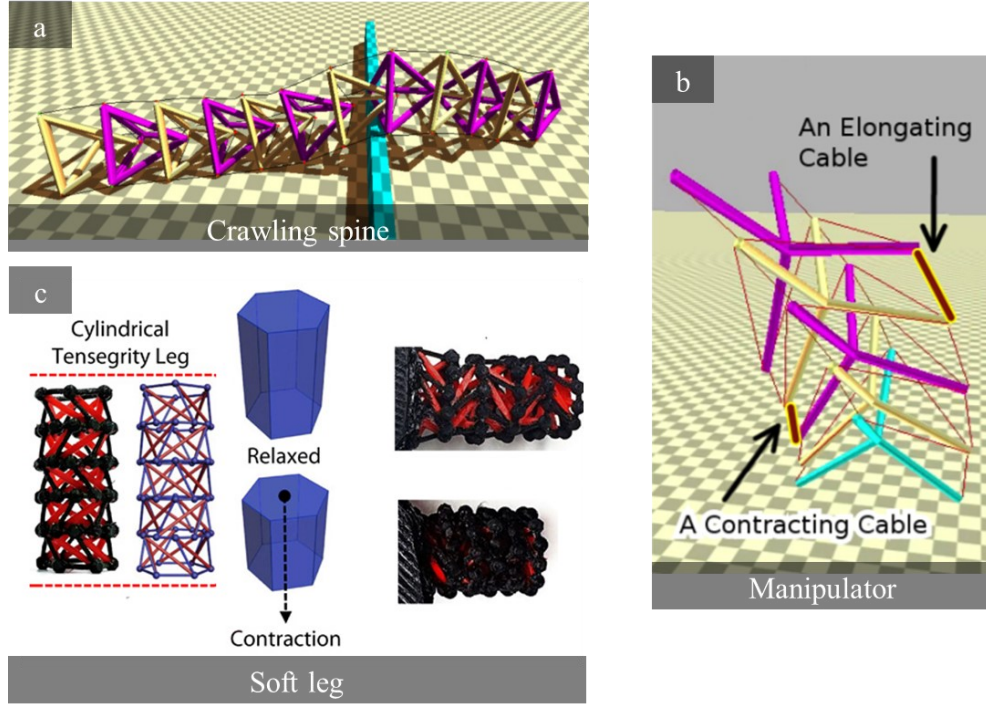


Figure 7. Examples of modular tensegrity robots in literature.

(a) Example of a tensegrity spine crawling robot [45], (b) example of tensegrity spine as a bending manipulator [60], (c) example of tensegrity modular soft legs [47].

## 1.2 Variable-stiffness tensegrity robots

Not many investigations exist on variable-stiffness tensegrity robots, although the use of tensegrity structures with low stiffnesses (i.e. Young Modulus in order of MPa/KPa) in soft robotics and as rigid structures in civil engineering (e.g.  $E$  = Modulus in order of GPa) are quite widespread and investigated. In only a few investigations, variable stiffness is addressed by enabling the change of cable pre-tensioning. [63] [64]. However, this approach generates relatively small stiffness change (by a factor of 3) or requires multiple actuators that increase the weight and bulkiness of the system [65].

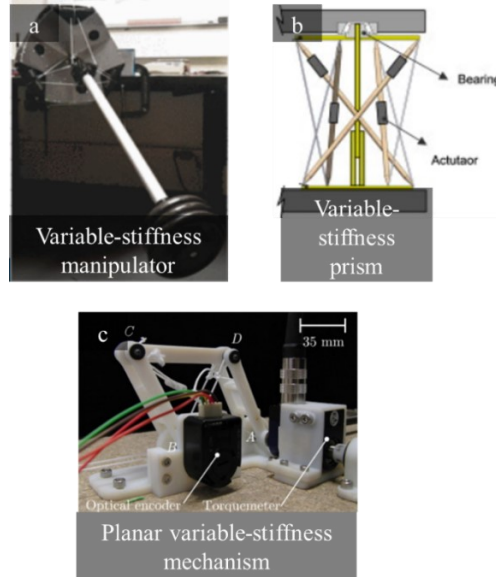


Figure 8. Examples of variable-stiffness tensegrity structures in literature.

(a) Example of a tensegrity variable-stiffness manipulator [61], (b) example of tensegrity variable-stiffness structure in simulation [62], (c) example of a two-dimensional variable-stiffness tensegrity mechanism [63].

### 1.3 Simulation of Tensegrity Robots

Simulation of tensegrity robots is one of the main challenges in the field. Simulations are indeed fundamental for designing morphology, mechanical properties, and controllers of such robots. A comprehensive simulator of tensegrity structures and robots requires modeling highly non-linear dynamic motions and contacts between struts and the ground including friction, strut-strut contact, and cable contacts.

Analytical formulations of the statics and dynamics of a tensegrity structure have achieved simulating high-level tasks such as morphology optimization and controller design [66] [67]. However, these analytical models make important simplifications, such as treating the cables with constant stiffness or struts as cylinders with rotation along the axis, ignoring end caps or other rigid structures, and assuming there is no collision between cables.

A few simulators exist able to modeling such behaviors [68] [69] [70], the most comprehensive is the open-source bullet-based NASA Tensegrity Robotics Toolkit (NTRT) [71] [72] which allows to model also cables to cables contacts and is the most popular choice for the design of tensegrity robots. However, dynamics motion obtained in simulation can be affected by inconsistencies that determine the so-called “reality gap” between simulation and hardware. Recently, new techniques based on an iterative process where simulation parameters are tuned after running experiments on physical robots have been successfully applied to increase the accuracy of NTRT and improve its applicability to real systems [73] [59].

Moreover, novel work on differentiable physics engines, showed that learning a physical model directly from data may further reduce the reality-gap [74].

### 1.4 Control of tensegrity robots

Classical control strategies which rely upon analytical models have been initially applied to provide effective equations of motion [94][92] using systems of differential-algebraic equations. [94] Alternatively, have also been used feedback linearization control laws [96] and Lyapunov-based controllers for 3D dynamic models [95]. However, the complex dynamics of tensegrity structures make classical controlling techniques challenging to be used and highly approximated [73].

Some researchers have found simpler heuristic controllers, such as hand-coded policies particularly appealing. However, such policies are system-dependent and do not use dynamic synergies that can lead to more efficient locomotion strategies [75]. To explore such synergies researchers have used several data-driven and bio-inspired techniques, such as Central Pattern Generators (CPGs), [60], [76], and evolutionary algorithms [59] [77]. In particular deep reinforcement learning (RL) seems to hold the promise of generating successful feedback control policies that map directly from sensory data to task-oriented actions [78]. For instance, RL has successfully facilitated the development of rolling controller policies for SUPER-ball [79].

### 1.5 Concluding Remarks

In conclusion, although several investigations have been made for designing tensegrity robots, the designers still make use of simple and hand-picked morphologies with the intuitive placement of actuators. A design methodology that allows exploring diverse morphological configurations and that can lead to more task-optimal and robust configurations are still missing. A modular approach that can lead to diverse morphologies and increased robustness has been investigated only for simple chain structures of artistic inspiration and is still limited by tethered technological solutions. Moreover, the great potential of variable stiffness is still not expressed and only a few studies exist in this direction with limited stiffness change.

Comprehensive simulators such as the NASA NTTR and promising control strategies such as data-driven bio-inspired strategies have been developed and are promising for designing also modular robots. However, finding an appropriate compromise between design parameters while ensuring that the corresponding robot is physically realizable is still challenging due to the reality-gap between tensegrity models and hardware prototypes.

# Chapter 2 Modular design strategy and novel manufacturing technique

Publication Note: The material presented in this chapter is adapted from:

- D. Zappetti, S. Mintchev, J. Shintake, e D. Floreano, «Bio-inspired Tensegrity Soft Modular Robots», in Biomimetic and Biohybrid Systems, lug. 2017, pagg. 497–508, doi: 10.1007/978-3-319-63537-8\_42 [95].

The first author contribution was to conceptualize the design strategies, manufacture and characterize tensegrity modules and robotic application, to analyse the results and to write the manuscript.

In this chapter, we introduce the modular design strategy for designing tensegrity robots and a novel manufacturing technique to facilitate the realization of tensegrity structures using planar manufacturing techniques. The chapter is organized as follows: In section 2.1, we give an overview of the modular design and actuation strategy and its bio-inspiration. In section 2.2 we present the novel planar manufacturing technique and its implementation in developing icosahedron tensegrity modules with programmable stiffness. In section 2.3 we describe how to actuate a module along a programmed DOF (i.e. Degree Of Freedom). Finally, in section 2.4 we present a proof-of-concept modular tensegrity robot obtained with such strategy,

## 2.1 A bio-inspired modular design strategy for tensegrity robots

In chapter one we have discussed how the design of the majority of the tensegrity robots still makes use of simple and hand-picked morphologies with the intuitive placement of actuators. In this chapter, the multi-cellular organization of

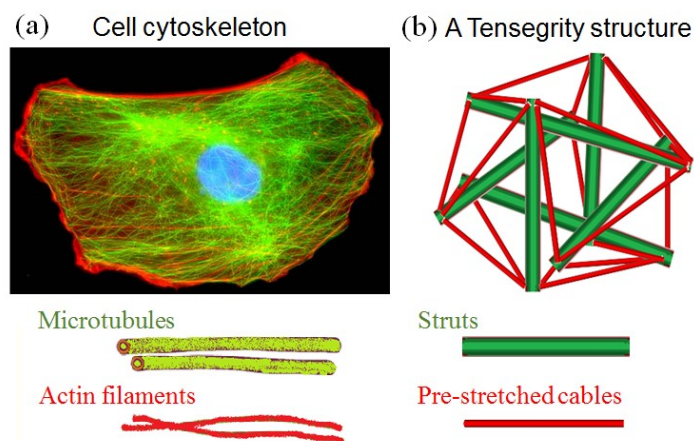


Figure 9 – The cytoskeleton of a cell and a tensegrity structure model.

(a) Image of a cell obtained with fluorescence microscopy. In blue is the nucleus of the cell and at the bottom a sketch of the two main constituents of the cytoskeleton: microtubules and actin filaments. (b) Example of a tensegrity structures: the icosahedron tensegrity structure composed of six struts and 24 cables.

biological structures inspired a novel design methodology that allows exploring diverse morphological configurations and that can lead to more task-optimal and robust configurations.

Biological multi-cellular organisms are heterogeneous systems made of cells with diverse functions and mechanical properties. The cells, and the tissues they compose of, display different degrees of stiffness: from very soft, such as fat cells, stiff, such as bone and ligament cells, to directional stiffness, such as hair cells, and variable stiffness, such as muscle cells, for example. However, every cell has a cytoskeleton, which is a network made of two types of interconnected fibers [80]: under compression microtubules and tensioned actin filaments (**Error! Reference source not found.**). This architecture and its components' mechanical properties are responsible for the shape, stiffness, and strength of the cell which can be formally described as a tensegrity structure [13].

By assembling in different configurations, these cells can form bodies and tissues with diverse morphologies and diverse mechanical properties that the organisms can take advantage of. Assemblies can range from completely soft bodies with variable-stiffness capabilities, such as worms, to complex hybrid rigid, soft, and variable-stiffness bodies, such as vertebrates.

Here we propose a design principle for designing variable-stiffness tensegrity robots inspired by the multi-cellular organization of biological organisms. This novel design strategy consists of designing a kit of individual tensegrity modules with programmable stiffness and variable stiffness capabilities that can be assembled in diverse robust task-optimal morphological configurations. Moreover, these modules can be divided into passive and active modules. While passive modules are used for assembling diverse morphologies, active modules include an actuation mechanism that allows controlled deformation along a specific direction axis or a variable-stiffness mechanism to modulate its mechanical properties. Different active actuated modules can be developed that can compress, bend, or rotate around a pre-programmed axis. Although this type of 1DOF actuation does not allow a single module to locomote or perform a task, just like single biological cells in multicellular systems, several actuated modules connected in series, in parallel or transversally could perform more complex movements and tasks, such as locomotion or manipulation (Figure 10). These modules can then be arranged in task optimal morphologies using state-of-the-art heuristic algorithms and optimization techniques, such as evolutionary algorithms.

### 2.1.1 Tensegrity Structures' kit selection

Different tensegrity structures already known in literature can be used to develop modules of a robotic tensegrity kit. They may differ for the number of struts and cables, the network configuration (e.g. struts and cables positions in the three-dimensional space), the cables' stiffness, and how much they are pre-stretched.

The main criteria for selecting structures for a kit is to display similar faces on the external surface to allow face-to-face connection in multiple directions between modules and allowing assembly of lattice-like structures to explore larger morpho-functional spaces. Additional criteria may be having a three-dimensional network as simple as possible (i.e. minimum number of struts and cables) to facilitate the manufacturing of several modules and exhibiting an inner empty volume to place and protect payloads such as actuators, batteries, and electronics.

Tensegrity structures resembling regular (or semi-regular) polyhedrons, such as "tensypolyhedrons" and symmetrical structures and are promising as building blocks for modular systems because of their regular external surface. Moreover, some of them have relatively simple networks and can be assembled into three-dimensional lattices. A comprehensive study of "tensypolyhedron" has been conducted by O. Foucher [81].

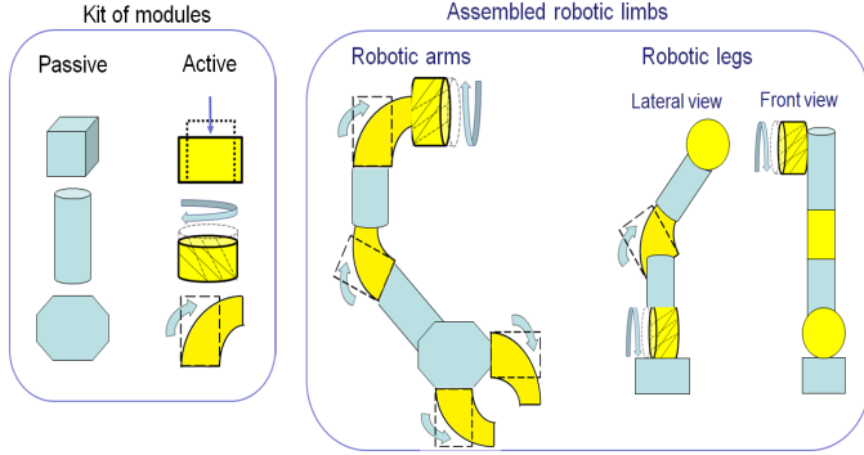


Figure 10 - Overview of conceptual tensegrity toolkit modules and assembled tensegrity robots.

## 2.2 Module Design and Manufacturing

In this work, we aim at studying robotic modules on a scale of few centimeters because they can be manufactured using affordable and simple manufacturing methods, incorporate off-the-shelf electronic components, and eventually be assembled into functional modular robots of a size comparable to the typical household or inspection robots.

In this study, we use the icosahedron tensegrity as a proof-of-concept tensegrity kit module. Three main criteria have been applied to select such a module. The first criterion is that the main tensegrity module can deform (e.g. stretch or contract) and connect in a three-dimensional lattice. The second criterion is that this tensegrity structure is composed of the smallest possible number of struts and cables to ease the manufacturing and assembling. The third criterion is that the icosahedron network configuration exhibits an inner volume not crossed by any cable or strut allowing placing and protecting a useful payload (e.g. actuator, microcontroller, energy storage, depending on the cell type).

The icosahedron tensegrity structure exhibits a symmetric network with an almost spherical shape [19] (Figure 11 a). It is composed of 6 identical struts and 24 cables of equal length. The cables are organized in 8 equilateral triangles interconnected by 12 vertices and distributed in 4 parallel opposite pairs (in Figure 11 b the pairs of triangles are marked with four different colors). Furthermore, the icosahedron tensegrity structure has an inner cubic volume that is not crossed by any cable or strut (Fig. 11 a), satisfying the third criterion.

When the icosahedron structure is compressed along a direction orthogonal to any of the four triangle pairs (Figure 11 c), it displays high deformability and can be collapsed to a flat configuration (Figure 11 d). These four directions, which we name “collapsibility directions”, allow the structure to deform in the three-dimensional space.

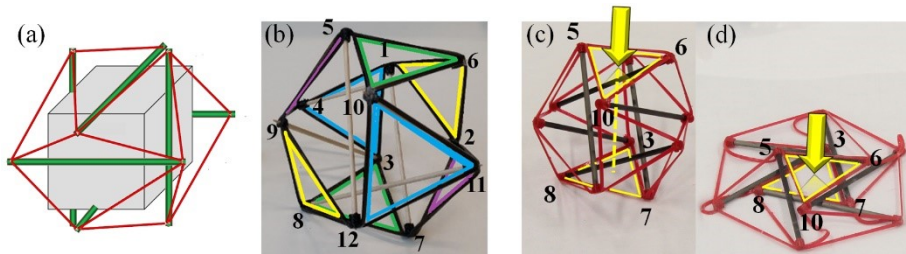


Figure 11. The icosahedron tensegrity module.

(a) Icosahedron tensegrity structure with a grey cube at the geometrical center to better display the inner cubic volume not crossed by any cable or strut. (b) Icosahedron tensegrity prototype with the 4 couples of parallel equilateral triangular faces marked with 4 different colors. (c) An external load is applied along the orthogonal direction to the two parallel triangular faces (a “collapsibility direction”). (d) The collapsed structure.

## 2.2.1 Novel Manufacturing strategy

Tensegrity structures are composed of rigid struts under compression and pre-stretched cables under tension assembled in a mechanically stable network. The assembly of tensegrity structures is particularly complex because the stability of every component is obtained only after assembling the last component (e.g. strut or cable), making highly unstable the structure during intermediate steps.

In our novel manufacturing strategy, instead of manufacturing and assemble every single component separately, we manufacture all cables as a single flat network that can be folded into a three-dimensional structure and subsequently filled with struts. The cable network can be rapidly manufactured using inexpensive 3D printers.

Two different materials are used for cables and struts. The cables require an elastic or rigid printable material; the struts instead require a stiff material that can withstand compressive forces without buckling [11]. In this study, we focus on developing soft cables and we use NinjaFlex, an elastic material compatible with commercially available fused deposition modeling 3D printers that can withstand 65% of elongation at yield. For struts, we use pultruded carbon rods (that are commercially available in different diameters and lengths) with a longitudinal Young's modulus of approximately 90 GPa, which is sufficient to withstand compression and buckling.

To design the flat cable's network, a 3D CAD model of the tensegrity module is realized (Figure 12a). The model is composed of the 8 equilateral triangles of the icosahedron tensegrity assembled with joints at the 12 vertices. The unfolded flat network is obtained by eliminating the 6 struts and disconnecting the cables at two vertices (see Figure 12b), and then rotating the triangles around the joints until obtaining a flat network's configuration (see Fig. 3c-d). The nodes of the network are marked according to the corresponding vertex of the 3D tensegrity model. The two vertices that were disconnected in software to unfold the network will be overlapped to close it back during the physical assembly.

To assemble the rigid struts in the elastic network, cylindrical housings are designed at all the nodes (see Figure 12d-e). The housings are 4 mm high and have an inner diameter equal to one of the carbon rods to ease the insertion. Thanks to this type of design, no additional connection elements or adhesives are required to connect the struts, which will be kept in place and secured by the pre-stretch of the cables after the physical assembly.

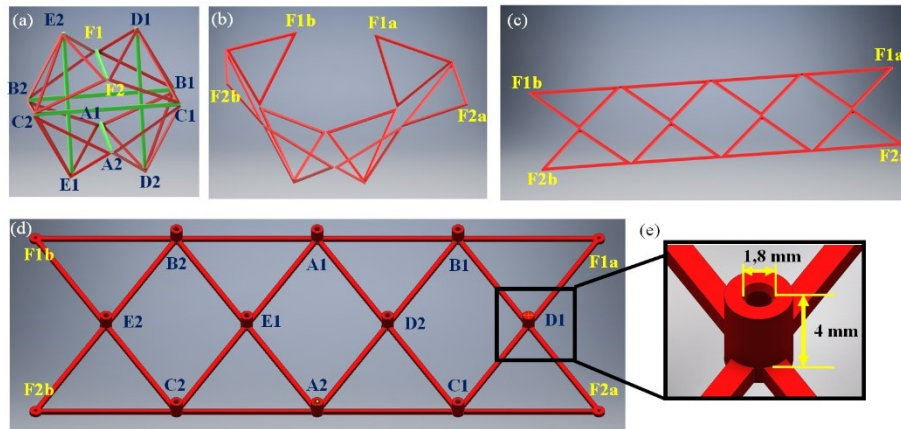


Figure 12. The novel flat manufacturing technique.

(a) 3D CAD model of a tensegrity icosahedron. In yellow are marked the two vertices disconnected to unfold the cable's network. (b-c) The unfolding sequence obtained by rotating the triangles around the joints in the vertices, in yellow is marked the 4 nodes that will be overlapped to generate vertices F1 and F2. (d) Flat cable's network with housings in the vertices to insert the carbon rods. (e) Detailed view of one of the housings.

The cable network is 3D printed with a Desktop 3D printer LulzBot TAZ 5. After 3D printing, the carbon rods are assembled following the illustration in Figure 12d: the two vertices of a rod are inserted in the two housings with the same letter starting from the housing "A" (e.g., the ends of the first strut will be inserted in A1 and A2 housings) and following the alphabetical order until the sixth and final strut "F" which has to be inserted in four housings (one side of the carbon rod is inserted in the two F1a-b housings and the other in the two F2a-b).

The icosahedron tensegrity prototype in Figure 11c is made of an elastic network of thickness and width of 1 mm and with cables long 4.75 cm each, has a height of 7.8 cm and can be approximated to a sphere of the same diameter, therefore occupying a volume of about 248 cm<sup>3</sup>. The printing process requires approximately 30 minutes for the icosahedron elastic network with an infill of 100 % and 0.25 mm of vertical resolution. When collapsed along any of the four different directions, the structure reduces its volume by 84 % to about 40 cm<sup>3</sup> (Figure 11d).

The stiffness of the tensegrity modules mainly depends on the stiffness of the cable networks that deforms when the module is compressed. Hence, by modifying the cable's stiffness, it is possible to tune the elastic behavior of the entire module. This can be achieved by changing some design parameters, such as the thickness, width, material of the cables, or their pre-stretch, which is defined by the ratio between struts and cables length. All cables have the same length and, if shortened, they become more stretched during the assembly (when the length of the strut is kept constant) and result in a stiffer module.

As validation of modules stiffness programmability. Different prototypes with different pre-stretches and thicknesses of the cables have been manufactured and tested. The pre-stretch ranges from less than 1 % up to 30 % (after which the manual assembly becomes difficult) and the thickness from 1mm to 3mm. Every module has been compressed 50% of its height and for every module, a load versus compression curve has been obtained. Figure 13a shows increasing stiffness of the modules with increasing values of pre-stretch at a constant thickness of 1 mm, although there is no sensitive variation over 15%. Figure 13b shows higher stiffness with increasing thickness.

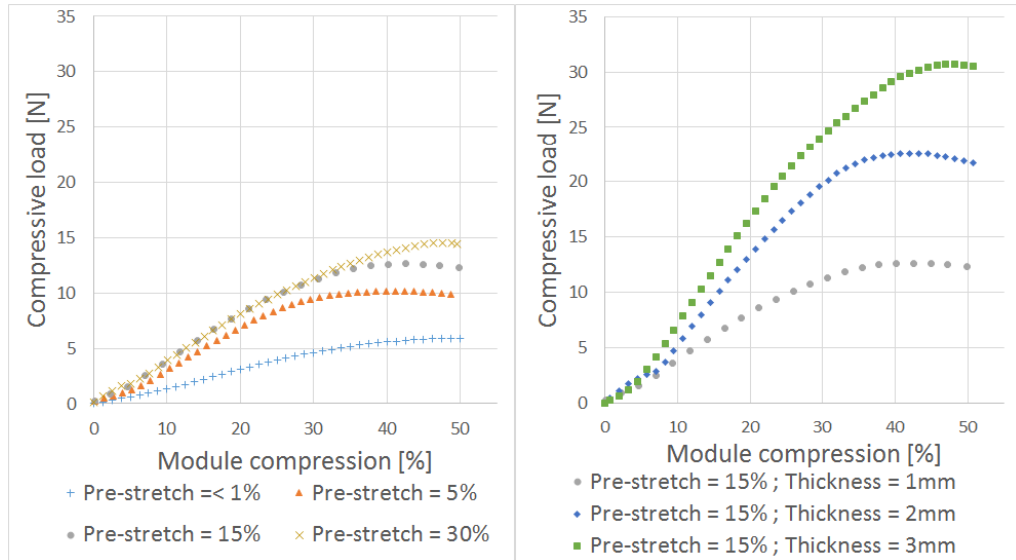


Figure 13. Stiffness programmability of the tensegrity modules.

(a) Compressive load versus module compression of manufactured modules with different pre-stretch and fixed 1mm thickness. The compression tests have been conducted with an Instron universal testing machine. (b) Modules with 15% pre-stretch and different thicknesses.

### 2.2.2 Connectivity

A connection mechanism is required to physically connect modules into a modular robot that can display some functionality. Connection points may also serve as a medium to transmit information and energy throughout the robot. Furthermore, the number and type of connection points in a module may affect the morphology and functionality of the robot. However, at this stage, we use only a simple mechanical latching that allows us to assemble modules into a proof-of-concept locomoting robot.

The mechanical latching system connects vertices and faces of different modules. The system is integrated into the flat cable's network configuration and therefore manufactured with all the other cables during the 3D printing process (see Figure 14a). The system consists of a pin and a hole at every vertex. The pin has a slightly larger diameter than the hole and when forced into it, it remains thanks to the friction between the lateral walls of the pin and hole. An opposite pressure is required to detach them. The pin and hole can be inserted inside one another when the vertex is not connected to another vertex (see Fig 14b-c) or can be latched to another vertex with each pin inserted in the hole of the other vertex (see Fig. 14d). Two triangular faces of two modules can be connected latching their 6 vertices in 3 pairs (see Fig. 14e).

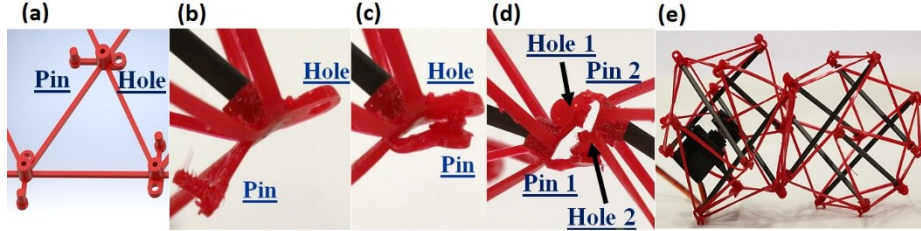


Figure 14. The latching-based connection system.

(a) Integration of the latching system in the cable's network. (b) Pin and hole of a vertex disconnected. (c) Pin and hole of a vertex connected. (d) Pin and hole of a vertex connected to another vertex. (e) Two triangular faces are connected through their 6 vertices.

## 2.3 Tendon-Driven Actuation

An actuation mechanism can be added to a module to control its deformation along the desired direction. In our case, we chose to actuate one of the four collapsibility directions to introduce a controlled compression of the module.

In this study, we propose to use a tendon-driven contractive system operated by a servo-motor. Although the servo-motor is a rigid component that can reduce the overall softness of the system [82] and the volume reduction in the fully collapsed state, the chosen motor has a small volume (5 cm<sup>3</sup>) compared to that of the module (248 cm<sup>3</sup>). The servo is strategically placed in a modified strut with rectangular housing. This design avoids rigid connections between two struts and the rigid servomotor and preserves the tensegrity nature of the structure and its deformability [83].

The tendon-driven actuation contracts the icosahedron tensegrity by simultaneously pulling two opposite triangular faces towards the geometrical center of the structure along the collapsibility direction (see Figure 15 a). The contractive mechanism comprises six tendons that connect each vertex of the selected triangular faces to a pulley that is activated by a servo-motor (see Figure 15 b). The pulley is placed at the geometrical center of the icosahedron structure (see Figure 15 b). When the servo is activated, the pulley starts to rotate wrapping the tendons, which in turn produces a contraction of the icosahedron (see Figure 15 c).

The six-tendon design can be directly included in the design process of the module's elastic network. The six tendons have one end attached to the vertices of the triangular faces and the other end free (see Figure 15 d-e).

The kinematic tests of the actuated module show that compression of about 25 % (the negative pick at about 3.5 seconds in Figure 15g) and a lateral diameter expansion of 9 % of the module height can be achieved. Improved design or different actuation technologies could further increase the contraction of the module if required.

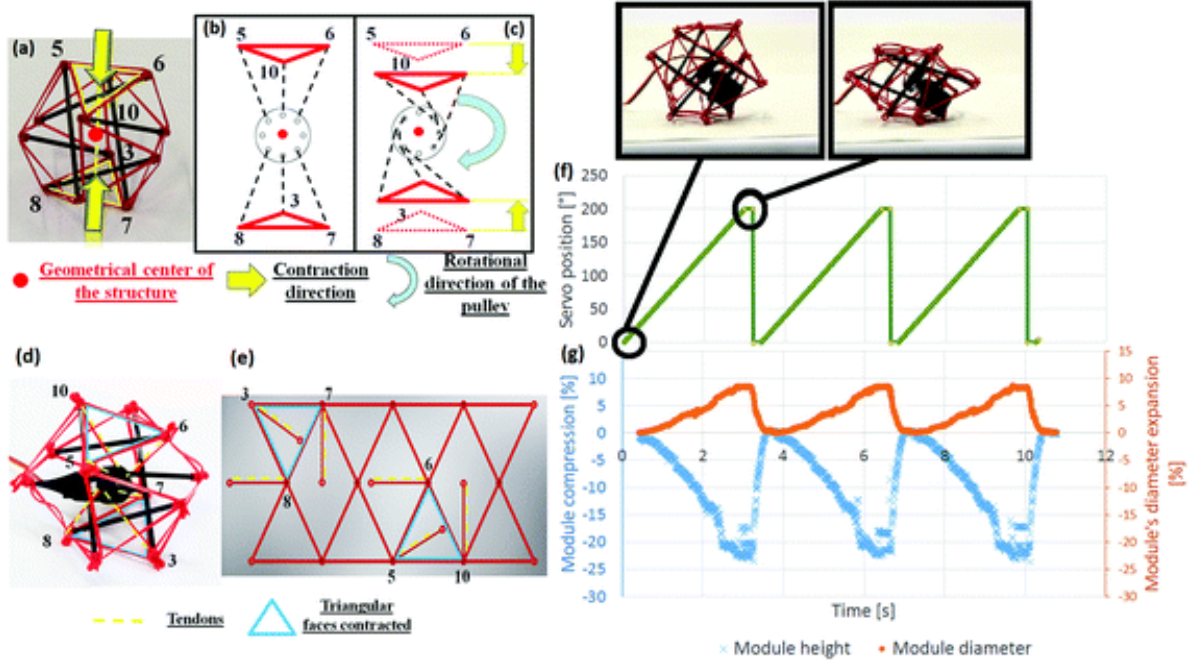


Figure 15. The tendon-driven actuation system for a tensegrity module with controlled compression.

(a) The arrows represent the contractive directions of the two triangular faces marked in yellow. While the red dot represents the geometrical center of the tensegrity structure toward which the two faces are contracted. (b) The six dashed lines represent the six tendons connecting the two triangular faces to the pulley placed at the geometrical center of the structure. (c) When the pulley is rotated, the six tendons are all pulled at the same time contracting the two triangular faces. (d) The assembled module with marked in dashed yellow lines the six tendons connecting the 6 vertices of the two opposite triangular faces (marked in blue) to the pulley in the geometrical center of the structure. (e) The unfolded network with the tendons. (f) Graph of the servo position driving signal generated by an Arduino Uno. (g) Corresponding graph of the module compression and lateral expansion recorder through motion capture system (i.e. Optitrack system recording at 240 Hz).

## 2.4 A proof-of-concept Crawling Modular Tensegrity Robot

We exploited the specific kinematic of the actuated module (i.e. lateral expansion when compressed) to develop a simple crawling modular robot using peristaltic locomotion as a proof-of-concept. The robot is composed of 3 actuated modules connected along the actuated axes with mechanical latching. The three modules are controlled with an external Arduino Uno board using three different signals (Figure 16a). A driving signal controls the contraction and expansion of a module along the actuated axis. At each step cycle, the three modules contract in sequence from left to right (see Figure 16a) and then expand very rapidly with the same order, thus producing contraction waves used in peristaltic locomotion [84]. This actuation pattern with different speeds in contraction and expansion generates directional friction on the ground which allows the assembly to move forward. The worm's head position has been tracked through a motion capture system and the result (Figure 16b) shows a travel distance of about 15 mm per cycle and a speed of 90cm/min. This speed could be further improved by adding directional patterning to the ventral surface of the robot.

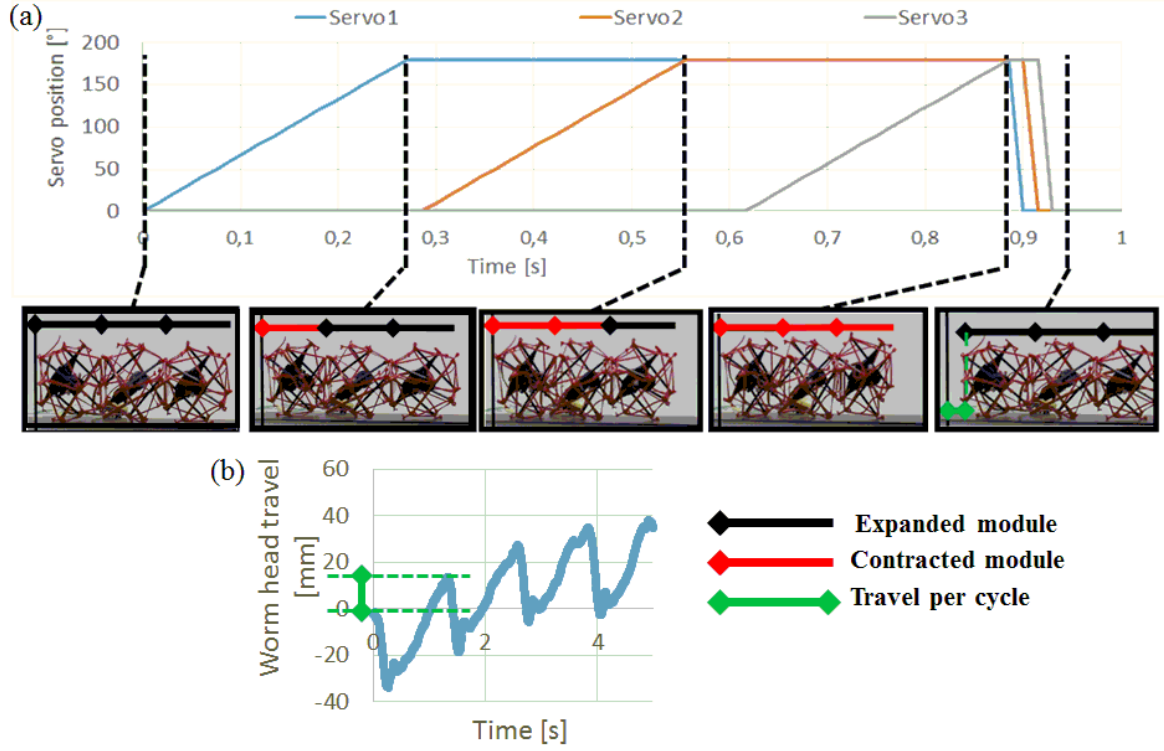


Figure 16. A proof-of-concept modular tensegrity locomoting robot.

(a) Contraction snapshots sequence of a peristaltic movement cycle compared with the servo position driving signal given by the Arduino board. (b) Graph of the worm's head movement in the longitudinal direction. Every cycle the worm moves forward of about 6.5 mm.

## 2.5 Discussion

In this chapter, we presented a bio-inspired design principle for designing tensegrity soft modular robots. Although the proposed design with an individual module displays many desirable features that could lead to the assembly of a variety of more complex robots with a diverse set of behaviors, other tensegrity modules with specialized functions can be included, such as modules with processing, power storage, and variable stiffness capabilities. Some of these modules will be presented in the next chapters.

The current system allows only the assembly of tethered robotic applications and requires a connection system that provides more functionalities than simple mechanical latching for untethered solutions. A novel connection strategy to solve this limitation is proposed in the following chapter three.

In this chapter, actuated tensegrity modules are intuitively assembled to develop a proof-of-concept locomoting robot, however, optimization algorithms coupled with a Tensegrity simulation tool, such as the NASA Tensegrity Robotics toolkit [72], can be used to find task-optimal morphologies. In chapter six of this thesis, preliminary results and insights on these methods are presented.

# Chapter 3 A bio-inspired connection strategy for untethered soft modular tensegrity robots

Publication Note: The material presented in this chapter is adapted from:

- D. Zappetti, W. J. Stewart., M. Boutot, and D. Floreano, «*Unleashing Soft Modular Robots by means of a Bio-inspired Connection Strategy*», *Robotic and Automation Letters* under review (2021)

The first author contribution was to conceptualize, assemble and characterize tensegrity modules and one robotic application, to analyse the results and to write the manuscript.

In this chapter, we present a new bio-inspired inter-module connection strategy that connects tensegrity modules mechanically and electrically. We show that our strategy allows connected modules to retain stiffness in the same order of magnitude as individual modules while providing low electrical resistance for passing energy and communication signals among modules. To demonstrate the connection strategy we developed a kit of four different tensegrity modules expanding the individual type of module kit presented in chapter two. Finally, we demonstrate the connection strategy with two proofs-of-concept untethered soft modular tensegrity robots: a gripper capable of holding two times its body weight and grasp objects of different shapes and a crawler that can move up to 4.5cm/min.

## 3.1 Introduction

A tensegrity modular robot can be considered a modular robot with modules that can have different stiffness. In the last decades, researchers have been extensively investigating the idea of modular robots as versatile robotic systems made of simple subunits that can be assembled into task-specific morphologies [85] [86].

Rigid modular robots are capable of untethered movement by using inter-module connection strategies that allow the transfer of mechanical loads as well as power and communication signals between the modules [87]. These strategies involve rigidly connecting the faces of neighboring modules with, mechanical latches [88] or magnets [89] to transfer mechanical loads and electrical plugs [88] [89] to transfer communication signals and power. Being untethered frees modular robots to navigate complex environments without risking entanglements with obstacles. Moreover, the presence of external tethers from each module can limit the set of possible connections among modules and, therefore, the set of potential morphologies [87].

Inspired by multi-cellular biological systems, researchers have recently investigated other approaches to develop modular robots composed of soft modules [90]. These soft modular robots provide safer interaction with the environment and span a larger morpho-functional space [91]. However, current soft modular robots make use of connection strategies between their modules that only transfer mechanical loads [91] [92] [93] [94] [95] [96] [97] [98] or have an electrical resistance that is too high to allow efficient power and communication transmission [99] [100] [101]. An alternative approach uses wireless communication [102]. However, this approach requires that every module with active components is equipped with a receiver, a sender, and a power supply that can increase weight and reduce the softness of the modules.

In this study, we aim at developing a novel connection strategy compatible with a generic soft modular system and we demonstrate it on our soft modular tensegrity platform.

Inspired by adherens junctions in soft pluricellular organisms, such as invertebrates and vertebrates' soft tissues, we propose a novel junctions connection strategy to not only transfer mechanical loads but also efficiently transfer power and communication signals using off-the-shelf copper wiring with low electrical resistance (i.e.,  $< 1\Omega$ ). Moreover, our strategy preserves the high deformability of the soft modules after being connected.

The rest of the chapter is organized as follows: in section 3.2, the *adherens junctions*, and the bio-inspired *junctions connection strategy* for soft modular robots are presented. A hardware implementation of the connectors is also described. Section 3.3 describes the implementation of the connection strategy in a soft modular tensegrity robot platform and the results of the mechanical and electrical characterization of connected pairs of modules. In section 3.4, two untethered soft modular robots: a soft robotic gripper and a soft crawling robot- are presented to demonstrate the potential of the proposed connection strategy.

## 3.2 Bio-inspired ball-joints connection strategy

In pluricellular organisms, cells in soft tissues are anchored to one another to transfer mechanical loads as well as to exchange energy and communication signals [103]. While connected, each cell preserves its softness and ability to deform.

To achieve this, soft cells have evolved points of contact, called *adherens junctions*, distributed on their external membranes (Figure 17a). These junctions consist of filiform cadherins proteins from each cell (Figure 17b). Because they occupy only a small part of the external surface of the cell and are filiform structures that can easily bend, the adherens junctions do not hinder the overall ability of the joined cells to deform [103].

There are two main types of specialized cadherins [103]. The first type is specialized in transferring mechanical loads. Being slender filiform structures, they only constraint relative translations between two membrane points while allowing relative rotations and can therefore be modeled as ball-joint constraints (Figure 17c) [104]. The second type of cadherins is specialized in transferring electrochemical energy and communication signals without hindering relative rotations between two membrane points. This type of cadherin can be modeled as a slack electrical conductive cable running in parallel to the ball-joint constraint (Figure 17c) [104].

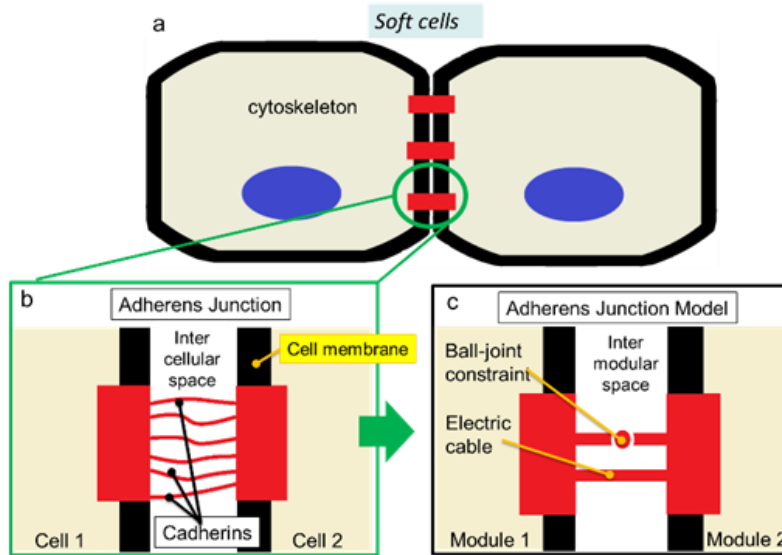


Figure 17. The Adherens Junctions in multi-cellular biological systems.

(a) A sketch of two living cells connected by adherens junctions. In red are three adherens junctions connecting the cell membranes (in black). In blue are the nuclei of the cells. (b) Zoomed in the depiction of an individual adherens junction. In red the filiform cadherins proteins lie in the intercellular space and comprise the junction (c) Sketch of a mechanical and electrical model of the adherens junction. The junction (in red) can be modeled as a ball-joint constraint and an electric cable with zero bending stiffness in parallel.

The *junctions connection strategy* for soft modular robots consists of anchored pairs of points on the external membranes of neighboring soft modules (Figure 18a). As with the biological counterparts, the novel *junction connector* is composed of two different cables. The first cable is stiff and short. It acts as a ball-joint constraint allowing the transfer of mechanical loads between modules. The second cable is a conductive electrical cable with low bending stiffness and low electrical resistance that allows the transfer of power and communication signals between the soft modules (Figure 18b and d). A male/female plug attachment system on both cables enables the modules to be connected and disconnected (Figure 18b and d).

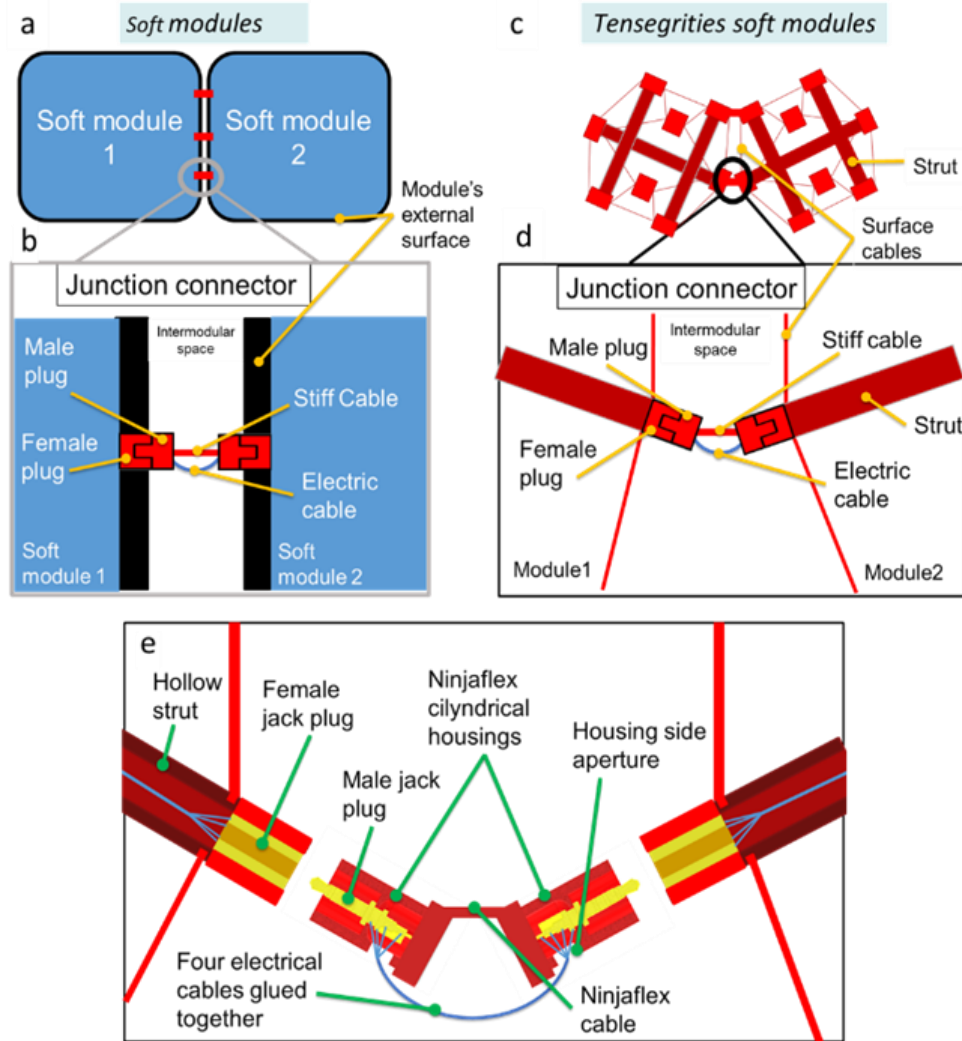


Figure 18. Bio-inspired junction connector for soft modular tensegrity robots.

(a) Schematic representation of two generic soft modules with a membrane in black and connectors in red. (b) Zoomed in section of the junction connector inspired by biological adherens junctions, in red the plug male-female system and the stiff cable, in light blue the electrically conductive cable. (c) Schematics of two soft tensegrity modules connected at their struts vertices. (d) Zoomed in section of a junction connector connecting two tensegrity soft module vertices. (e) Detailed section of a hardware implementation of a junction connector. In yellow the male-female jack plug system, in light blue electric cables connecting the two jack male plugs, and in red structures 3D-printed in ninjaflex.

According to classical mechanics (*chains law*) [105] and its application on *soft kinematic chains* [106], for two three-dimensional modules to be considered connected, it is required that one or more connectors constrain all three relative rotations and all three relative translations between the modules at mechanical equilibrium [105]. Individual ball-joint constraint constrains three relative translations but still allows three relative rotations, while two ball-joint constraints would still allow one relative rotation between the modules, thus three ball joints are required to fully constrain two modules [106].

### 3.3 Implementation of the junctions connection strategy

We implemented the *junctions connection strategy* on a soft modular robotic kit composed of tensegrity modules with two morphologies (Figure 19c-d). Each tensegrity module is composed of rigid struts enveloped in a flexible network of elastic cables (Figure 19) [15]. The two types of tensegrity structures used as modules in this work are an icosahedron structure from chapters 2 and 3 and a novel three-box-prism module developed as part of this work (Figure 19 a-b). The icosahedron tensegrity module is composed of six struts and 24 cables. It has eight triangular faces all around its external surface (Figure 19a). Its face to face distance is about 10cm, and each strut has an approximate length of 9cm from vertex to vertex. The three-box-prism module is composed of three planar box tensegrity submodules [11] measuring 10cmx3.5cm (Figure 19b).

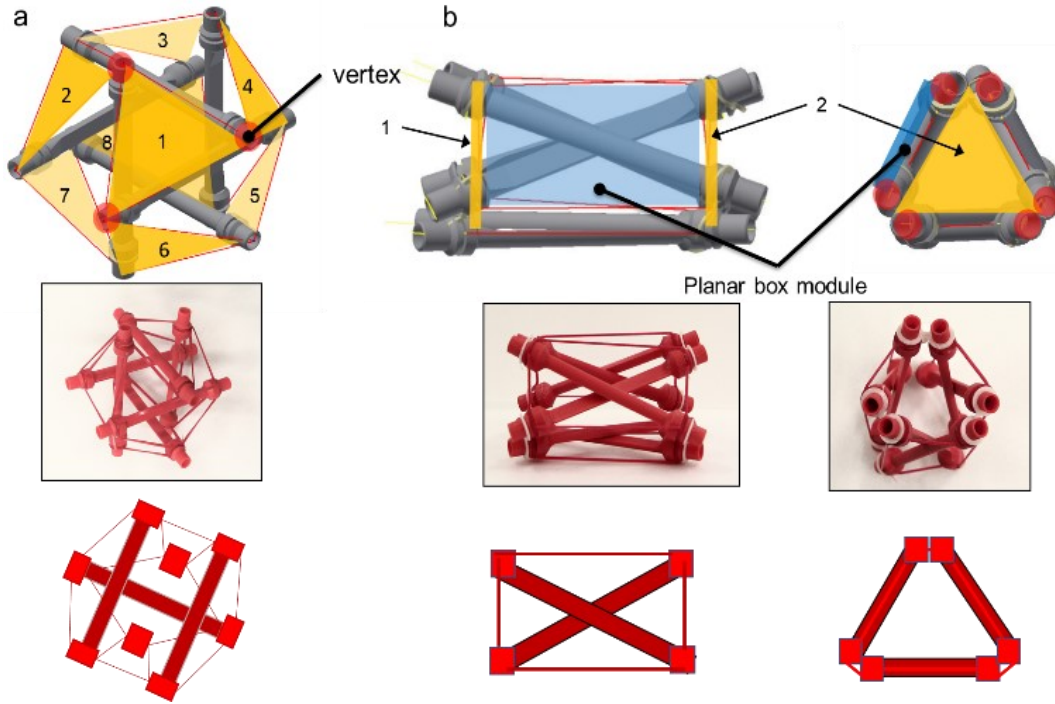


Figure 19. The two modules morphology tensegrity kit.

(a) Schematic representation of an icosahedron tensegrity module. The eight triangular faces displayed on the external surface are highlighted in yellow. Three circular red dots highlight the three vertices of one of the faces. Below, a photograph of one icosahedron module and its schematic representation used in the results section of the chapter. (b) Schematic representation of a three-box tensegrity module in side view on left and front view on the right. The two triangular faces displayed on the external surface are highlighted in yellow. One of the rectangular surfaces is highlighted in light blue. Circular red dots highlight the six vertices of one of the faces. Below, a photograph of one of the modules and its schematic representation used in the result section of the chapter.

The three planar box submodules are connected together along their longer side into a three-dimensional tensegrity prism (Figure 19b). The three-box-prism module is composed of six struts and 12 cables. It displays two opposite symmetric triangular faces on the external surface with the same dimensions as the icosahedron modules. Each soft module can be connected by means of three *junction connectors*, one at each corner of one of its triangular faces.

Each *junction connector* is composed of two cables and an off-the-shelf male-female jack plug connection system (Digikey - diameter 2.5mm) (Figure 18e). The stiff cable that transfers mechanical loads is 3D printed in ninjaflex with sufficiently large dimensions (2.5mmX2.5mm and length of 5mm) to exhibit around ten times the stiffness of the individual tensegrity module cables (31kN/m vs. 3kN/m). The stiff cable is 3D printed in a single print together with two cylindrical housings, one at each end of the cable. These housings contain the two male jack plugs (Figure 18e). The bendable electrically conductive cable is composed of four low gage, and low electrical resistance wires glued together and soldered to the male jack plugs.

These cables pass through openings on the side of the cylindrical housings. The female part of the jack plug system is glued to the tips of the vertices on the external surface of the tensegrity modules (Figure 18e).

To validate that our strategy does not reduce the deformability of the modular robot, we performed a set of experiments where we compared the deformability of individual modules with the deformability of pairs of connected modules. We compressed individual modules, pairs of identical modules, and pairs of mixed types of modules in different directions (Table 1). The deformations of individual modules were then compared with pairs of connected modules in compressions to assess how the connections affect deformability. During the experiments involving two connected modules, the electrical resistance of the connection was recorded to assess if an efficient transfer of energy and communication signals (i.e., low average electrical resistance) can be assured throughout the entire range of deformation.

### 3.3.1 Results

Table 1. Set of experiments and results for validating the novel connection system.

	Tested structure	Control parameter: Deformation of 50% length in the load direction	Measured parameters	Measured max Load [N]	Measured resistance [mΩ]
1	Individual icosahedron	Side compression 5 cm	Load	7	
2	Two connected icosahedron modules	Longitudinal compression 5 cm	Load + electrical resistance	7	10.2 ( $\sigma \pm 1.4$ )
3	Individual icosahedron	Side compression 5 cm	Load	7	
4	Two connected icosahedron modules	Side compression 5 cm	Load + electrical resistance	13.8	8.7 ( $\sigma \pm 1.7$ )
5	Individual three-box-prism module	Side compression 2.5 cm	Load	5.2	
6	Two three-box-prism connected	Side compression 2.5 cm	Load + electrical resistance	10.9	9.8 ( $\sigma \pm 1.7$ )
7	Individual three-box-prism module	Longitudinal compression 5 cm	Load	38	
8	Two three-box-prism connected	Longitudinal to the connection 10 cm	Load + electrical resistance	38	11.3 ( $\sigma \pm 1.8$ )
9	Mixed two modules connected	Longitudinal to the connection 10 cm	Load + electrical resistance	29	9.4 ( $\sigma \pm 0.4$ )
10	Mixed two modules connected	Side compression 2.5 cm	Load + electrical resistance	14	9.7 ( $\sigma \pm 0.3$ )

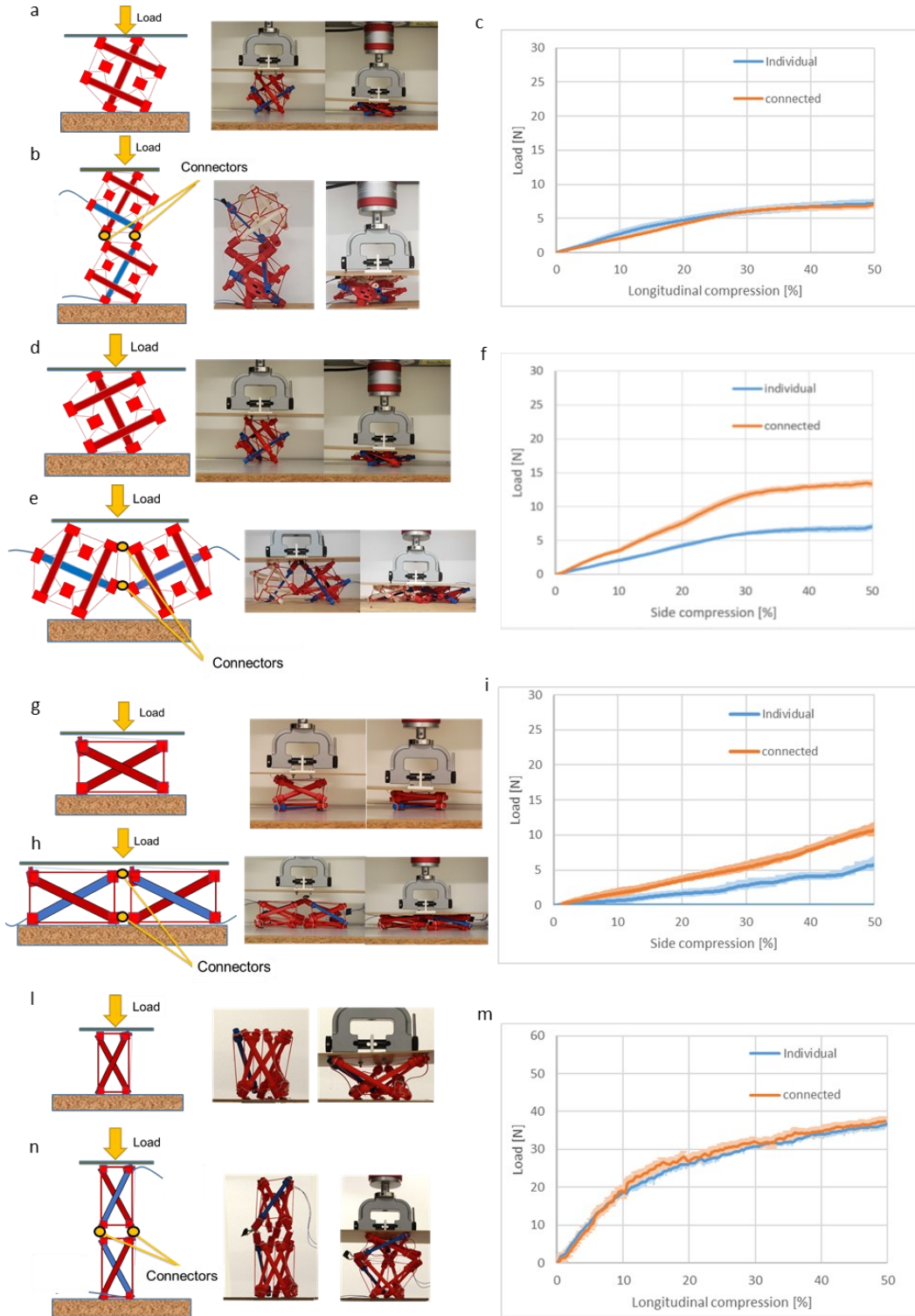


Figure 20. Experimental results of experiments 1-8.

(a, b, d, e, g, h, l, n) On the left, diagrams of the specimens and experimental setup used in experiments 1 through 8; on the right photographs of the modules during experiment at rest and at 50% compression. In blue are represented the struts that contain the electric cables to pass communication and energy throughout the module; while the yellow dots represent the junction connectors to connect pairs of modules. (c) Comparison of experiment 1 and 2: individual vs two connected icosahedron modules compressed longitudinally. (f) Comparison of experiment 2 and 4: individual vs two connected icosahedron modules compressed from the side. (i) Comparison of experiment 5 and 6: individual vs two connected three-box-prism modules compressed from the side. (m) Comparison of experiment 7 and 8: individual vs connected two three-box-prism modules compressed longitudinally.

In each experiment, the tested specimen was compressed to 50% of its length in the tested direction. Each experiment was repeated three times. An Arduino board was used to read and record electrical resistance during each experiment involving

pairs of connected modules. The average resistance and a range of the minimum and maximum resistance recorded in the experiments are then presented.

The results of experiments with connected modules show that pairs of two connected modules of the same type require the same load as an individual module when compressed longitudinally (Figure 20 b-c and n-m) and approximately, double the load when compressed laterally (Figure 20 e-f and h-i). These results are in line with the equivalent springs law [105], where two identical modules compressed laterally behave as two identical springs in parallel and require double the load to compress 50% of their length, and two identical modules compressed longitudinally behave as two identical springs in series and require the same load to compress 50% of their length. Moreover, experiments 1-8 show an average electrical resistance of 10m $\Omega$ , a minimum of 8,6 m $\Omega$  and a maximum of 12,5m $\Omega$  throughout the entire range of deformation, showing that a stable and efficient electrical communication and power exchange can be maintained.

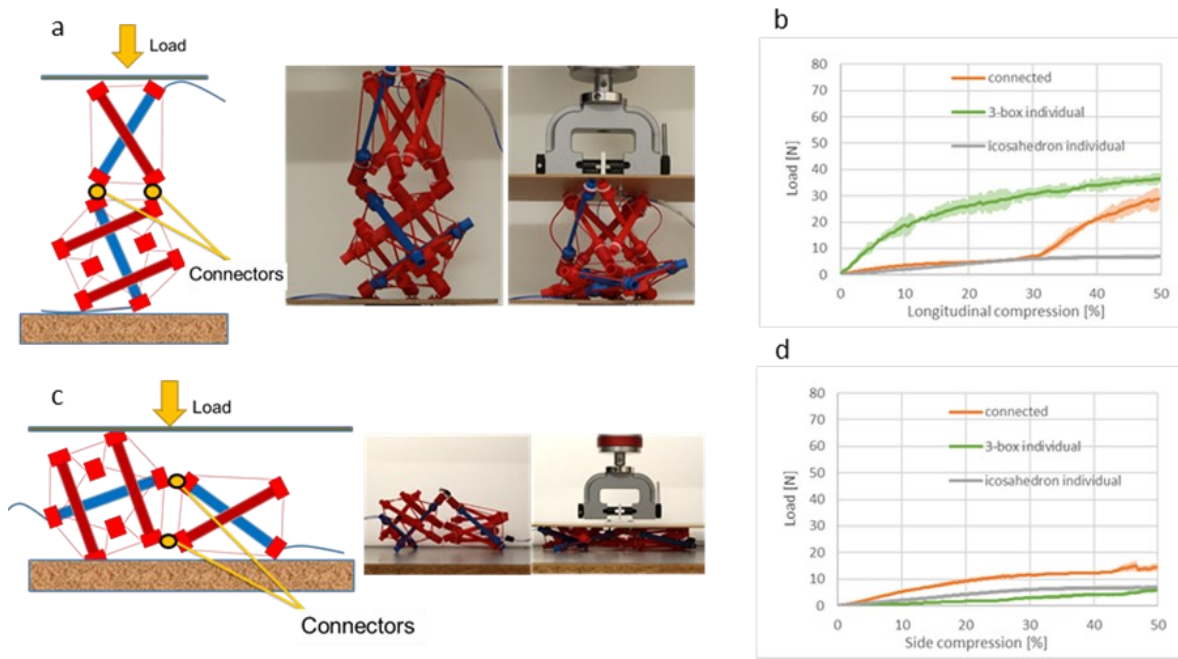


Figure 21. Experimental results of experiments 9-10.

(a,c) On the left, sketches of the specimens and experimental setup used in experiments 9 and 10; on the right photographs of the prototypes during the experiment at rest and at 50% compression. In blue are represented the struts that contain the electric cables to pass communication and energy throughout the module; while, the yellow dots represent the junction connectors to connect pairs of modules. (b) Comparison of experiments 1, 6, and 8: individual icosahedron, individual three-box-prism, and the two connected together and compressed longitudinally vs connected two icosahedron modules compressed longitudinally. (d) Comparison of experiments 1, 4, and 9: individual icosahedron, individual three-box-prism vs the two connected and compressed from the side.

The results of experiments 9-10 show that pairs of two different types of connected modules require a higher load when compressed laterally than for identical modules (Figure 21c-d) and a lower load when compressed longitudinally (Figure 21a-b). This result can be explained by the fact that when two different modules are compressed longitudinally, the softer module compresses more than 50%, reducing the overall stiffness. Moreover, experiments 8-9 show an average electrical resistance of 9,5m $\Omega$  a minimum of 8,7 m $\Omega$ , and a maximum of 9,9m $\Omega$  throughout the entire range of deformation, validating that an efficient electrical communication and power exchange can also be established among mixed pairs of connected modules. The manual soldering of the copper cables to the jack connectors explains the small difference in average electrical resistance among the two sets of experiments.

### 3.4 Soft modular untethered tensegrity robot demonstrators

Two robotic demonstrators have been developed to demonstrate the potential of the novel soft connection strategy: a soft untethered gripper and a soft untethered crawling robot. The two robots were assembled using a kit of four different tensegrity modules. The kit consists of two types of icosahedron modules: a passive module with no additional components

inside (Figure 22a) and a brain module equipped with a microcontroller and battery (Figure 22b). The kit also includes two types of three-box-prism modules: a passive module with no additional components inside (Figure 22c) and a bending module equipped with an actuation system (Figure 22d). These electronic components do not hinder the modules' deformability because they are attached to the rigid struts [38].

The functionalized icosahedron has a TinyZero basic kit (TinyDuino) attached to one strut (Figure 22b). The TinyZero kit consists of a 3cmx3cm controller, two motor controller boards, and a battery (Figure 22b). The functionalized three-box-prism bending module has an actuation system consisting of a motor with pulley (Pololu, torque 2.6N/m) attached to one of its struts, and a tendon, running parallel to one of its edges, to control bending motion (Figure 22e).

The gripper consists of two fingers and was assembled using a brain module, four bending modules (two for each finger), and 18 *junction connectors* (Figure 22f). The gripper is controlled with a simple control signal which closes the two fingers by bending the four bending modules at the same time towards each other and opens the fingers after a set time when the microcontroller cuts off the current (Figure 22f). The two bending module vertices closest to the grasping point are equipped with two small 3D printed ninjaflex fingertips to increase the friction with the grasped object. The gripper is able to successfully grasp and hold up to two times its body weight and different object shapes (Figure 22h). Mechanical deformation tests were performed on the robot using the same test setup as in section 3.3. These tests showed that the gripper deforms to 50% of its height with a maximum of 10N around 30% compression (Figure 22g).

The crawling robot was built using a brain module, a passive icosahedron module, a passive three-box-prism module, two bending modules, and 12 *junction connectors* (Figure 22i). The crawling robot is controlled with an oscillatory control signal at 0.5Hz frequency that deflects the two bending modules in the same direction pushing against the ground (Figure 22i). The vertices that push on the terrain have been equipped with the same ninjaflex pads used for the gripper fingertips to increase friction with the ground. The robot is able to achieve a speed of 4.5cm/min (Figure 22m) and is deformed to 50% of its height with 35N (Figure 22l). These results show that it is possible to use the connection strategy to assemble soft untethered tensegrity modular robots.

### 3.5 Discussion

This chapter has presented and demonstrated a novel bio-inspired connection strategy for developing untethered soft modular tensegrity robots. The results show that the connection strategy allows the transfer of mechanical loads as well as enables an efficient transfer of power and communication signals without hindering deformability of the individual modules.

We demonstrated the connection strategy on a tensegrity soft modular system of type two [11]. In the robots developed here, the junction connector connected vertices of rigid struts from neighboring modules together. However, if tensegrity soft modular systems are developed as type-one structures or the connection strategy is applied on other types of soft modular systems, there may be no vertices where to attach the female parts of the connectors. In these cases, the female parts of the junction connectors can be incorporated into membranes or attached to elastic cables with 3d-printed housings on the external surface.

The junction connectors used in this project could be further improved by replacing the electrical cables with CANbus cables that can carry a significantly higher number of independent signal channels, thereby increasing the maximum number of modules in a robot. Moreover, in the future, the advancement of multi-material 3D printing [107] could allow the printing of the stiff cable, conductive cables, and the plug system at the same time in a unique component, making faster the manufacturing and more replicable the contact resistances given by manual soldering.

We believe that the results presented in this chapter demonstrate the potential that the junctions connection strategy has to be used in the future development of untethered soft modular tensegrity platforms and paves the way to foster research in the growing field of soft modular robotics.

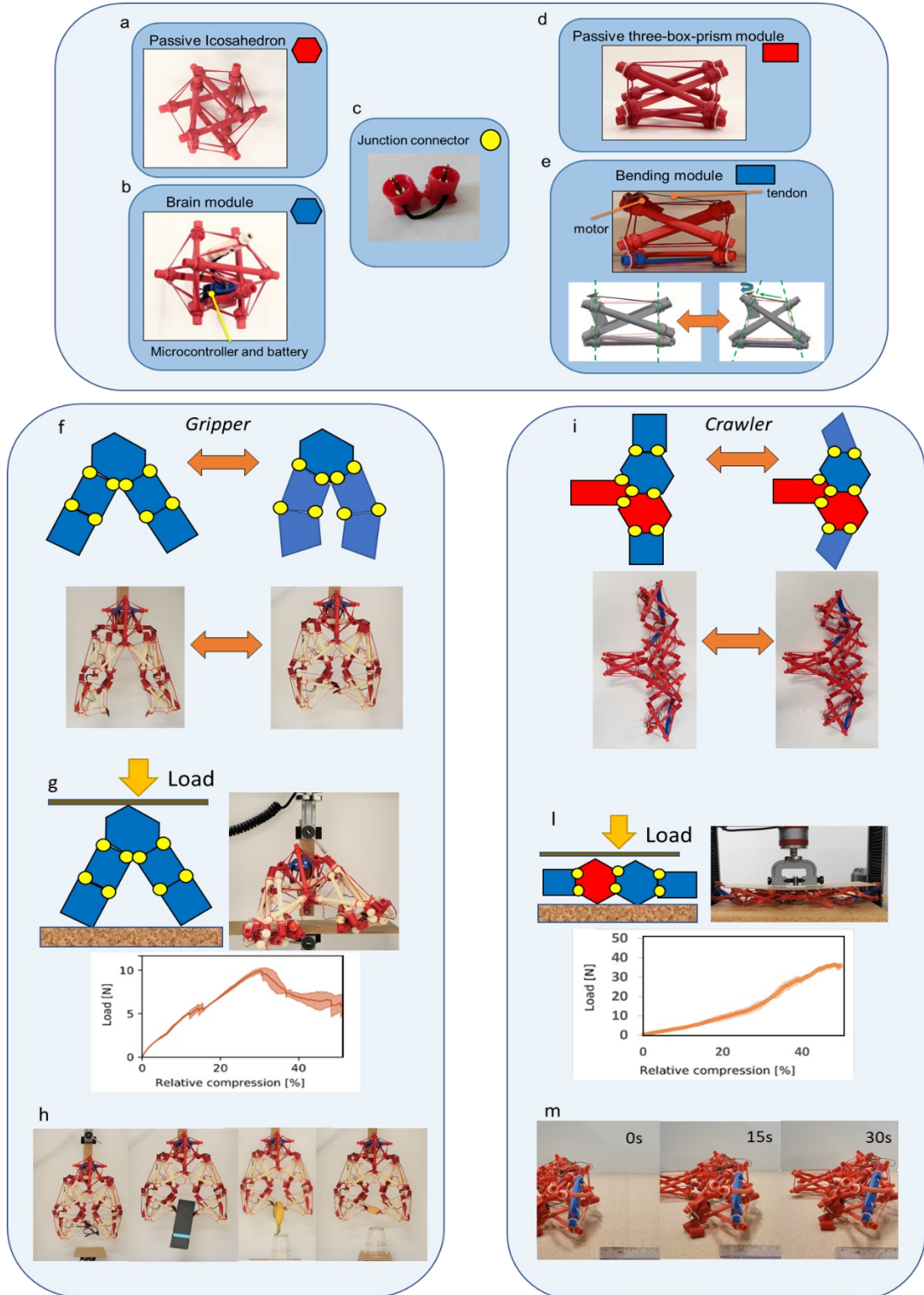


Figure 22. The modular tensegrity kit and the two soft untethered robotic demonstrators.

(a-e) Representation of the soft modular kit developed to demonstrate the connection strategy. (a) The passive icosahedron. (b) The brain module. (c) A junction connector. (d) The passive three-box-prism. (e) The bending module. At the bottom a sketch to show its deformation when actuated. (f) Schematic representation and photographs of the robotic gripper. On the left, the gripper in its configuration at rest, on the right, after closing its fingers. (g) Schematic representation of the experimental setup to test mechanical deformations of the gripper. On the right a photograph of the experiment. At the bottom the load-strain graph of the gripper. (h) Examples of the gripper grasping from left to right, a pair of glasses, a remote controller, a banana and a mandarin. (i) Schematic representation and photographs of the robotic crawler. On the left, the crawler in its configuration at rest, on the right, after it pushed its limbs backwards. (l) Schematic representation of the experimental setup to test mechanical deformations of the crawler. On the right a photograph of the experiment. At the bottom the load-strain graph of the crawler. (m) Sequence of images demonstrating movement of the crawler over time.

# Chapter 4 Design strategies for active stiffness-change of tensegrity modules

Publication Note: The material presented in this chapter is adapted from:

- D. Zappetti, S. H. Jeong, J. Shintake, e D. Floreano, «Phase Changing Materials-Based Variable-Stiffness Tensegrity Structures», *Soft Robotics*, dic. 2019, doi: 10.1089/soro.2019.0091 [120].
- D. Zappetti, R. Arandes, E. Ajanic, e D. Floreano, «Variable-stiffness tensegrity spine», *Smart Mater. Struct.*, 2020, doi: 10.1088/1361-665X/ab87e0 [121].

For the first publication, the first author contribution was to conceptualize, assemble and characterize tensegrity modules and the robotic applications, to analyse the results and to write the manuscript.

For the second publication, the first author contribution was to conceptualize, and characterize the the robotic applications, to analyse the results and to write the manuscript.

In the previous chapters, soft modular tensegrity structures are investigated as a biologically inspired design principle for soft robots. However, as biological evidence suggests, a core challenge of soft robotics research is to develop an integrated approach, where rigid structures and soft structures are merged with variable-stiffness technologies to increase soft robot applications in all types of tasks and environments.

In this chapter, we investigate how to implement variable-stiffness capabilities in tensegrity modules. The strategies discussed in this chapter focus on controllable *active stiffness-change* obtained through activation of smart materials or with bio-inspired type-changing tensegrity structures.

## 4.1 Controllable active stiffness-change through activation of smart materials

As discussed in chapter one, only a few examples of tensegrity structures with variable stiffness exist in literature. However, they display relatively small stiffness change (i.e. by a factor of 3) or resort to multiple and bulky actuators. In this section, we describe a novel design approach to variable-stiffness tensegrity structures (VSTSs) that relies on the use of variable-stiffness cables (VSCs). In the following sections, we describe the design and characterization in simulation and hardware of LMPA-based VSCs within a 3-strut tensegrity module (Figure 23a). We then validate the novel capabilities of the proposed concept in three demonstration scenarios: 1) a two-modules beam with tuneable load-bearing capability (Figure 23b), 2) a

tensegrity module that can self-deploy and lock its shape in both deployed and undepleted states (Figure 23c), and 3) a two-modules joint with underactuated shape deformations (Figure 23d).

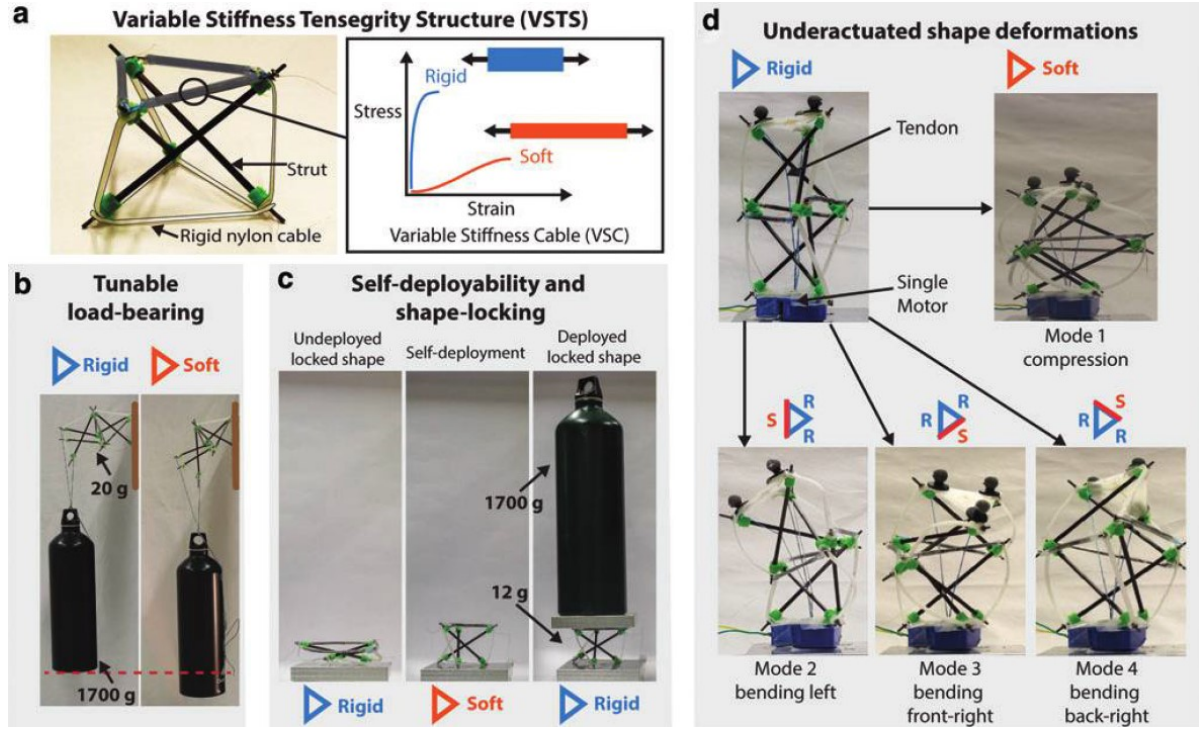


Figure 23. Overview of the active stiffness-change strategy based on LMPA Variable-stiffness cables.

The VSTS design strategy implementing VSCs and the three demonstration scenarios to validate the novel capabilities. (a) A 3-strut tensegrity module structure with LMPA-based VSCs implemented in the upper structure's triangle. (b) A 20 grams VSTS two modules beam is rigidly connected at one end and with a load applied at the other (e.g., the weight of approximately 1.7 kg water-filled bottle). The beam displays tunable load-bearing capability in bending. It can increase globally its stiffness to manipulate the bottle without bending (left) or globally decrease its stiffness to comply (right). (c) A 3-strut VSTS module with the ability to lock its shape in undepleted (left) and depleted configuration (right) by changing its global stiffness. When the VSTS in a locked undepleted shape configuration softens, the structure self-deploys without needing any external actuator. (d) An underactuated VSTS joint and its shape deformations. The VSTS joint can compress or bend in three different directions using only one actuator after changing the stiffness of all three VSCs simultaneously (top right) or one at a time (bottom).

#### 4.1.1 Methods

##### VSTS design and model

The design strategy consists of replacing cables of a tensegrity structure with VSCs. We make use of the NASA Tensegrity Robotics Toolkit (NTRT) [72] to predict how one or more VSCs affect the tensegrity structure stiffness. The NTRT uses the BulletPhysics Engine (version 2.82) mixed with linear complementary problem-solvers for rigid body dynamics. This software has been proven to estimate the rigid body and internal cable dynamics within 1.3% error on position [59]. The internal dynamics of the spring-cable is an implementation of Hooke's law representing a first-order linear approximation of the real response of springs and other elastic bodies. All our simulation experiments are performed in quasi-static load conditions and no damping is applied in the model of the cables' dynamics. The internal dynamics of the spring-cable is an implementation of Hooke's law linear spring.

To assess the effectiveness of the proposed strategy, we use VSCs in a 3-strut tensegrity structure that can function as a module for modular tensegrity robotic kit. The 3-strut tensegrity is one of the simplest three-dimensional tensegrity structures proposed in the literature to create lattices [108]: it consists of 3 struts and 9 cables. We modeled the structure with predefined and fixed stiffness cables as in Figure 24a and we investigated replacement of which cables with VSCs could allow controlling of the structure's stiffness along with selected deformations. In this study, we selected compression and bending as two of the fundamental structures of deformation in mechanical design.

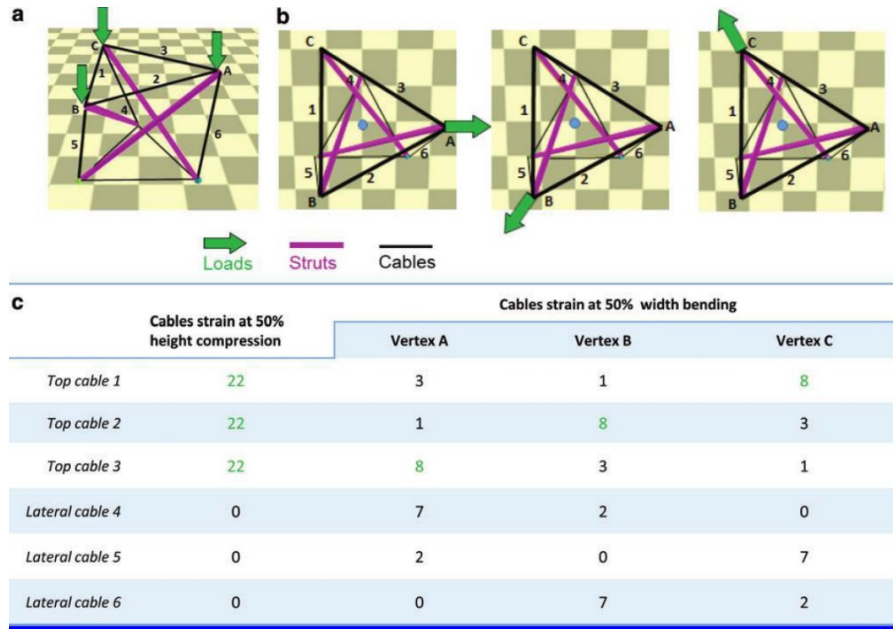


Figure 24. 3-strut tensegrity structure cables analyses.

Cable strain analyses in compression and bending load conditions. (a) Lateral view of the 3-strut tensegrity model under compression load. Compression load is divided in three vertical loads on the three top face vertices. (b) Top view of the three bending load conditions. Bending load is applied to one top face vertex at a time, parallel to the top face and on the direction intersecting the top face geometrical center (indicated with a blue dot in the figure) (c) Table of the six cables strain at 50% deformation in compression and bending. In red-green, the cable/s with highest strain at each loading condition.

## 4.1.2 Results

### 3-strut tensegrity structure with fixed stiffness in compression and bending

In the simulated 3-strut tensegrity structure, struts are modeled as cylinders with 3 mm diameter, 80 mm length, and infinite rigidity, while cables are modeled as springs of 50 mm length with the stiffness of 35000 N/m, which is comparable to the stiffness of a rigid plastic cable, such as nylon. The cable stiffness is calculated as  $EA/L$ , where  $E$  is the Young's modulus of the material,  $A$  the cross-sectional area, and  $L$  is the length of the cable. The structure is attached to the ground by ball joint constraints connected to the bottom vertices and compressive and bending forces are applied to its top vertices to reveal how structural deformations affect cable strain. Due to the ball joint constraints, the three cables on the bottom face are constrained and only six cables strain are recorded (Figure 24a and c). Compression is simulated by applying three equal loads at top vertices (Figure 24a). Bending is simulated by pulling each vertex individually in the direction opposite to intersecting the geometrical center of the structure (Figure 24b). The loads are applied incrementally until the structure compresses up to 50% of its height (i.e., 27.5 mm) and bends up to 50% of its width (i.e., 43.3 mm). The strain of the six passive cables and the overall deformations in compression and bending of the structure are recorded (Figure 24c).

These experiments reveal that the rigid cables on the top face experience the highest strain along with the selected deformations (Figure 24c). These results suggest that providing the tensegrity structure with variable stiffness along with the selected deformations could be sufficient to replace only the rigid cables on the top face with active VSCs, simplifying the realization of the hardware prototype. The resulting structure is a 3-strut tensegrity structure with three active VSCs cables on the top face (

Figure 25a).

### 3-strut VSTS in compression and bending

We added to the 3-strut tensegrity model three Variable-stiffness Cables on the top face. The VSC stiffness is defined as  $S_{VSC} = x \cdot S_r$ , where  $S_r$  is the stiffness of the rigid passive cables and  $x$  is the “stiffness change ratio”. When  $x = 1$ , VSCs and rigid passive cables have same stiffness  $S_{VSC} = S_r = 35000 \text{ N/m}$ , and when  $x = 0.01$   $S_{VSC} = 350 \text{ N/m}$ . We then repeated the compression and bending simulation experiment (

Figure 25a and c) for the two VSC stiffness levels and observed the resulting stiffness of the tensegrity structure, measured as the slope of the load-displacement curves in both compression and bending. To evaluate the stiffness in a linear range, we analyzed the curve in the initial 5% range of the deformation (Figure 3b and 3d).

The results indicate that VSC stiffness change affects the stiffness of the entire tensegrity structure in both compression and bending. When VSCs have the same stiffness as the rigid passive cables (i.e.  $x = 1$ ), the VSTS display an overall stiffness in compression of 27000 N/m; instead, when the VSCs stiffness is reduced 100 times ( $x = 0.01$ ), the VSTS overall stiffness decreases to 490 N/m, displaying a total stiffness change of around 55 times (

Figure 25 b). Similarly, in the case of bending, the stiffness is reduced by a factor of 28 times (

Figure 25 d).

Based on the simulation results, we developed a hardware implementation of the 3-strut VSTS replacing top-triangle 3 cables with VSCs (

Figure 25a and c). We fabricated VSCs using LMPA encapsulated in a silicone tube. Stiffness change is activated by the Joule effect when applying an electrical current. The VSCs are equipped with dedicated connectors for mechanical assembly in VSTS and for applying electric current through them. The fabrication process is described in the SI section. The fabricated VSCs have 50 mm length and 2.5 mm diameter. Their stiffness calculated in their first 5% deformation can change from 347 N/m to 35700 N/m when a current is applied, which corresponds to a stiffness change of approximately 102 times. The VSTS struts are made of carbon rods and the rigid cables are made of 3D printed nylon with a length of 50 mm and a cross-section area of  $1 \text{ mm} \times 0.6 \text{ mm}$ . The dimensions of the rigid nylon cables are selected to have the same length as the VSCs. Moreover, nylon cables cross-section area has been selected such that the rigid cables have approximately the same stiffness as the VSCs in the rigid state: 36000 N/m in rigid nylon cable and 35700 N/m in the VSCs. Therefore, according to equation  $S_{VSC} = x \cdot S_r$ , when VSCs are soft ( $x$  is approximately 0.01) their stiffness is reduced 102 times. The fabricated VSTS was tested in both compression and bending (

Figure 25a and c) with a universal Instron testing machine. The prototype displays a stiffness change of 28 times in compression and 13 times in bending (Figure 3b and 3d). Measured stiffness values in the soft state are in good agreement with the simulation results (error < 5%), while measured stiffness values in the rigid state are around 50% lower than those estimated in simulation (

Figure 25b and d). The main reason is the limited kinematic model used in the simulation to estimate the positions of the vertices and strain of the cables. The implementation of a Hooke’s law linear spring neglects the non-linearity of the VSC stress-strain behavior and its lower stiffness at the beginning of the deformation as shown in Figure 55 in Appendix A. Additional reason may be the presence of defects in the VSCs manufacturing process and 3D printing of the nylon passive cables, such as non-uniformity of the cross-section area along the cable length, which reduce VSTS stiffness.

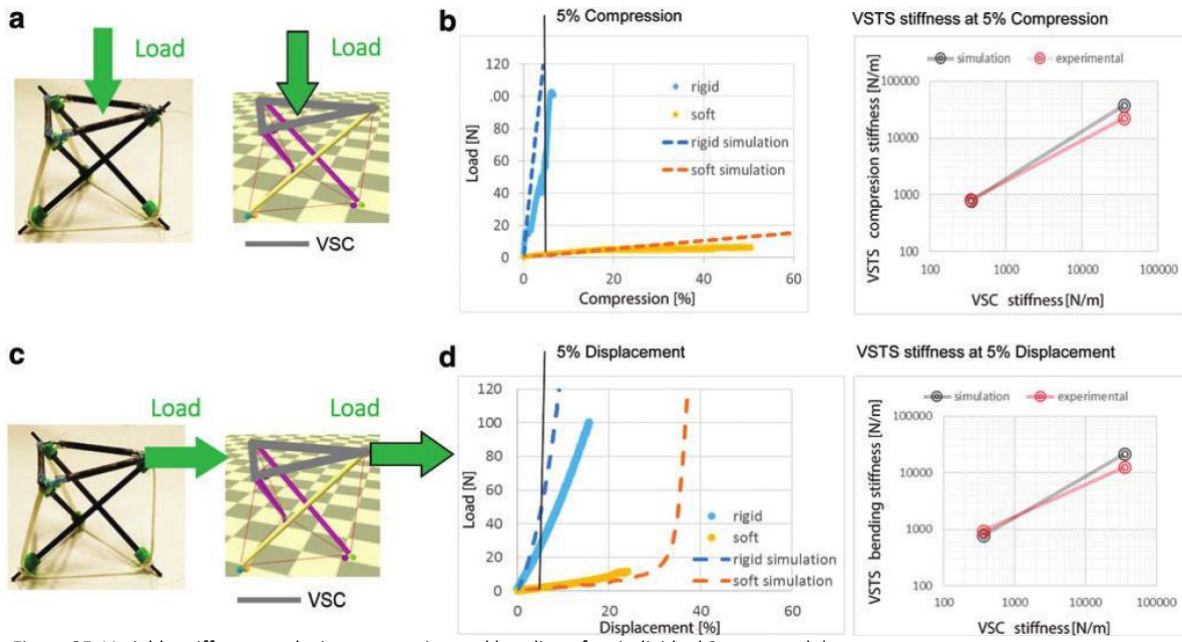


Figure 25. Variable-stiffness results in compression and bending of an individual 3-strut module.

Simulation and experimental results demonstrating stiffness change of a 3-strut VSTS in compression and bending. (a) Schematics of the VSTS under compression. On the left VSTS prototype with three VSCs mounted on the top face. On the right VSTS model in the simulation. (b) On the left load versus percentage of compression curves of the VSTS in both soft and rigid state. Simulation results are represented in dashed lines and experimental results with continuous line. A vertical line representing the 5% deformation defines the upper range used to calculate the stiffness of the overall structure. On the right, relationship between VSCs stiffness and overall stiffness change in compression of the VSTS. (c) Schematics of the VSTS under bending load. On the left VSTS prototype with three VSCs mounted on the top face. On the right VSTS model in the simulation. (d) On the left load versus percentage of lateral displacement curves of the VSTS in both soft and rigid state. Simulation results are represented in dashed lines and experimental results with a continuous line. A vertical line representing the 5% deformation defines the upper range used to calculate the stiffness of the overall structure. On the right, the relationship between VSCs stiffness and overall stiffness change in compression of the VSTS.

### VSTS beam with tuneable load-bearing capability

We designed and manufactured a proof-of-concept VSTS beam composed of two 3-strut modules with tuneable load-bearing capability. (Figure 26a). The cables shared by the two 3-strut stages at their junction were replaced by three VSCs. The VSTS beam was characterized with a universal testing machine in both compression and bending, and the results were compared with the simulations. The change of stiffness was around 26 times in compression and 7 times in bending. The experimental data showed a good agreement (error < 5%) with the simulated one in the soft state, while in the case of the rigid state, the experimental values were around 50% lower than the simulated ones (Figure 26b and d), similarly to the results discussed in the previous section.

In the soft state, the 20-gram VSTS beam bent more than 100% of its width under external force (weight of a 1700-gram bottle corresponding to 85 times its own weight), while in the rigid state it was able to hold the same external load with bending of less than 10% its own width (Figure 23b).

### VSTS with self-deployment and shape locking capabilities

The VSCs can be used to lock a tensegrity structure in different shapes. As an example, when a 3-strut VSTS module (Figure 27a) becomes soft by joule heating, it can be compressed to a flat configuration (Figure 27b) and hold its shape after cooling to room temperature (Figure 27c). Since the extended VSCs cable store strain energy in the stretched silicone tube, when heated again the tensegrity structure can recover its original shape (Figure 27d) and lock in the originally deployed shape after cooling (Figure 27a).

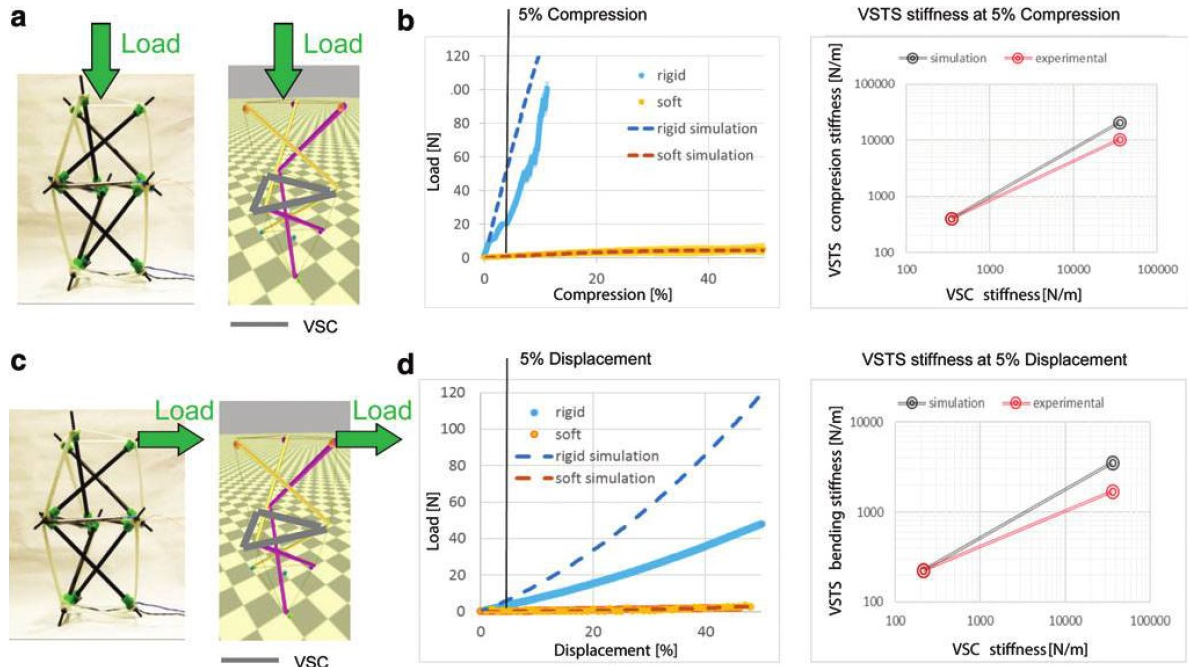


Figure 26. Variable-stiffness results in compression and bending of a two 3-strut modules beam.

(a) Schematics of the VSTS beam under compression. On the left VSTS beam prototype with three VSCs at its stages junction. (b) On the left, load versus percentage of compression curves of the VSTS beam in both soft and rigid states. Simulation results are represented in dashed lines and experimental results with a continuous line. A vertical line representing the 5% deformation defines the range used to calculate the stiffness of the overall structure. On the right, the relationship between VSCs stiffness and overall stiffness change in compression of the VSTS beam. (c) Schematics of the VSTS beam under bending load condition. (d) On the left, load versus percentage of lateral displacement curves of the VSTS in both soft and rigid states. Simulation results are represented in dashed lines and experimental with a continuous line. A vertical line representing the 5% deformation defines the range used to calculate the stiffness of the overall structure. On the right, the relationship between VSCs stiffness and overall stiffness change in bending of the VSTS beam.

The VSTS module shown in Figure 27 weighed 12 grams and in the soft state required 10 N of external load to achieve a compression of 70% of its height (Figure 27 b), which corresponded to a volume reduction of approximately 90%. In deployed state, it could withstand up to 80 N with only 5% compression. The transition time from rigid to soft was around 2.5 minutes by applying 1.5 A at 12 V to heat the VSC at 47°C. Transition time from soft to rigid was around 4 minutes at room temperature. In a first approximation, considering a constant spring coefficient, the strain energy stored in the stretched silicone tubes during compression can be estimated using the elastic potential energy equation of a spring  $U_s = 1/2 kx^2$ , where  $U_s$  is the elastic potential energy,  $k$  is the spring constant and  $x$  is the extension of the tube. The three VSCs in the VSTS have  $k=347$  N/m, and a measured extension of  $x=15$  mm at 70% VSTS compression. The resulting  $U_s$  stored in the undeployed VSTS was 0.117 J. The VSTS displayed in Figure 23 could withstand the weight of a 1700-gram bottle (141 times its own weight) with only 2% compression.

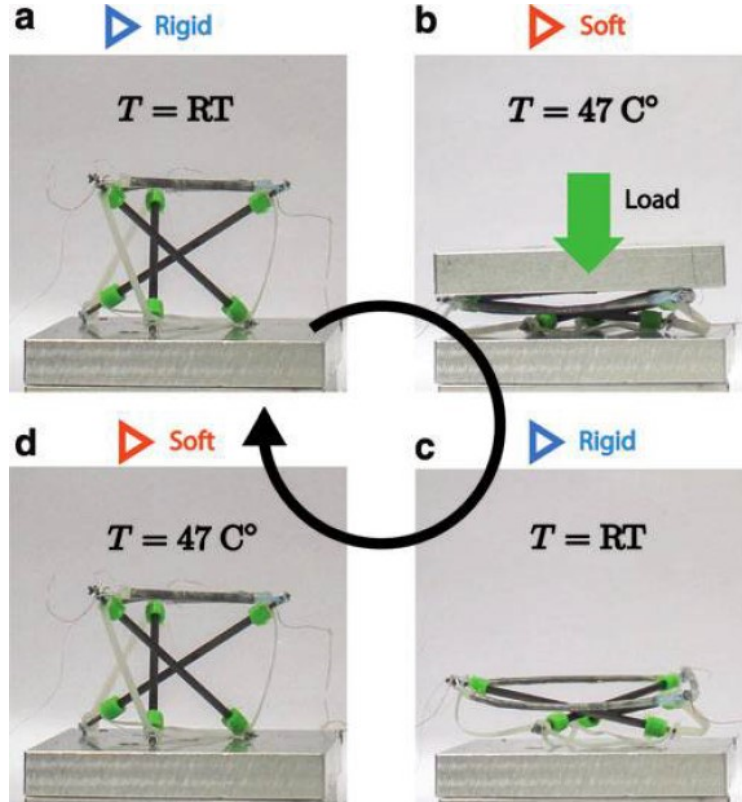


Figure 27. A 3-strut VSTS module with the ability to self-deploy and lock its shape in both deployed and undepleted states.

(a) The VSTS in its deployed shape configuration locked. No electric current is applied to its VSCs and the structure lays at room temperature. (b) The soft VSTS is compressed around 70% of the original height with an external load of around 10N. Electric current is applied to its VSCs which are kept at around 47°C degrees in temperature (c) After removing the electrical current and let the VSCs cool down to room temperature (RT), the external load is removed and the undepleted shape configuration is locked. (d) When the VSCs transition to soft again by temperature increase, the self-deployment of the VSTS occurs by releasing the stored energy in the VSCs.

#### VSTS joint with underactuated shape deformations

The integration of individually controlled VSCs in a tensegrity structure could enable diverse shape deformations. Differential distribution of the same actuation force throughout the tensegrity structure can be obtained by selectively controlling the stiffness of a subset of VSCs. The advantage of this approach to differential deformation of the structure is that it does not require the use of actuators for each deformation direction, which could increase the size and weight of the tensegrity structure.

As a proof of concept, we developed an underactuated VSTS joint module capable of deforming in four different directions using only one actuator. The dual-stage VSTS joint module was composed of two connected 3-strut tensegrity modules with three shared VSCs at the junction (Figure 28a and b). The two rigid surfaces of the structure, one at the top and the other at the bottom, could be connected to other modules or components, such as robot bodies or end effectors. The VSTS joint was actuated by means of a tendon-driven mechanism placed at the base that uniformly pulled all the top surface vertices towards the base (Figure 28b). The four different modes of actuation were achieved by simultaneously changing the stiffness of the three VSCs (Figure 28c) or by selectively changing the stiffness of only one VSC at a time (Figure 28d).

Experiments were performed by actuating the motor at low speed (5 °/s) until it reached maximum torque (7.25 N\*cm) while the position of the geometrical center of the top surface was tracked by means of a motion capture system. When the three VSCs were simultaneously softened, the structure could compress up to 40% of its height at the maximum torque (Figure 28e). Instead, when only one of the three VSCs was softened, the structure could bend around 40° (Figure 23 lateral view) in three different directions (Figure 28b-e top view).

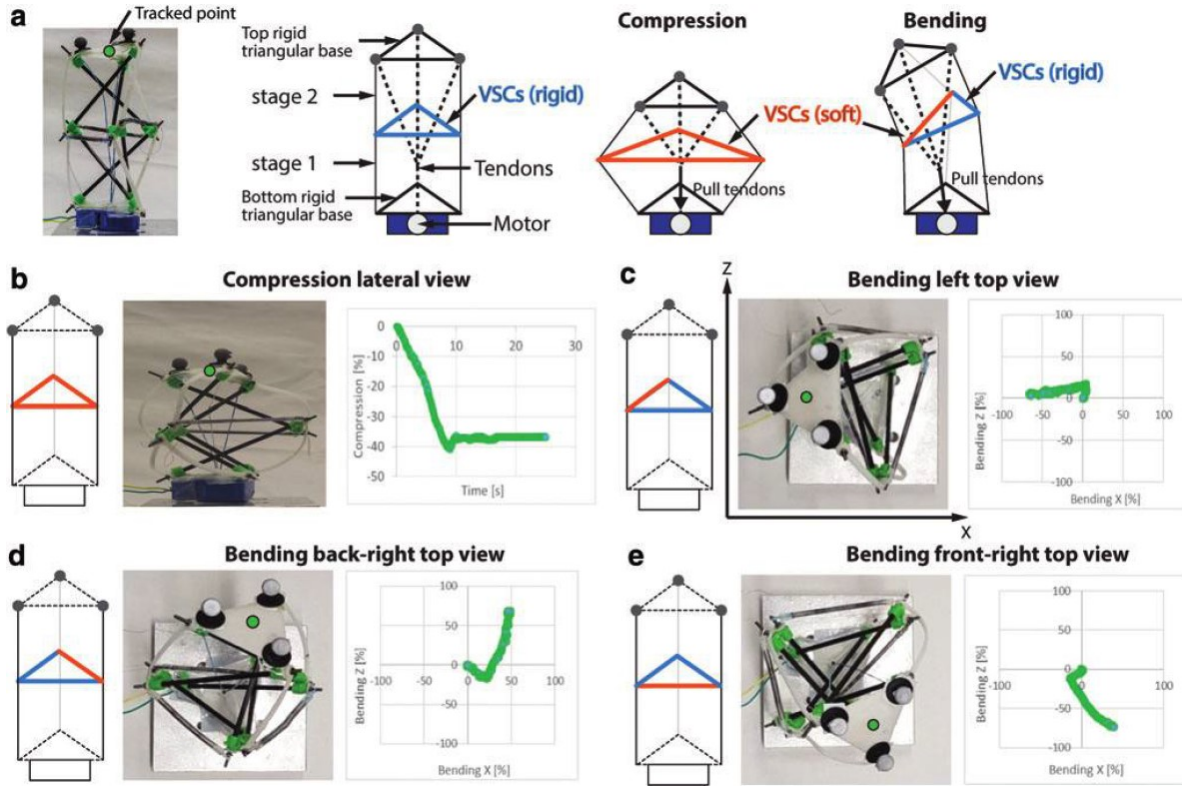


Figure 28. Underactuated VSTS joint module and its shape deformations.

(a) The VSTS joint prototype with in green highlighted the upper triangle geometrical center tracked in the motion tracking system, (b) schematics of the VSTS joint components, (c-d) schematics of compression and bending. The schematics show soft VSCs in orange and rigid VSCs in blue. (e-h), shape deformations of the VSTS are obtained by changing soft-stiff states of the three VSCs at the junction of the two 3-strut stages. Each deformation has schematics of the soft-stiff states on the left and plots showing trajectories of the tracked point on the right. Deformations are expressed in percentage of height over time for the compression and percentage of the beam width along Z and X axes for the bending. The VSTS with all soft VSCs compresses, while VSTS with only one soft VSC bends. Bending produce an initial twisting due to manufacturing asymmetries of the structure represented by the initial curve of the bending trajectory.

### 4.1.3 Discussion

The variable-stiffness tensegrity modules and assemblies described in this project offer tuneable load-bearing properties, shape locking, and controllable deformations in underactuated structures without significantly affecting the size and weight of the structures. While the cables described in this project were based on LMPAs encapsulated in stretchable tubes, other variable stiffness technologies could be used according to the force, speed, magnitude, or transition time required.

Moreover, given the scalability of tensegrity structures, the proposed VSTS strategy could be applied for modular systems at different scales. For example, large VSTSs could serve as a scaffold for lightweight and self-deployable modular bridges, infrastructures, manipulators, antennas, and buildings with the ability to lock into their deployed and undeployed configurations [109]. Human scale VSTSs are promising for load-bearing tuneable modular robotic frames and joints or underactuated appendices of robotic bodies [110] (e.g. wings, arms, tails, fingers, etc.), while smaller scale VSTSs could be useful to develop modular underactuated and minimally invasive surgery devices where reduced bulkiness and mechanical compliance to soft tissues is important [111].

The overall mechanical performance of the modular structures considered in this work, including the stiffness change capability, are essentially influenced also by the applied geometrical boundary conditions and the mechanical parameters (e.g. length and initial stiffness) of the non-actuated passive modules. It is therefore fundamental to develop an appropriate modeling tool to predict mechanical performances in different application scenarios involving different morphologies, scales, and boundary conditions. Improved modeling of tensegrity VSCs within the state of the art physics engines, or the use of Finite Element methods, could also pave the way to the development of more accurate simulations to predict

stiffness change and which cables should be selectively stiffened to achieve desired deformations and load-bearing configurations. In turn, such models could be leveraged by heuristic optimization methods to explore the morphological and behavioral space of future soft modular tensegrity robots.

## 4.2 Controllable active stiffness-change with type-changing tensegrity structures

In this section, we describe a novel bio-inspired active variable-stiffness design strategy based on type-changing tensegrity structures. We investigate the strategy on a bio-inspired proof-of-concept tensegrity module which uses an active mechanism to add or remove a ball-joint constraint among its rigid components, allowing transition among different tensegrity types and stiffness modes. We demonstrate the variable-stiffness strategy by developing a variable-stiffness robotic manipulator that can operate in different stiffness modes.

### 4.2.1 Introduction

New biological studies have highlighted the mechanical complexity of biological spines that are composed of not only rigid components under compression (vertebrae) with pivots functioning as joints but also of intervertebral muscles that are under tension [112] [113] [9]. These muscles help to distribute loads and increase the robustness of the whole system (Figure 29(a)) [9]. The biological spine has a pre-defined bending stiffness given by the intervertebral muscles at rest, which can globally increase when all muscles are simultaneously actuated, pulling the vertebrae against each other [113]. Furthermore, directional bending stiffness (i.e., exhibiting different bending stiffness in different directions) and controlled bending (i.e., repositioning of the spine in a bent configuration) are achieved by actuating a subset of the spines' muscles [113] [9].

Recently, to explain the mechanical complexity of the spine behavior, a novel bio-inspired model of the spine has been proposed: the tensegrity-truss system, where the rigid vertebrae are stabilized by intervertebral muscles (i.e., pre-stretched elastic cables). However, the existing solution in the state of the lack the ball-joint constraints among the vertebrae art [60] [61], not allowing the adaptation of the spine stiffness by pulling the vertebrae against each other (Figure 29(c)).

In this study, inspired by the biological spine, we propose and investigate a novel type-changing tensegrity structure that uses an active mechanism to add or remove ball-joint constraints among its rigid components, allowing transition among different tensegrity types and stiffness modes. Such a tensegrity structure can be used as a module to develop a robotic spine with variable-stiffness capabilities. The developed variable-stiffness tensegrity module can transition between different bending stiffness modes: *soft*, *global stiff*, and *directional stiff* as a biological spine. Moreover, in each of these states, its bending can be actively controlled. Finally, we demonstrate the novel variable stiffness tensegrity structure in a robotic spine used as a continuous manipulator (Figure 29(f)), which can adapt its mechanical stiffness.

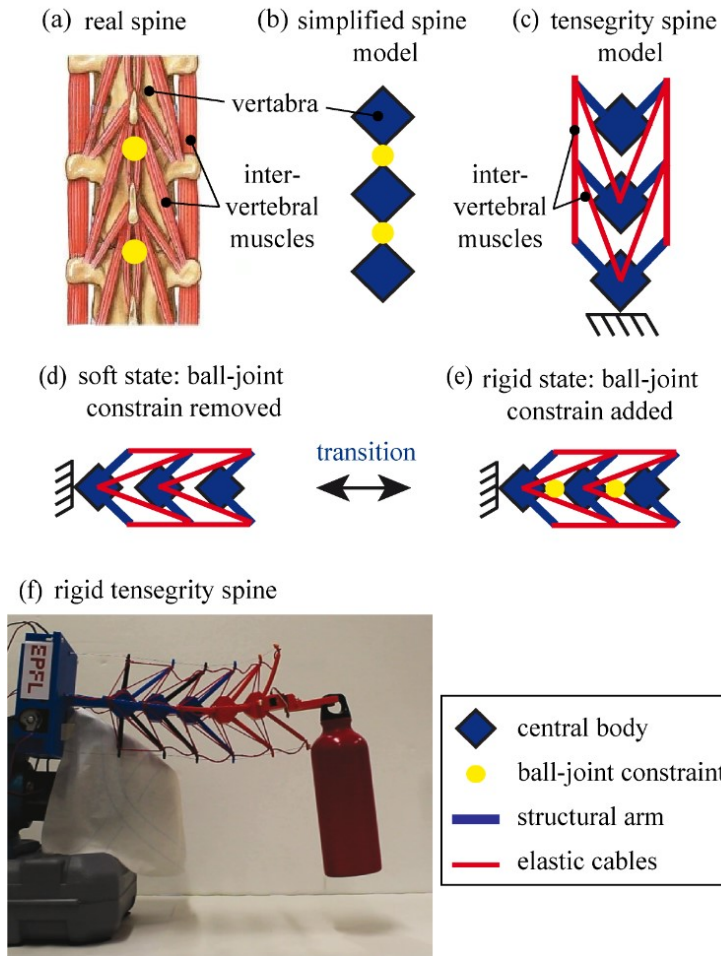


Figure 29. Schematic representation of a type-changing variable-stiffness tensegrity structure and its bio-inspiration from a vertebrate spine.

(a), a simplified artificial spine model (b), and the artificial tensegrity spine (c). The blue rhombus represent the vertebrae, the yellow dots represent the ball-joint constraints. The red lines represent intervertebral muscles (c). Schematic representation of the variable stiffness tensegrity module placed horizontally (d-e). A tensegrity type-changing module is used as continuous manipulator capable of lifting a 300 grams bottle stiff mode (f).

#### 4.2.2 Class-changing variable-stiffness strategy for tensegrity systems

A tensegrity structure is composed of rigid bars under compression in a network of tensioned cables, while a tensegrity system is defined as a set of rigid bodies of any shape stabilized by a network of tensile elements [11]. Various classes of stable tensegrity structures or systems exist. In *class 1* tensegrity system, the rigid bodies are not in contact and do not have ball-joint constraints (Figure 29(d)); in *class 2*, tensegrity systems at least two rigid bodies are constrained by a ball-joint constraint (Figure 29(e)). A *class 1* tensegrity structure is stable in a three-dimensional space thanks to the cable network. By adding ball-joint constraints, it is possible to augment its resistance to deformations and therefore increase its stiffness [11]. Our novel variable-stiffness strategy relies on the principle of transitioning from a *class 1* tensegrity system where the rigid bodies, i.e., named vertebrae, are not in contact with each other, to a stiffer *class 2* tensegrity system with ball joint constraints among the rigid bodies (Figure 29(e)). We applied this strategy to a well-known *class 1* tensegrity structure inspired by the biological spine. The structure is named *Tetrahedral Tensegrity Spine* [14-16], and we included a mechanism to add constraints between the vertebrae when a stiffer configuration is required.

#### 4.2.3 Hardware implementation

The simplest stable module of a *Tetrahedral Tensegrity Spine* is composed of an internal vertebra suspended in a network of tensioned cables connected to two external vertebrae at the top and the bottom (Figure 30(b)). The rigid bodies named

vertebrae of our variable-stiffness tensegrity spine module are composed of two main components: the *central body* and the *structural arms* (Figure 30(a)). The *central body* facilitates the positioning and the assembly of four *structural arms* for each vertebra. The *structural arm tips* serve as vertices where tensile elastic elements are attached to stabilize the structure.

In order to provide the mechanism with variable-stiffness, we added a pin with a spherical tip at the bottom face of the vertebra's central body; the spherical pin tip can fit a socket shaped into the top face of the central body. All the components of the vertebrae were made of polylactic acid (PLA) with a Stratasys DimensionElite 3D-printer and are manually connected with hot glue. The vertebrae arms are 50 mm long and with a cross-section diameter of 2 mm. The distances between the end tip of the arms and the geometrical center of a central body are 60 mm.

The tensioned cables to stabilize the three vertebrae of the spine present the same configuration design as described in [61] for the *Tetrahedral Tensegrity*. However, we designed cable tensile elements as a flat network that can be folded into the three-dimensional (3D) spine structure, as we described in chapter one. Our methodology allows to easily manufacture the cables with 3D-printed thermoplastic polyurethane (TPU), which has the required elastic properties. The network is first designed with the help of computational aided design (CAD) for the three-vertebrae spine. Then, the unfolded network can be retrieved by eliminating the vertebrae and rotating the cables until a flat configuration is obtained (Figure 30(b)). The *tensile-element* network has a cross-section of 1 mm<sup>2</sup> and each cable is designed to exhibit a 10% pre-stretch when assembled. Although the presented assembled spine is a 3-vertebrae segment (Figure 30(c)), it can be extended by adding n-internal vertebrae and extending the cable network.

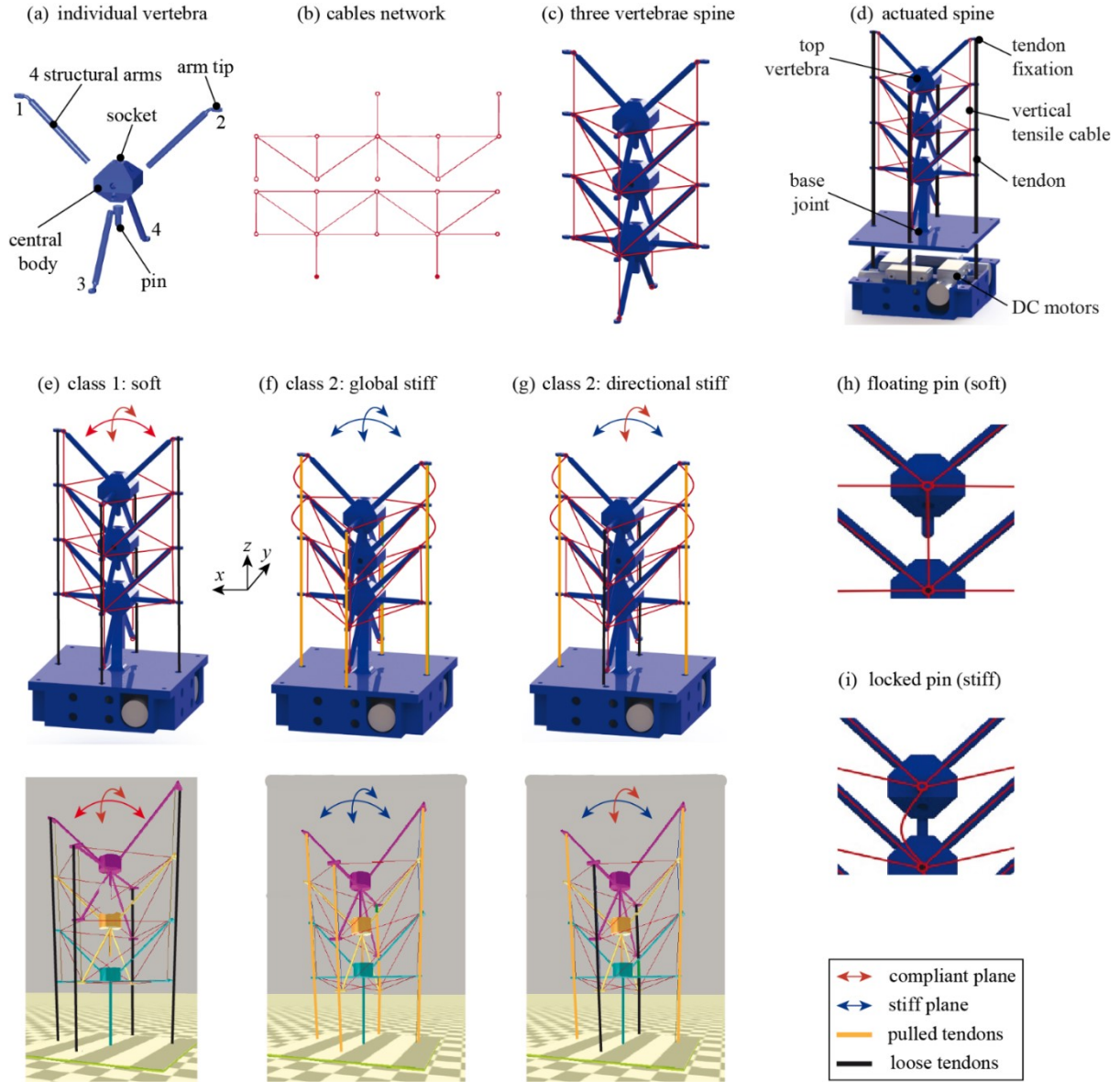


Figure 30. Tensegrity type-changing module design.

The upper part of the figure presents the variable-stiffness tensegrity module hardware implementation in detail. (a) Exploded view of a vertebra design. The numbers highlight the four structural arms. (b) The flat elastic network to assemble a three vertebrae tensegrity module. (b) The assembled 3 vertebrae tensegrity module. (d) Exploded view of the tensegrity module's base containing the motor actuators and in black the four tendons connecting the top vertebra arm's tips to the motor actuators in the base. (e-f) Representation of the three stiffness modes both in hardware prototype and simulation model. The arrows represent the two orthogonal planes where the four tendons stand. The red arrows represent a compliant plane of bending, while blue arrows represent a stiff plane of bending. Green lines represent pulled tendons while black lines loose tendons. (e) The four tendon are loose and the tensegrity module is compliant in the two planes. (f) The four tendons are pulled and the module is stiff in the two planes. (g) Two tendons are loose and two are pulled. The plane where the two loose cables stand is compliant the other is stiff. (h-i) Detailed 2D view of the pin floating in the soft mode and inserted in the socket in the stiff modes.

To change the stiffness and to actively bend the module in the vertical plane, we implemented a tendon-driven clustered actuation system (Figure 30(d)) [114] in a rigid base at the bottom of the first rigid body. This system is composed of four tendons made of Dyneema wires (ultra-high molecular weight polyethylene with a rigid Young Modulus of approximately 110GPa), each actuated by a DC electrical motor (DC12V25RPM from Pololu) and controlled by an Arduino Uno microcontroller (Figure 30(d)). Each of the four tendons is running in parallel to the vertical elastic tensile cables connecting the vertebrae arms displayed at the four edges along with the height of the spine (Figure 30(d)). While the vertical elastic tensile cables are fixed to each of the vertebrae arms tips (Figure 30(d)), the four tendons are fixed only at the tip of the top

vertebra arms (Figure 30(d)) and they run freely throughout holes in the tips of the bottom vertebrae arms. This clustered tendon-driven actuator design reducing the number of actuators necessary to compress all the vertebrae reducing mass, bulkiness, and energy consumption of the actuation system.

#### 4.2.4 Stiffness transition mechanism and tensegrity module's stiffness modes

In the developed type-changing tensegrity module, the variable-stiffness is achieved by removing or adding ball-joint constraints between the vertebrae. According to which tendons are pulled, the tensegrity system can transition between three different stiffness modes: *soft mode*, *global stiff mode*, and *directional stiff mode* (Figure 2(e-g)).

- **Soft mode:** When all the tendons are loose, and the pins are not inserted (Figure 2(h)), the vertebrae are stabilized in space only by the elastic cables and with small loads can experience relative translations and rotations (Figure 2(e)). The tensegrity system is *class 1*.
- **Global stiff mode:** When the four tendons are pulled simultaneously, the *spherical pins* are inserted in the *sockets* of the underneath vertebrae adding a ball-joint constrain among the vertebrae and locking relative translations (Figure 2(i)), while the rigid pulled tendons constrain relative rotations in all longitudinal planes (Figure 2(f)). The tensegrity module is a *class 2* tensegrity system.
- **Directional stiff mode:** When two opposite tendons are simultaneously pulled, the *spherical pins* are inserted in the *sockets* of the underneath vertebrae constraining relative translations (Figure 2(i)), while the two rigid tendons constrain relative rotations only in the plane where they stand. The bending in the orthogonal plane is constrained by the elastic cables that allow deformations (Figure 2(g)). The tensegrity module is a *class 2* tensegrity system.

In each of the three modes, it is possible to actively control the tensegrity module's bending with the same actuation system. The bending can be controlled in four directions by pulling individually one of the four tendons (Figure 4(a)). When only one cable is pulled, the opposite one is simultaneously loosened not to increase its pre-stretch. Therefore, in the soft mode, the opposite tendon remains loose during bending, while in the stiff modes, it keeps a certain pre-stretch to keep the pin inserted without hindering the bending.

#### 4.2.5 Model

To investigate the three stiffness modes, we developed a model of the tensegrity module using the NASA Tensegrity Robotics Toolkit (NTRT). Similar to the hardware prototype, the model consists of a three-vertebrae tensegrity module with four tendons running through holes at the tips of the vertebrae arms and attached to the tip of the top vertebrae arms (Figure 30(e)). The vertebrae are modeled with arms as cylindrical rods of length 50 mm, and the distance of 60 mm between end arms tips, and geometrical center of the central body is respected. At the arms tips of central and bottom vertebrae, a hole through which the tendons run is approximated with a three-rod hollow triangle because of simulator limitations. The density of all vertebrae components is  $1.25 \text{ g/cm}^3$ , an approximation of the 3D printed PLA density. Likewise, in the hardware prototype, the bottom vertebra is rigidly constrained to a square base. The elastic cable network is modeled as a set of cables between the vertebrae arms tips with a Young's Modulus of 12.5 MPa corresponding to the value of the 3D printed TPU. Their pre-stretch is set to match 10% of the real prototype. The tendons are modeled with a Young modulus of 110 GPa like their hardware counterparts.

To simulate the *soft mode*, the four tendons are not pulled (Figure 30(e)), while to simulate the *global and the directional stiff modes*, the tendons are pulled until the pins touch the upper faces of the central bodies of the underneath vertebrae (Figure 30(f) and (g)). Given the difficulty to model the round tip of the pin and concave shape of the socket, a translational constraint (i.e. a constraint that locks in-plane movements of the pin's tip, while allowing rotations) is added between the tip of the pin and the center of the upper face of the bottom vertebra. Such a constraint is used to model the real constraint of the pin insertion in the socket.

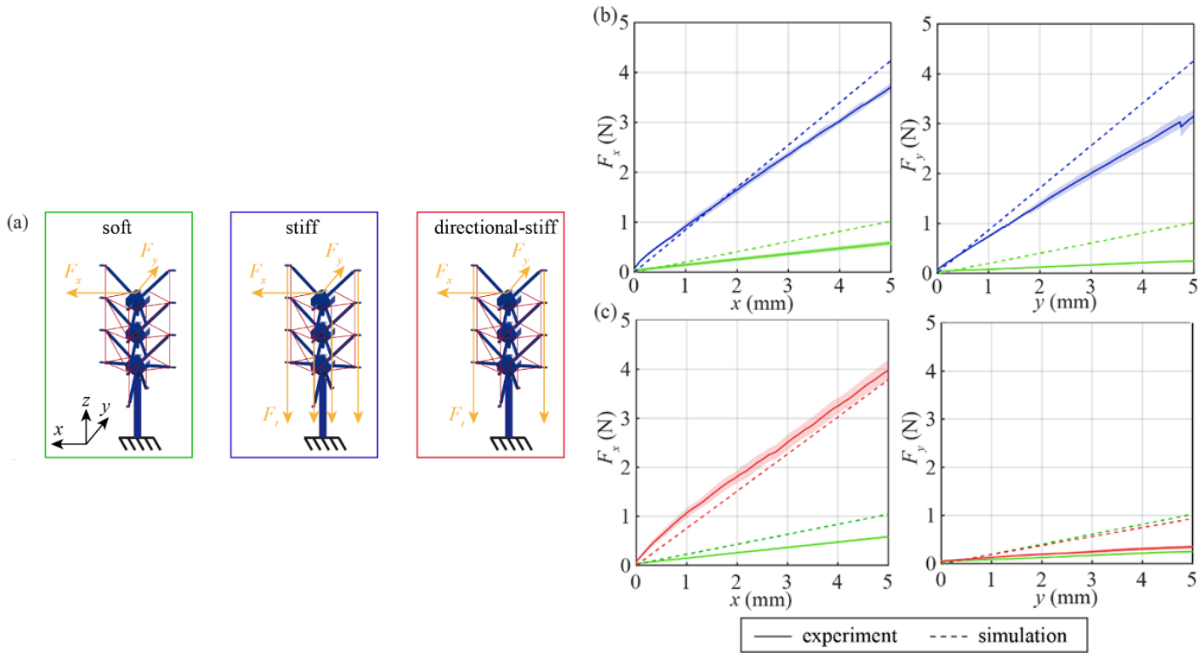


Figure 31. Type-changing tensegrity module stiffness characterization.

Results of the bending load characterization with the experimental setup in (a). The results of the experiment (solid lines) and the simulation (dashed lines) are shown in (b) for the soft (green) and stiff (blue) mode in the x-z-plane (force  $F_x$ , displacement  $x$ ) and in the y-z-plane (force  $F_y$ , displacement  $y$ ). (c) shows the results of the experiment and the simulation for the soft and directional stiff (red) modes in the x-z-plane (force  $F_x$ , displacement  $x$ ) and in the y-z-plane (force  $F_y$ , displacement  $y$ ). The shaded areas represent the standard deviation of the experimental measurements.

## 4.2.6 Results

To validate the variable-stiffness strategy and the three stiffness modes, we performed load-displacement bending characterization in both reality and simulation in each mode (Section A). In section B, we investigated in the simulation how the mechanical properties of the elastic cables affect the transition among modes and the bending stiffnesses of the spine in each mode. In section C, we characterized the reachable workspace when actively control the tensegrity module bending in each of the three modes.

### Load-displacement bending characterization at each mode

For the hardware bending experiments, we fixed the tensegrity spine's base and applied loads  $F_x$  and  $F_y$  along the orthogonal planes to the last vertebra (i.e., planes x-z and y-z) by an Instron testing machine (5960 Series), which caused displacements in the  $x$  and  $y$  directions (Figure 31(a)), this allows calculating bending stiffness in  $x$  and  $y$  directions. The same conditions were applied to the model. For this study, in all experiments, the maximum displacement was  $x = y = 5$  mm to stay abreast of the small-angle approximation and linear load-displacement range.

Three different stiffness modes were tested. In the *soft mode*, all actuation tendons were relaxed (Figure 31(a), green). In the *stiff mode*, all tendons were pulled by symmetric forces until the pins entered their sockets (Figure 31(a), blue). In the *directional stiffness mode*, only two opposite tendons in the x-z plane were pulled until the pins entered the sockets (Figure 31a, red). For the latter two modes, the stiffness of the system could be further increased by applying a greater tendon force  $F_t$ . However, this further stiffening of the system has already been widely discussed in [115], [116], [117], and thus, it is not investigated in this work.

The experimental results confirm that in the stiff mode (Figure 31(b), blue), the bending stiffness can be increased by a factor of approximately six times the bending stiffness in the soft mode (Figure 31(b), green). The bending stiffness in the y-direction shows a decreased stiffness as compared to the x-direction. This could be explained by mechanical imperfections of the prototype that result in asymmetric stiffness. The slight deviations of the measured forces between the hardware

and the model are probably due to slightly loose tendons fixations caused by manual knotting and to the 3D printing (Figure 30(b)) of the elastic cables that result in non-uniform cross-sectional areas. By pulling only the two tendons in the x-z-plane, it is possible to achieve directional bending stiffness (Figure 31(a), red). When the movement in this plane is constrained (similar to Figure 31(b) right), the bending stiffness in the x-direction is increased (Figure 31(c) left), while the bending in the y-direction exhibits a stiffness comparable to the soft state.

#### **Elastic cables influence bending stiffness and mode transitions.**

The type-changing tensegrity module's bending stiffness in the soft and stiff modes and the tendons pulling load to transition among the modes is dependent on the mechanical properties of the elastic cables. To gain a better understanding of this interplay, we changed the cable stiffness (Figure 32(a)) and pre-stretch (Figure 32(b)) of the elastic cables (Figure 32(b)) in our simulator and investigated how this affects the bending stiffness in the soft and global stiff mode and the tendons pulling load applied to transition from the soft to the global stiff mode.

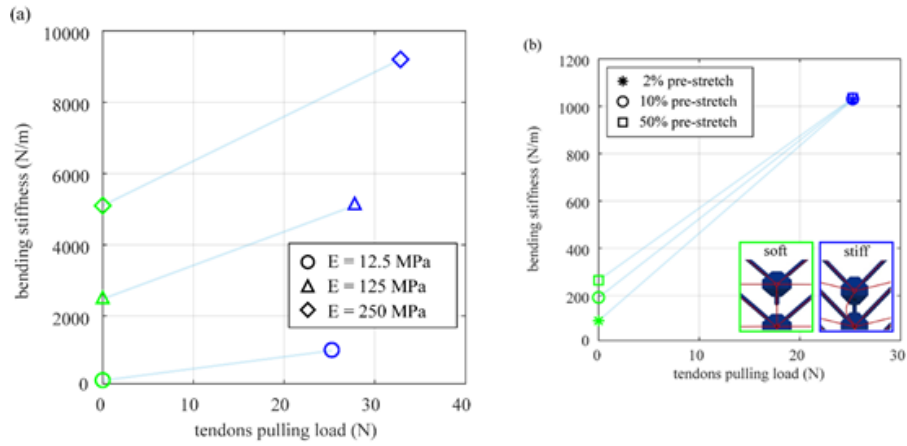


Figure 32. Type-changing tensegrity module parameters study.

(a), the graph shows the type-changing tensegrity module's bending stiffness in the x-z plane versus the tendons pulling load. Each symbol represents a result of a simulation performed with our model. Circles are simulations of a module with 12.5 MPa stiffness of the elastic cables, triangles 125 MPa, and diamonds 250 MPa. The green symbols represent the results of the simulations in the soft mode when the tendons are loose and the tendons pulling load is zero; while the symbols in blue represent the results of the simulations in the global stiff mode, when the pins are inserted and the ball-joint constraint is added. Light blue lines are added to highlight couples of simulations performed with the same elastic cables mechanical properties. (b) the graph shows the module bending stiffness in the plane x-z versus the tendons pulling load. Each symbol represents a result of a simulation performed with our model. Circles are simulations of a module with 10% initial pre-stretch of the elastic cables, asterisk 2% pre-stretch and squares 50% pre-stretch. Light blue lines are added to highlight couples of simulations performed with the same elastic cables mechanical properties.

#### **Passive cables stiffness**

In the first set of experiments, we simulated different elastic cable stiffnesses by applying three Young's modulus  $E = 12.5$ , 125, and 250 MPa. To calculate the bending stiffness of the type-changing tensegrity module, we constrained the base of the module and applied a fixed load  $F_x$  in the x-z plane (Figure 31(a) to the last vertebra, as seen in section A). The displacement is recorded to calculate the bending stiffness  $K = \frac{F_x}{displacement}$ . In the soft mode, we immediately applied the load when the simulation was initialized. In the global stiff mode, however, first, we pulled all four tendons in symmetry until the pins touched the vertebrae. Then, we added a translational constraint to model the pin insertion (as described in chapter III) and applied the load  $F_x$ . Furthermore, we also recorded the pulling load in the tendons when the pins are inserted.

The results in Figure 32 (a), show that the stiffness of the elastic cables affects the bending stiffnesses in the soft and the global stiff mode and the tendons pulling load to transition among the two. Indeed, when the elastic cables are stiffer, compressing the tensegrity spine to insert the pins and transition to the global stiff mode, requires higher tendons pulling loads (blue triangle and blue diamond in Figure (a)). Higher loads in the pulled tendons also mean a greater tendon pre-stretch, which, in turn, increases the bending stiffness of the system in the stiff mode (blue triangle and blue diamond in Figure 32(a)). At the same time, stiffer elastic cables increase bending stiffness in the soft mode (green triangle and green

diamond in Figure 32 (a)). Although with higher elastic cables stiffnesses, we observe an increase of both soft and stiff bending stiffness, these don't scale similarly. Therefore, at different elastic cables stiffnesses, we observe different stiffness changes among the modes: approximately a factor of six times at 12.5 MPa, two times at 125 MPa, and less than one at 250 MPa.

#### Elastic cables pre-stretch

With the second set of experiments, we investigated in the simulation how the passive cables' pre-stretch affects the load to transition from the soft to the global stiff mode and the bending stiffnesses in the two modes (Figure 32(b)). We applied a pre-stretch of 2%, 10%, and 50% to the elastic cables while setting their Young's modulus to 12.5 MPa. Then, we performed bending simulations at both soft mode and global stiff mode for each pre-stretch value. The bending stiffnesses and the tendons pulling loads to transition between the soft and the global stiff modes were recorded analogous to the first set of simulation experiments.

The results show that the elastic cables' pre-stretch affects the bending stiffness of the spine in the soft mode (Figure 32(b), blue). Increasing the pre-stretch from 2% to 10% increases the bending stiffness by 105%. Likewise, increasing the pre-stretch from 2% to 50% increases the bending stiffness by 183%. In the global stiff mode (Figure 32 (b), blue), however, no clear change in bending stiffness can be observed (difference < 1%). We can hypothesize, that since increasing pre-stretch of the elastic cables does not result in an observable change in the tendons pulling load in the stiff state, the tendons experience similar pre-stretches and therefore the bending stiffness it is not affected (Figure 32(b)).

Based on these results, we can discuss two design principles for class-changing variable stiffness tensegrity modules. First, the stiffness of the elastic cables can be tuned to program the range of bending stiffness in both modes. However, when increasing the stiffness of the elastic cables, the change in bending stiffness from soft to global stiff mode is decreased. Second, the pre-stretch of the elastic cables can be tuned to program the bending stiffness in the soft mode without influencing noticeably the bending stiffness in the global stiff mode. Therefore, lower pre-stretch of the elastic cables can be designed to increase the stiffness change when transitioning from soft to global stiff mode.

#### Workspace experiments

By pulling one of the four actuation tendons individually (Figure 30(d)) and simultaneously releasing the opposite one, it is possible to actively control the tensegrity module bending.

To assess how the stiffness modes influence the tensegrity module's reachable workspace (i.e., maximum bending angles of the spine segment in the four actuated directions), we studied the workspace of the variable-stiffness tensegrity module in the soft mode and the global stiff mode, assuming that the workspace of the directional stiff mode is a combination of the two (i.e., the same maximum bending angle of the stiff mode reachable in the stiff plane and maximum bending angle of the soft mode reachable in soft direction). The bending experiments are conducted by pulling only one tendon at a time while releasing the opposite one by the same cable length. The experiment is repeated in each mode until the external arms are in contact, which prevents any further bending (Figure 33 (a)). A human operator can control the rotations of the motor that pull the tendons throughout a custom made Arduino interface. This interface allows applying small incremental rotations (e.g., 90°) to the motors until desired positions are reached. To track the movement of the system with an Optitrack motion capture system (solid lines in Figure 33(b) and (c)), four reflector markers are fixed at the base of the tensegrity spine system as a reference, while one reflector marker is attached on the upper face of the top vertebra's central body. The trajectories are measured in the x-z-plane and the y-z-plane, as shown in Figure 33(solid lines).

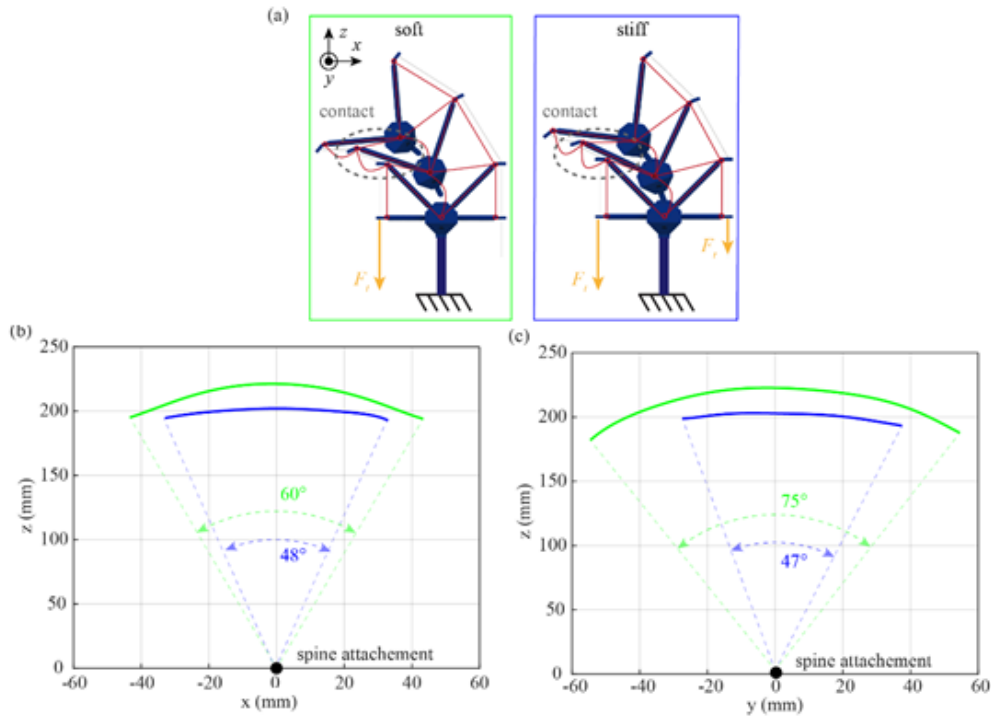


Figure 33. Type-changing tensegrity module workspace characterization.

In the workspace experiment, the soft and stiff mode were considered as shown in the schematic in (a) and the bending was induced by applying a force  $F_t$  and pulling the tendon on one side, or asymmetrically on both sides, respectively. The measured trajectory of the central point of the upper face of the top vertebra in the x-z-plane for soft (green) and stiff (blue) are represented by the solid lines in (b), while the trajectories of the last vertebra in the y-z-plane for soft and stiff are shown by the solid lines in (c).

The results show that a trade-off exists between stiffness and workspace. The measured workspace angle in the stiff mode is 20% smaller for the x-z-plane and 37% smaller in the y-z plane compared to the soft mode. The main reason for this decreased workspace angle between soft and stiff mode lies in the compression of the spine. When the spherical pins touch the central bodies, the distances between the vertebrae are reduced (see Figure 30(e-g)), and consequently, the radius of their relative rotation is shorter. The bending angles in the positive and negative direction of both orthogonal planes are not perfectly symmetric. (see Figure 2(c)). These differences can be explained by the different lengths of the actuated tendons in the two planes. Indeed, the top vertebra arms tips have different heights measured from the base (Figure 30(d)). Moreover, the measures could be affected by small asymmetries of the assembled spine or errors of the human operator that manually actuated the motors.

Here, we also want to highlight two design principles which affect the workspace of the tensegrity module. First, increasing the distance between the vertebrae increases the distance between the arm tips (Figure 30 (a)), which increases the bending range of the tensegrity spine and thus the workspace. Second, increasing the length of the pin reduces the decrease in the workspace between the two modes (Figure 30 (b)).

#### 4.2.7 A continuous tensegrity spine manipulator

To demonstrate the potential of the type-changing variable-stiffness tensegrity module and its different stiffness modes, we developed a continuous tensegrity manipulator based on the variable-stiffness tensegrity module described above.

The manipulator is composed of a 5-vertebra tensegrity module, the top vertebra is equipped with a gripper (Figure 34(a) and (b)). The total height of the manipulator is 400 mm from the top of the base to the tip of the gripper. The gripper is based on an open-source design [118]. It is composed of a servo motor-driven claw that can close and open to grasp objects (Figure 34(b)). The four motors of the tendon-driven actuation system and the servo are driven by an Arduino UNO and

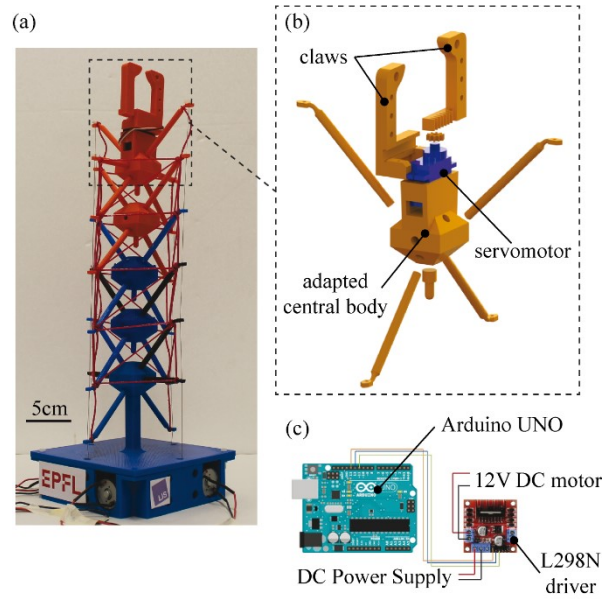


Figure 34. A tensegrity spine manipulator designed with an adapted type-changing tensegrity module composed of five vertebrae. The continuous manipulator design with a 5 vertebrae variable-stiffness tensegrity module (a). In blue, the 3 original vertebrae of the characterized type-changing tensegrity module in orange the 2 additional vertebrae. The top vertebra is modified with a built-in gripper composed of two claws actuated by a servo-motor (b). Schematics of the electronics to allow open loop user control (c).

four L298N motor drivers (Figure 34(c)). A human operator, thanks to an Arduino Uno user interface, can control the manipulator. The human operator can bend the manipulator in four directions by pulling one individual tendon or control the transition from the *soft mode* to the *global stiff mode* by pulling all four tendons at the same time or change to the *directional stiff mode* by pulling only two opposite tendons at the same time.

The three different stiffness modes of the manipulator are demonstrated in three different task scenarios highlighting the advantage of each stiffness mode. In each demonstration, the manipulator is actively bent with the same control input (i.e., the same number of incremental rotations of the tendon-driving motor) in a specific direction before and after a stiffness transition to highlight different behaviors.

1. *Soft mode*: the manipulator is capable of complying with 300 grams objects while moving in its workspace to demonstrate safe interaction with the environment (Figure 35(a))
2. *Stiff mode*: the manipulator is capable of lifting a 300 grams object (i.e., approximately the same weight of the spine system) thanks to increased stiffness to demonstrate on-demand load-bearing capability (Figure 35(b)).
3. *Directional stiff mode*: the manipulator is capable of lifting a 300 grams object in the vertical plane (i.e., orthogonal to the table surface) and safely comply with objects of the same weight in the horizontal plane (i.e., parallel to the table surface) to demonstrate load-bearing capability and compliance in different directions (Figure 35(c)).

## 4.2.8 Discussion

In this chapter, we proposed a novel type-changing variable-stiffness design strategy for tensegrity structures and systems. We developed a variable-stiffness tensegrity module capable of transitioning among three different stiffness modes. The mechanical adaptability given by the three stiffness modes has been validated in a proof-of-concept continuous tensegrity manipulator capable of manipulating heavy objects and complying with obstacles while moving.

The proof-of-concept module that we developed to demonstrate the type-changing variable stiffness strategy is not a type-one tensegrity structure -as the modules in the other chapters- but a tensegrity system, where rigid bodies have more complex morphologies than bars. However, tensegrity structures can be developed with the same strategy by adding or removing ball-joints between vertices of the bars. This can be obtained with clustered actuation like in this study or with

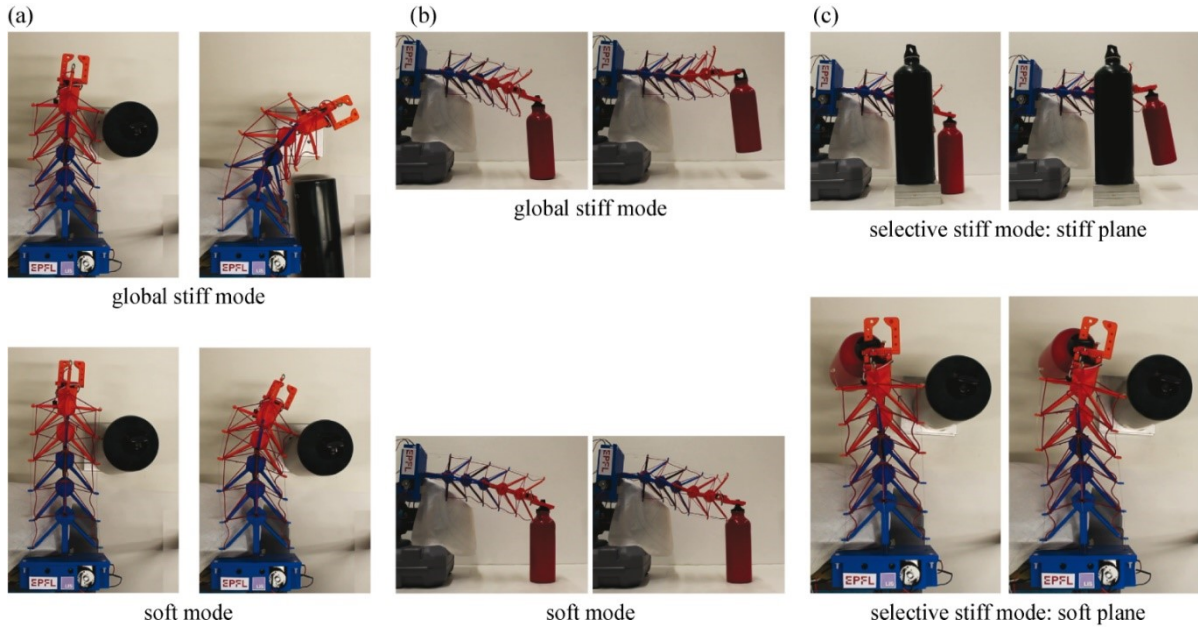


Figure 35. Variable stiffness tensegrity manipulator stiffness modes.

(a) Top view of the manipulator clamped at one side and placed horizontally to a table surface. A bottle weighting around 500 grams is placed in its reachable workspace. A sequence of two images show the manipulator bending on the right while in global stiff mode (top) and in soft mode (bottom). In the first case, the manipulator is too stiff and pushes the bottle to fall on the table, while in the soft mode the manipulator is able to comply with the bottle avoiding its fall on the table. (b) Side view of the manipulator clamped at one side and placed horizontally to a table surface while grasping a bottle weighting 300 grams. A sequence of two images show the manipulator bending upwards while in global stiff mode (top) and in soft mode (bottom). In the first case the manipulator is able to lift the bottle. In the second its stiffness is not sufficient to transmit a high enough force to lift the bottle. (c) Lateral view and top view of the manipulator clamped on one side and standing horizontally to a table surface. A bottle weighting around 300 grams is grasped by the gripper, while a bottle weighting around 500 grams is placed in its reachable workspace. The manipulator is in selective stiff mode, the plane orthogonal to the table surface is stiff while the parallel plane is soft. In the two top images of the sequence, the manipulator is able to lift the bottle in its stiff plane. In the two bottom images of the sequence, while the manipulator is lifting the bottle, it bends on the right in its soft plane and it is able to comply with the second bottle avoiding its fall on the table.

other mechanisms such as spherical magnets. Moreover, the module developed in this chapter is not compatible with other chapters' modules. However, using form-finding techniques, compatible type-changing modules with similar faces on their external surface could be developed.

In this project, the variable-stiffness is achieved by actively adding or removing a ball joint constraint among the rigid bodies, named vertebrae, by means of tendon driven clustered actuation system. The mechanism allows changing the tensegrity system class from *class 1* with no constrain between the rigid bodies to a *class 2* with ball-joints constraints among the vertebrae. In the future, more advanced modeling or use of optimization algorithms [75], may allow programming of the morphological and mechanisms space design in terms of stiffness range and workspace, by optimizing passive cables' mechanical properties and components dimensions. Furthermore, more reliable manufacturing techniques, such as molding instead of 3D printing, could improve the quality of the elastic cables to match the stiffness of the uniform cross-section cables of the model.

### 4.3 Concluding remarks

In this chapter, we have presented two different active stiffness-change design strategies for developing tensegrity modules: through activation of smart materials or with bio-inspired type-changing tensegrity structure.

While the first strategy can be implemented in any type of tensegrity module morphology including structures with no actuators. The second needs a more advanced form-finding technique to design compatible morphologies. However, smart materials, investigated in the current state of the art, are still prone to some disadvantages like high energy consumption or low speed. We believe that the two strategies are complementary and that in some applications type-changing tensegrity variable stiffness may be a preferable strategy to include variable stiffness capabilities in tensegrity modular robots.

# Chapter 5 Dual-stiffness design strategy for passive stiffness change of tensegrity structures

Publication Note: The material presented in this chapter is adapted from:

- D. Zappetti, S. Mintchev, e D. Floreano, « Dual Stiffness Tensegrity Structures for highly resilient robots», to be submitted in 2021

The first author contribution was to conceptualize and characterize the tensegrity modules and the robotic applications, to analyse the results and to write the manuscript.

In the previous chapters, we investigate how to implement a controllable active stiffness-change in tensegrity modules. Active-stiffness change is a desirable feature to have on-demand mechanical adaptability and multifunctionality in tensegrity robots. However, active stiffness-change has disadvantages as well. An active stiffness component requires more energy, additional electronics that may increase the weight of the system, and a more complex control system [119]. Moreover, according to the variable stiffness technology used, for some applications, the time of the stiffness transition could be too high (e.g. when using the smart-materials-based variable-stiffness strategy [120]), or can add weight and bulkiness to the system as for the type-changing tensegrity variable-stiffness strategy [121].

## 5.1 Introduction and design strategy

Nowadays the use of robots to navigate and explore cluttered environments is spreading. Although detection and control systems have become always more effective [122], the risk of a collision cannot be completely eliminated. A possible approach towards collision resilience is to develop completely soft robots, able to deform easily at impact and absorb the energy of the collision [7]. However, such an approach has downfalls as well. Locomoting robots, such as drones and wheeled robots often need a rigid frame to efficiently navigate the environment. For instance, a drone with a soft body can have the relative position among its propellers change due to wind disturbances and accelerations making controlled flight difficult or highly energy consuming [110]. A similar issue may arise when relative positions among wheels of a cart robot change.

Recently, some researchers have suggested that variable-stiffness capabilities [119] may be key to solve this trade-off. However, collisions happen as very sudden events during navigation and in unpredicted ways [117]. For this reason, researchers have highlighted the importance of designing passive variable-stiffness mechanisms into robotic bodies rather than active ones [123] [124] [125]. A passive variable-stiffness change allows bypassing the detection and processing of the collision simplifying the design of collision-resilient robotic applications. Passive variable-stiffness strategies employ dual-stiffness materials or structures with the ability to transition to a lower stiffness when an external load increases over a certain pre-programmed threshold. After transitioning, a dual-stiffness material can withstand much larger deformations without failure, storing the energy of the impact, which will be later dissipated or employed after the collision to assume the pre-collision configuration.

Tensegrity structures are a promising framework for developing collision-resilient robotic applications. Rigid tensegrity structures are very lightweight therefore exhibiting lower inertia and less energy to dissipate during collisions. Coupled with dual-stiffness technologies, tensegrity structures can be even more resilient resulting in a promising approach.

Several investigations exist in the literature on creating dual-stiffness materials for robotic applications, such as dual-stiffness membranes [126] and magnetic fuses [127]. However, one of the most promising for developing is the use of buckling-instabilities [128] [129] [130]. Buckling is an instability that is exhibited by materials under compression. These materials can have high rigidity and, after a certain compressive load threshold, transition to a softer stiffness allowing them to withstand high deformation and store energy.

A tensegrity structure is made of elements in compression, the struts, and elements in tension, the cables. With rigid struts and inextensible cables, the structure is stiff [20](Figure 36a). By allowing buckling of the struts is possible to develop a highly lightweight dual-stiffness tensegrity structure that can be used as a module to develop robotic applications for collision resilient navigation (Figure 36b).

In the rest of the chapter, we first describe how to functionalize a tensegrity strut for buckling with high deformations up to 30% of its length. Then we assemble and characterize dual-stiffness tensegrity modules and finally, we validate the approach by developing a tensegrity dual-stiffness wheeled rover and a drone multi-copter, both with dual-stiffness behaviors and the ability to withstand collisions.

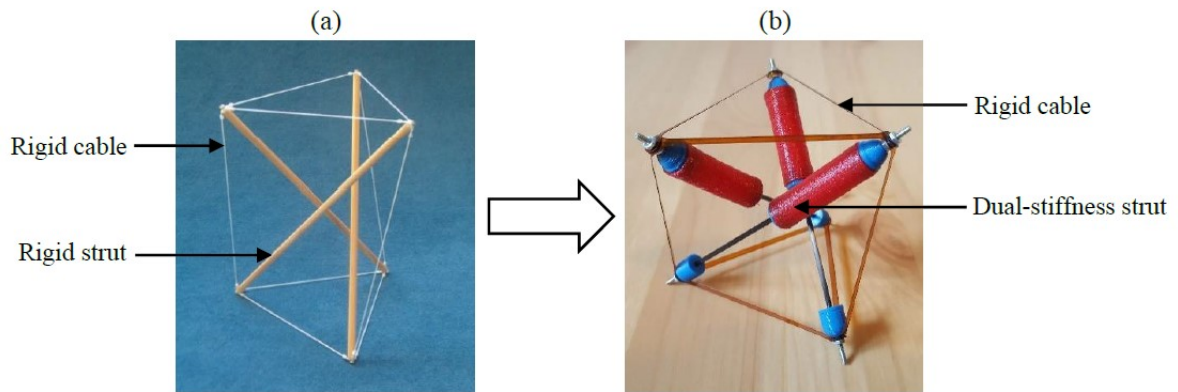


Figure 36. Examples of a rigid tensegrity module and a dual-stiffness tensegrity module.

(a) A 3-strut tensegrity module with nylon cables and wooden struts. (b) Our 3-strut dual-stiffness module with highlighted the dual-stiffness strut and rigid cables made of Kapton.

## 5.2 Buckling strut design and its characterization

A strut of a tensegrity structure is usually made of a rigid material able to withstand compression without buckle. Some researchers explored the idea that buckling is not only a failure mode but can be used to make improve the deformability of a soft tensegrity structure [131]. In our work, we develop a rigid tensegrity structure that is composed of rigid cables and dual stiffness buckling strut. Our aim is to develop a structure that deforms as little as possible before buckling, making the buckling the only activation of large structural deformation. Moreover, we developed a strut able to highly deform after buckling up to 30% of its length.

The chosen design for the buckling strut is shown in Figure 38(a). The strut consists of two main parts: a tube (the red part in Figure 38(a)) made of NinjaFlex, a printable elastic material, and a pultruded carbon rod (the black part in Figure 38(a)). These two parts are connected with a rigid connector, made of ABS (blue parts in Figure 38(a)). At the two ends of the strut, two screws are attached to insert the cables during the assembly and to add connectors between the modules. The parts of a strut are glued together. Both NinjaFlex tube and ABS parts are 3D printed. The tube has an inner diameter of 7 mm, and an outer diameter of 9 mm (Figure 38(b)). It measures 30 mm but on both ends, the ABS parts are glued inside on 4 mm, so the effective length is 22 mm. The strut measures 93 mm with the screws and 79 mm without. In the strut, the buckling part is the NinjaFlex hollow tube. The advantage of using the NinjaFlex hollow tube is that it is stiff during

compression with small loads and and, at the same time, it can highly bend after buckling. Indeed, the tube behaves as a thin shell [128]. First, the tube is stiff in compression. When the tube starts to buckle, a small deformation appears at first and then propagates quickly until the collapse of the tube.

The carbon tube part allows increasing the length of the strut without increasing the length of the NinjaFlex tube that, in turn, would decrease the buckling load. Indeed, both stiffness and buckling load of a hollow tube increase by reducing the length of the tube, or by increasing its thickness [123].

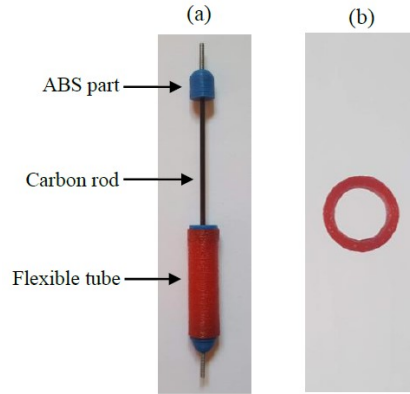


Figure 38. Dual-stiffness strut design and model.  
(a) Dual stiffness strut design. (b) Flexible hollow tube section

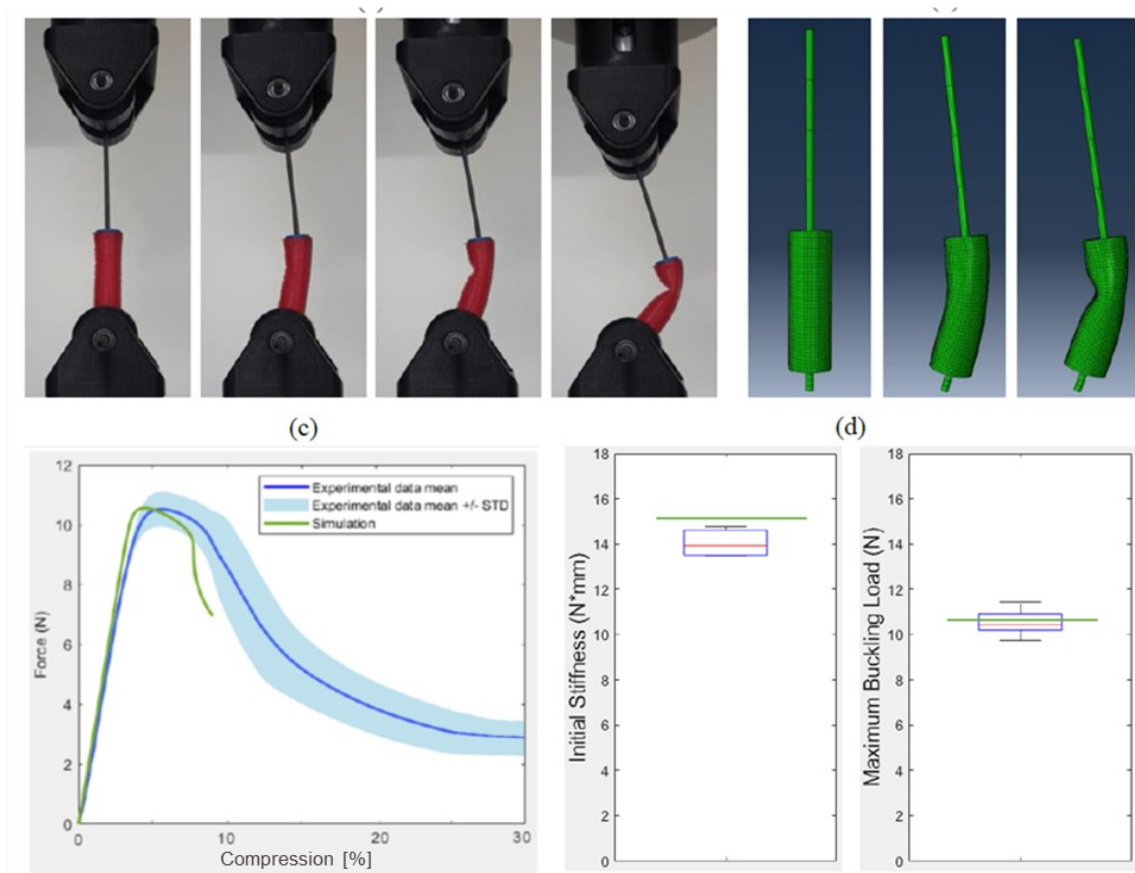


Figure 37. Dual-stiffness strut characterization.  
(a) Pictures in sequence of the real experiment. (b) Pictures in sequence of the FEM simulation (c) Force vs Displacement results of hardware and simulation experiments. In Blue the average curve of hardware experiments. In light blue the standard deviation. In green the simulated curve. (d) bar plots to compare initial stiffness and buckling load of real experiments and simulations.

To study the dual stiffness behavior of the strut, we performed experiments in hardware and developed a FEM simulation using the Abaqus software. For both hardware and simulation, we used a simplified geometry of the strut without the ABS rigid caps that are used for assembly of the cables in the module (Figure 37(a-b)). The material used for the tube has the mechanical properties of the NinjaFlex (Young Modulus of 12Mpa and Poisson's ratio of 0.48), while the carbon tube and rigid attachments to the tube are rigid (Young's modulus of 107 MPa and Poisson's ratio of 0.3). As for the real strut, the tube measures 30 mm but its effective length is 22 mm as the rigid parts fit inside.

To characterize the mechanical behavior of the hardware prototypes, we did compression tests on an Instron 5965. The struts are inserted in special supports allowing its ends to rotate (Figure 37a). A compression displacement of 30% of the length is applied on the top of the strut while recording the reaction force along the vertical axis. With the recorded force versus displacement plot, we can extract the initial stiffness and the maximum buckling load. The stiffness is the slope of the initial linear part of the curve, and the maximum buckling load is the maximum load, at which there is a sudden change in stiffness ( $\Delta \text{Stiffness} > 20\%$ ). Since the struts are assembled by hand and the print quality differs slightly from one strut to another, the stiffness and the buckling load also differ. Therefore, we tested three different struts, to study the average and the standard deviation of the buckling behavior.

In the simulation, the strut has the same dimensions and mechanical properties and has ball-joint constraints applied at its ends as with the real experiment. A downward displacement is applied on its top end and the reaction force is recorded (Figure 37b).

The results are presented in Figure 37c and d and confirm that the struts have a dual-stiffness behavior. Initially, the struts are stiff and after the buckling of the flexible part, the reaction force decreases, which is the expected behavior. Due to limitations in simulating the post-buckling behavior, the simulations stops at around 10% compression due to the inability to simulate the contact between the inner surfaces of the elastic tube after buckling. Nevertheless, we observe very similar buckling loads and a slightly higher initial stiffness in simulation Figure 37d. This may be due to defects in the thickness of the 3D printed flexible tube which can lead to not uniform thickness and, in turn, lower stiffness.

### 5.2.1 Parametric study to design stiffness and buckling load

Both initial stiffness and buckling load of the strut can be programmed by changing the thickness  $W$  of the flexible tube. We performed simulations to assess how the thickness influences the performances. In Figure 39 are presented the results of the simulations. The initial stiffness  $S$  and the buckling load  $B$  can be programmed with the following functions:  $S = 17xW$ ;  $B = 18.8xW + 1.5$

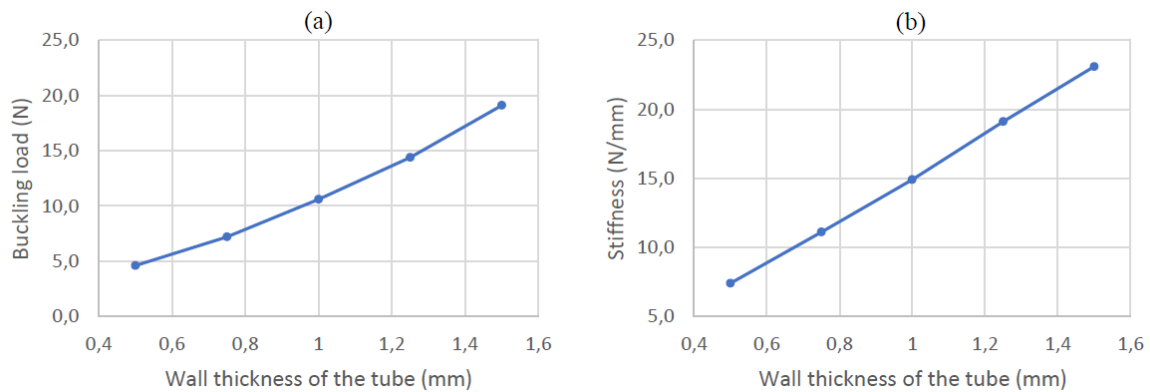


Figure 39. The programmability of the dual-stiffness behavior.  
(a) Buckling load vs tube's thickness. (b) Initial stiffness vs tube's thickness.

### 5.3 Dual-stiffness tensegrity module design and characterization

To assess the effectiveness of the proposed strategy, we implement the dual stiffness on a 3-strut tensegrity structure that can function as a module for a modular tensegrity robotic kit Figure 40a and d. The 3-strut tensegrity is one of the simplest three-dimensional tensegrity structures proposed in the literature to create lattices [108]: it consists of 3 struts and 9 cables.

We used the 3-strut tensegrity to develop a dual-stiffness module composed of dual-stiffness struts and cables made of rigid Kapton Figure 40c. The cables have a hole-to-hole length of 55 mm, a thickness of 140  $\mu\text{m}$ , Young's modulus of 2500 MPa, and Poisson's ratio of 0.3. They are cut with a laser cutter and inserted on a screw mounted on top of the strut, a nut system is used to avoid slipping out of the cables Figure 40b.

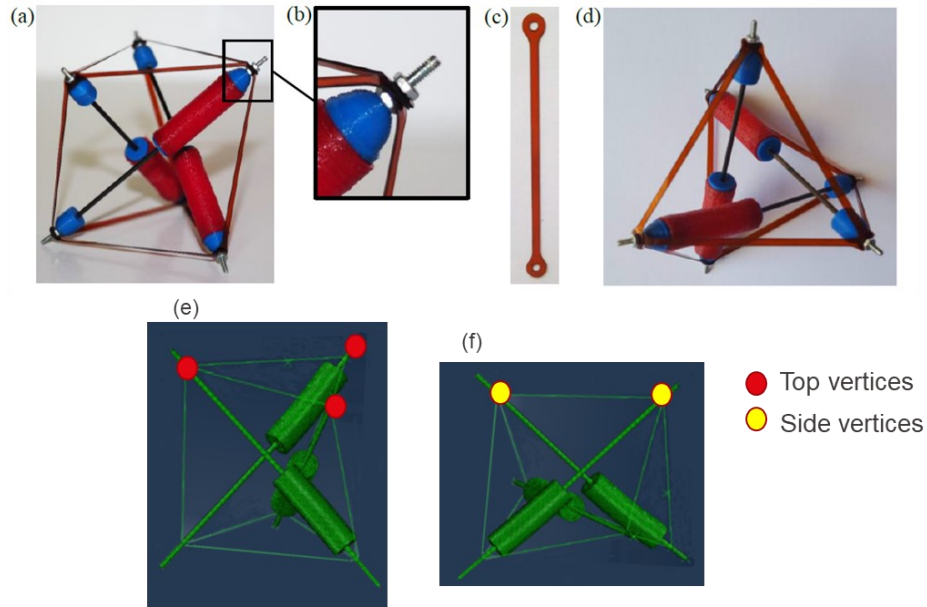


Figure 40. Dual-stiffness tensegrity module design.

(a) Dual-stiffness 3-strut module. (b) Enlarged section of the cables' attachment system. (c) Rigid cable made of Kapton. (d) Top view of the dual-stiffness module. (e) 3-strut FEM model with highlighted top vertices. (f) 3-strut FEM model with highlighted side vertices.

The 3-strut model is composed of the same dual-stiffness strut models previously characterized connected by truss elements to model the cables. The truss elements have the same cross-section of the cables (i.e., 0.28 mm<sup>2</sup>) and the material properties of Kapton (Young's modulus of 2500 MPa and Poisson's ratio of 0.3). These truss elements are set to act like cables, being stiff in tension and completely soft in compression.

To assess the dual-stiffness behavior of the module, we performed compression experiments in both hardware and simulation from two different directions: top (applying a vertical load equally distributed on the three top vertices Figure 40e) and side (applying a vertical load equally distributed on the two side vertices Figure 40f).

In both hardware and simulation, the bottom vertices are attached to a platform with ball-joint constraints to allow rotations of the struts (Figure 41a and b). A displacement is applied in the tested direction to compress 30% of the structure while the load is recorded. Each experiment is repeated with 3 different modules and the average with standard deviation is plotted. The maximum buckling load is recorded as the load before the stiffness changes abruptly (stiffness change > 20%). The initial stiffness is calculated with a linear interpolation of the curve before the buckling load.

The Results for the top direction are presented in Figure 41 c and d and confirm the dual-stiffness nature of the module. The higher stiffness of the results in the simulation may be explained by the loose cables manually assembled on the modules. The Results for the side direction are presented in Figure 42 a and b and confirm the dual-stiffness nature of the module also in the side direction. The higher stiffness of the results in simulation, as for the top results, may also be explained with the loose cables manually assembled on the modules.

These results confirm that by implementing a dual-stiffness strut in a rigid tensegrity module is possible to develop tensegrity structures exhibiting dual-stiffness behavior when compressed by external loads.

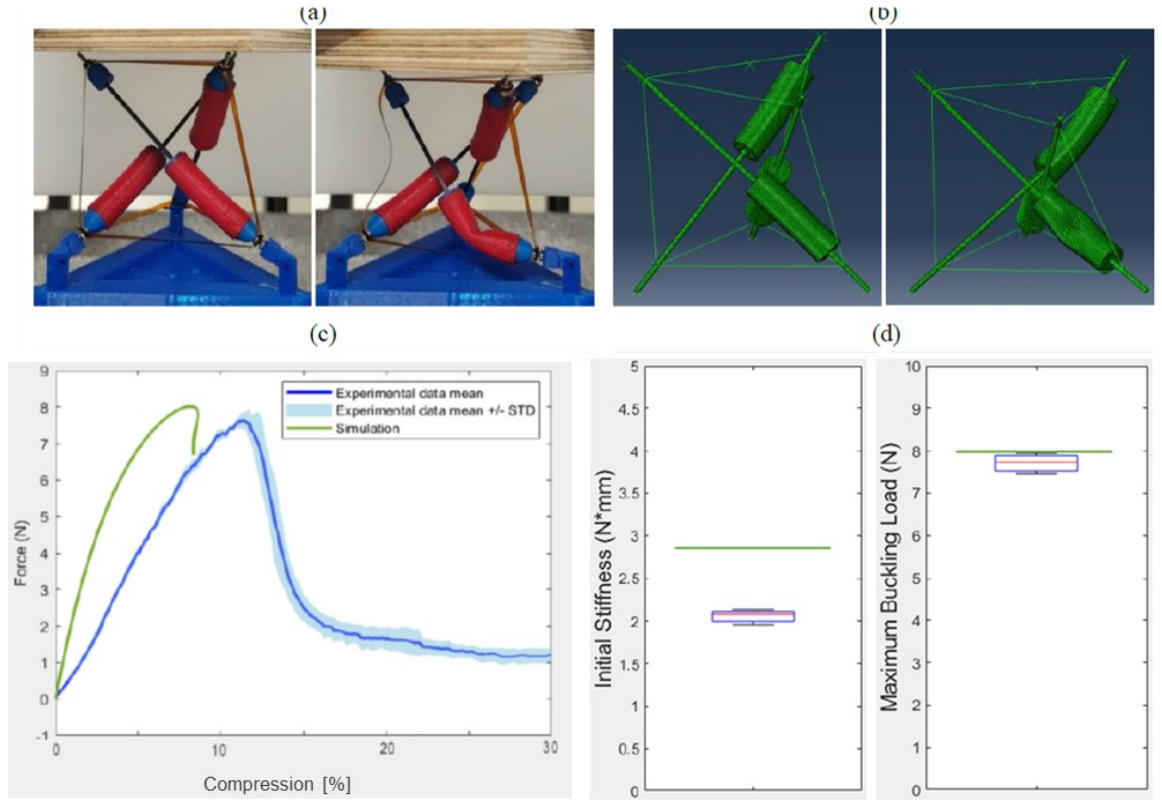


Figure 41. Dual-stiffness module characterization.

(a) Pictures of a module buckling during a compression test. At the bottom the platform that allows rotation of struts with ball-joint constraints. (b) Pictures of a module buckling in the simulation. (c) Comparison of the displacement vs load curve during top compression of the module. In blue the average curve of the hardware experiments. In light blue the standard deviation. In green the simulated curve. (d) Bar plots to compare initial stiffness and buckling load of real experiments and simulations.

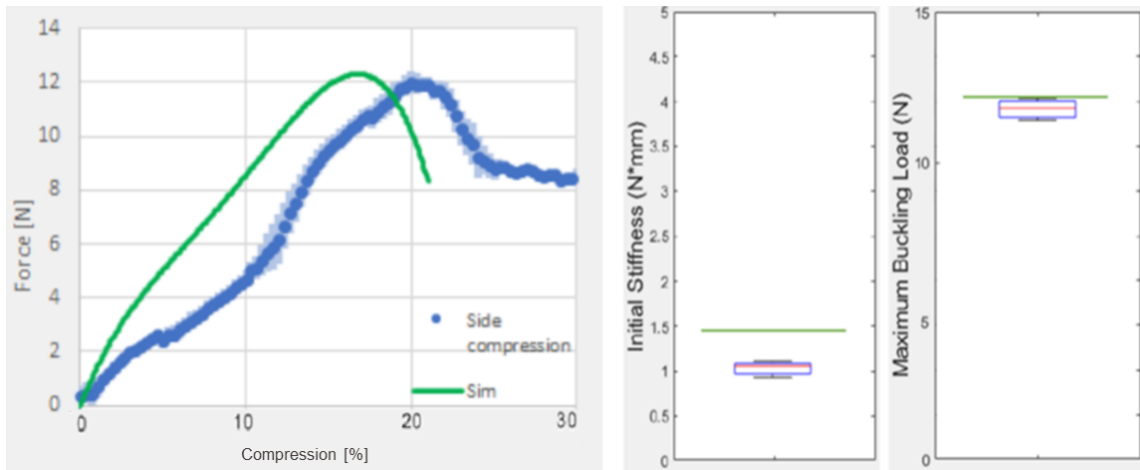


Figure 42. Dual-stiffness module characterization.

(a) Comparison of the displacement vs load curve during side compression of the module. In blue the average curve of the hardware experiments. In light blue the standard deviation. In green the simulated curve. (b) Bar plots to compare initial stiffness and buckling load of real experiments and simulations.

## 5.4 Dual-stiffness tensegrity robot demonstrators

To demonstrate the potential of the dual-stiffness strategy to design collision-resistant robotic applications we used 3-strut dual-stiffness tensegrity modules to assemble two robotic demonstrators: a drone quadcopter and a wheeled rover. Both demonstrators are mechanically tested with an Instron machine to assess their dual-stiffness behavior. Moreover, crash tests have been performed to assess from which height they can safely fall.

### 5.4.1 Dual-stiffness Tensegrity drone quadcopter

The dual-stiffness tensegrity drone quadcopter is composed of four dual-stiffness tensegrity modules connected in a frame where the microcontroller, battery, and propeller are mounted.

The frame is composed of four modules (Figure 43a and b). The modules are connected by rigid ball-joint-like connectors to allow rotations of the struts and therefore deformations of the modules after buckling (Figure 43c). The connectors are 3D printed in ABS. The frame weighs 30 grams, with dimensions of 130 x 150 x 70 mm. At the geometrical center of the frame, the battery and autopilot board are mounted on a 3D printed ABS platform which is connected to the frame with four ball-joint constraints that allow rotations of the struts after buckling Figure 44d. The four motors - required for a quadcopter drone configuration - are mounted on four modified connectors among couples of modules' vertices Figure 44c. The autopilot is a BetaFPV F4 2-4S AIO Brushless Flight Controller 12A (BLHeli\_S), and the motors used are some DYS BE1104-4000KV motors with 3 blades 65 mm HQ propellers.

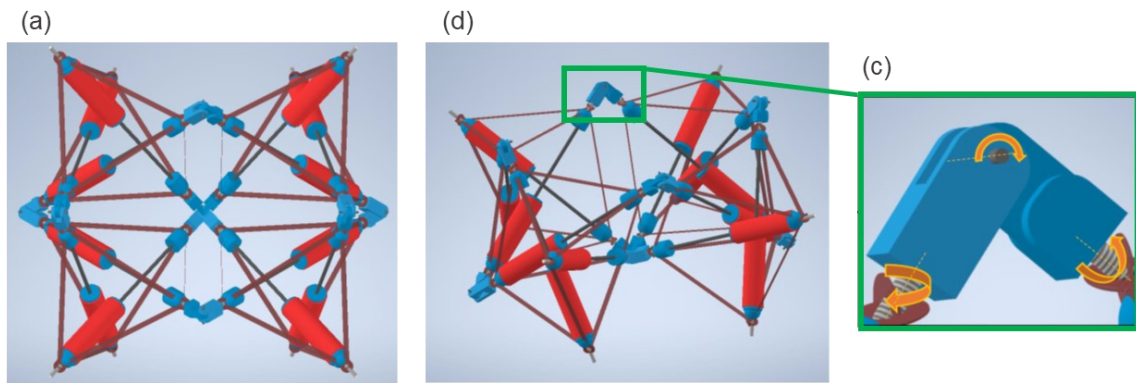


Figure 43. Four modules dual-stiffness frame.

(a) Top view frame CAD. (b) Isometric view frame CAD with highlighted rigid ball-joint connector. (c) Detailed view of the connector and arrows indicating free rotations.

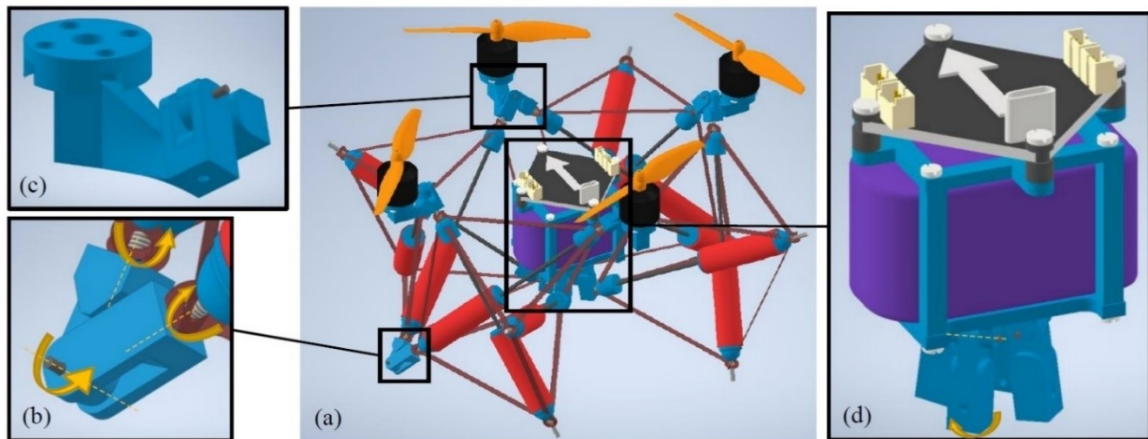


Figure 44. Dual-stiffness Tensegrity drone quadcopter design.

(a) CAD image of the drone with highlighted the ardupilot and battery mounted in the geometrical center (d), a ball-joint connector (b), and a modified connector to mount motors (c).

To validate the dual-stiffness behavior of the prototype of the tensegrity-based drone quadcopter (Figure 45a) we performed mechanical tests with an Instron machine 9560 compressing the drone from the top (Figure 45) and side directions up to 30% of its dimension while recording the loads. The experiments are repeated three times.

The results in Figure 45 confirm that the drone has dual stiffness behavior in both directions although a two-step initial stiffness is shown for the top direction. This may be because one of the modules has a defect of 3d printing manufacturing that leads to an early first partial buckling of the structure.

Moreover, we performed crash-landing experiments to test the collision resistance of the drone. We switched off the drone during hovering from different heights assessing that it can survive crashes up to 100% of the times up to a height of 2 meters after which the connector of the motors breaks. A snapshot sequence of a collision with deformations due to the buckling is shown in Figure 45e-h.

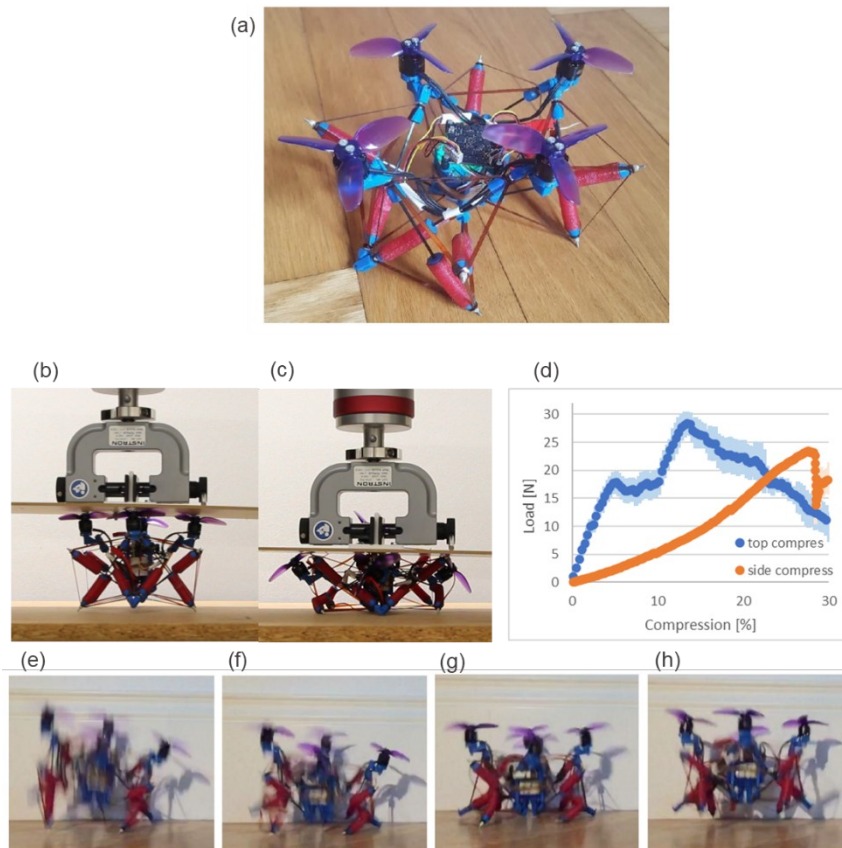


Figure 45. Dual-stiffness tensegrity drone characterization.

(a) Prototype of the dual-stiffness tensegrity drone. (b-c) Snapshots of a top compression experiment of the drone. (d) Comparison of the top (in blue) and side (in orange) compression experiments. Curves are average of three experiments, in light color is represented the standard deviation. (e-h) Snapshots of a drone collision with the ground. In f and g the buckling of the struts is more evident. In h the drone is bouncing back reassuming its shape after the collision.

## 5.4.2 The wheeled rover demonstrator

The dual-stiffness tensegrity wheeled rover is composed of two dual-stiffness tensegrity modules connected in a frame where microcontroller, battery, and motors equipped with wheels are mounted.

The frame is composed of two modules (Figure 46). The modules are connected by rigid ball-joint-like connectors to allow rotations of the struts and therefore deformations of the modules after buckling (Figure 46). The connectors are 3D printed in ABS. The frame weighs 15 grams, with dimensions of 130 x 70 x 70 mm. At the geometrical center of the frame, a microcontroller board is mounted on a 3D printed ABS platform which is connected to the frame with three ball-joint constraints that allow rotations of the struts after buckling Figure 46. The battery is encapsulated in a flexible 3D printed cover and

attached to the microcontroller frame throughout an elastic beam. The two motors are mounted at the two extremities of the connected modules they are kept in position at the center of the modules' triangular faces by cables attached to the faces' vertices. The microcontroller is a TinyDuino, and the motors used are Pololu 5601 with stall torque of 2.1kg/cm. The two wheels are 3D printed with an elastic material (Ninjabflex).

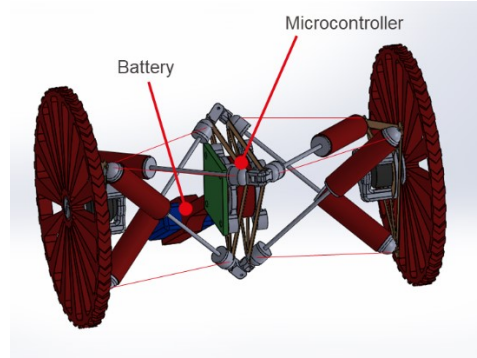


Figure 46. Dual-stiffness wheeled rover design.

To validate the dual-stiffness behavior of the prototype of the tensegrity-based drone quadcopter we performed mechanical tests with an Instron machine 9560 compressing the rover from the top (Figure 47) and side directions up to 30% of its dimension while recording the loads. The experiments are repeated three times. The results in Figure 47 confirm that the rover has dual stiffness behavior in both directions.

Moreover, we performed crash-landing experiments to test the collision resistance of the rover. We made the rover fall from different heights assessing that it can survive crashes up to 100% of the times up to a height of 5 meters after which the cables may break. A snapshot sequence of a collision with deformations due to the buckling is shown in Figure 47e-h.

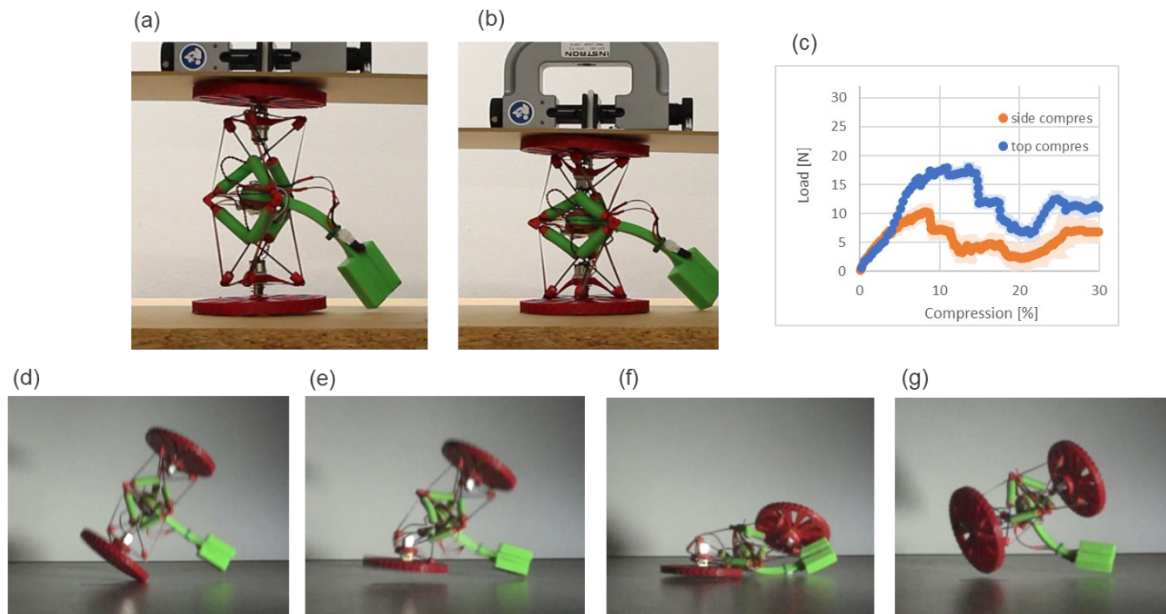


Figure 47. Dual-stiffness wheeled rover characterization.

(a-b) Pictures of a side compression experiment of the rover prototype. (c) Comparison of the top (in blue) and side (in orange) compression experiments. Curves are average of three experiments, in light color is represented the standard deviation. (d-g) Snapshots of a drone collision with the ground. In f and g the buckling of the struts is more evident. In h the drone is bouncing back reassuming its shape after the collision.

## 5.5 Discussion

The dual-stiffness tensegrity modules and assemblies described in this project offer collision resilience capability. While the dual-stiffness struts described in this project were based on Ninja flex elastic tubes, other materials and metamaterials that make use of elastic instabilities can be used to customize dual-stiffness properties such as initial stiffness and buckling load of tensegrity modules and assemblies [128] [129] [130].

Moreover, given the scalability of tensegrity structures, the proposed dual-stiffness strategy could be applied for modular systems at different scales. For example, large dual-stiffness modular tensegrity structures could serve as a scaffold for lightweight and collision resilient modular bridges, infrastructures, manipulators, antennas, and buildings with the ability to survive unexpected external loads [109]. Human scale dual-stiffness modular tensegrity are promising for modular robotic frames [110] and other collision-resistant structures such as (e.g. wings, arms, tails, fingers, etc.), while smaller scale dual-stiffness modular structures could be useful to minimally invasive surgery devices where the ability to soften passively after a certain load threshold can increase safety and protect tissues [111].

The overall mechanical performance of the structures considered in this project, including the initial stiffness and buckling load, is essentially influenced also by the applied geometric topology and boundary conditions, as well as the mechanical parameters (e.g., length and initial stiffness) of the cables and connectors. It is therefore fundamental to develop appropriate modeling tools to predict mechanical performances in different application scenarios involving different morphologies, scales, and boundary conditions. Improved modeling of dual-stiffness tensegrity assemblies could also pave the way to the development of more accurate simulations to predict stiffness change and a reduction of dual-stiffness struts required to achieve desired collision-resistant morphologies.

In conclusion, we believe that the presented dual-stiffness strategy for tensegrity structures can lead to the development of highly resilient, lightweight, and safe robots.

# Chapter 6 Heuristic algorithms to design task-optimal morphology, stiffness, and control of modular tensegrity robots.

Publication Note: The material presented in this chapter is partially adapted from:

• D. Zappetti, J. M. Bejjani, e D. Floreano, «Evolutionary Co-Design of Morphology and Control of Soft Tensegrity Modular Robots with Programmable Stiffness», arXiv:2101.11772 [cs], gen. 2021, <http://arxiv.org/abs/2101.11772>.<sup>[170]</sup>

The first author contribution was to conceptualize the design strategy, design the experiments, to analyse the results and to write the manuscript.

In this chapter, we present preliminary results and insights on using heuristic algorithms to design task-optimal morphologies, stiffness, and control of modular tensegrity robots. The chapter is divided into three parts.

In the first part of the chapter, we demonstrate the feasibility of using a heuristic algorithm to design soft tensegrity modular robots with open-loop controllers. Moreover, we demonstrate the importance of including the cables' stiffness as a design parameter of the tensegrity robot optimization.

In the second part of the chapter, we present preliminary results on co-evolving morphology, stiffness, and control of tensegrity modular robots. Moreover, we give insights on how to perform the sim-to-real transfer of modular tensegrity robots evolved with the presented design method and we show the first successfully transferred to reality modular tensegrity robot.

## 6.1 Introduction

The design of morphology, control, and actuation placement of tensegrity robots is still a difficult task. As discussed in chapter one, most tensegrity robots have simple polyhedral tensegrity bodies (i.e., tensegrity structures resembling polyhedral convex solids) and intuitively placed actuators. Moreover, tensegrity robots in literature are not optimized in terms of stiffness. These designs could be suboptimal according to the task or the goal of the robot. Therefore, in chapter two, we proposed a modular approach, using simple and easy to assemble tensegrity structures with programmable stiffness and actuation as building blocks for constructing diverse robotic morphologies with programmed stiffness. However, how to optimally connect, program the stiffness, and control each module, according to a specific task, is still an open challenge.

Recently, researchers have applied heuristic algorithms, such as Evolutionary Algorithms (EAs) to design soft modular robots. Designing soft robots and soft modular robots is notably difficult due to the hard-to-model dynamics of soft materials and the non-trivial interactions between morphology and controller [7]. These difficulties, together with the lack of analytical methods, make Evolutionary Algorithms (EAs), coupled with physics simulators, one of the most promising design tools [75]. EAs can discover unconventional high-performing solutions and provide a pool of possible designs by "illuminating" the design space [132]. This is a significant aspect since it determines the number of eligible candidates for the physical realization.

Moreover, Evolutionary algorithms have been shown to be a promising approach to co-design robot morphologies, their stiffness, and control [133] [134] [75] [135]. So far evolutionary algorithms have been successfully applied to evolve tensegrity morphologies without control [136] or control strategies of fixed tensegrity morphology [59] [137] [138] [77]. In this first part of the chapter, we apply evolutionary algorithms to perform co-evolution of body and brain (e.g. morphology and control) of tensegrity modular robots, and we show the importance of determining the appropriate stiffness in tensegrity soft robots given a specific task. Indeed, we show how changing the stiffness of the modules -remaining in a soft domain- affects not only the body shape and control of the robot solution but also evolves different locomotion strategies.

## 6.2 Co-evolution of body and brain of the tensegrity modular robots with programmed stiffness

In this section, we describe how we perform simulations and body-brain evolution of modular tensegrity robots with programmed stiffness based on our design. For co-evolving body-brain, we developed a Modular Tensegrity evolution platform named: “TensSoft”, which is built with additional libraries on top of the NASA Tensegrity Robotics Toolkit (NTRT) [72]. The NTRT allows simulating modular tensegrity robots based on our current hardware including friction with the ground and cable-cable interaction. “TensSoft” implements input structure definition for modular tensegrity robots based on our current modular design. The input allows the user to define any robot with a tree-shaped structure.

We also implemented an evolutionary algorithm layer named “TensSoft Evolution” that can evaluate and evolve the body and brain of modular robots to optimize a certain behavior with a fitness function. For that layer, we used the “GAlib 2.4” library for genetic algorithms developed at MIT [26].

The evolution layer currently uses a direct encoding where each robot is defined by two types of genes; morphological genes that define the morphology and control genes that define the open-loop input signals for each independent module of the structure. The morphology encoding includes global properties, affecting the entire robot, and local ones, specific to each module. In this project, the global gene is only the number of modules. Instead, the local morphological ones include only the number  $p$ , which identifies the triangular face that is connected to the next module in the chain. This influences also how the robot is actuated since the servomotor acts always on the same pair of faces.

The control genes affect the controller parameters. The control parameters can modulate the open-loop servo-motor signal of each module. The signal given is a sawtooth modulated by the amplitude, frequency, and offset parameters (Figure 48).

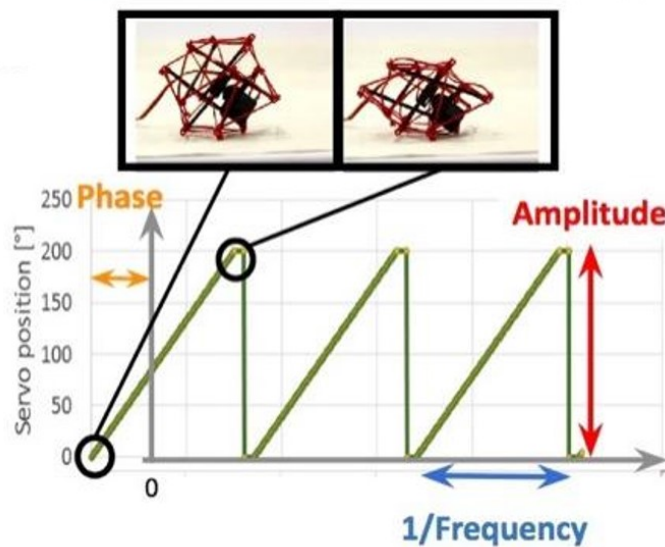


Figure 48. Module actuation control parameters.

We use a binary genome from the “GAlib” library for the encoding. The genetic layer sends the configuration it wants to test to the simulator which returns the fitness value.

The allowed mutations included by the genetic algorithm are the addition of a new module in a random position; the deletion of a random module in the chain; the change of the connection face to the next module (local mutation). For the control, a mutation is applied to each module to the frequency, amplitude, and phase.

In this project, the evolutionary algorithm used is the “ $\mu+\lambda$ ” [139]. A highly exploitative algorithm that converges towards a single solution for each run.

In this first investigation, a few constraints have been introduced. The connected faces in between modules are not changed resulting in chain modular structures.

## 6.2.1 Results

Ten experiments of body-brain evolution were initially run to validate the effectiveness of the “TensSoft Evolution” body-brain co-evolution platform and to investigate the effect of different modules’ stiffness. The objective of the evolution (i.e. fitness function), for all the experiments, was to maximize the distance reached by the robot after 10 seconds.

### Experimental conditions

We ran two sets of experiments to compare robotic modules with two different stiffnesses. The two sets were composed of 5 experiments each for a total of ten experiments. These were all initialized with different random seeds. The following ranges were applied for the evolved parameters.

- Range of number of modules: 2-9
- The frequency range of module actuators: 0-1 Hz
- Amplitude range of module actuators: 0-1
- Offset range of module actuator: 0, 1.57, 3.14, 4.71

The evolutionary algorithm settings were:

- Number of Generations: 200
- Number of Individuals: 50

The previous actuation parameters were chosen to match the servo capabilities used in the real hardware. The only changing parameter between the 2 sets was the modules’ stiffness:

- HIGH Stiffness = 10 MPa
- LOW Stiffness = 100 MPa

Both stiffnesses are in the elastic domain similar to the soft materials ones.

Table 2. Set of experiments and results.

Evolution	1	2	3	4	5	6	7	8	9	10
Stiffness	High	High	High	High	High	Low	Low	Low	Low	Low
Best Individual's number of modules	8	8	7	8	6	2	2	3	2	2
Best Individual's Fitness	307	320	450	339	405	136	212	175	172	155
Best Individual's Strategy	CAT	CAT	CAT	CAT	CAT	Hop	Hop	Hop/Rol	Hop	Hop/Rol

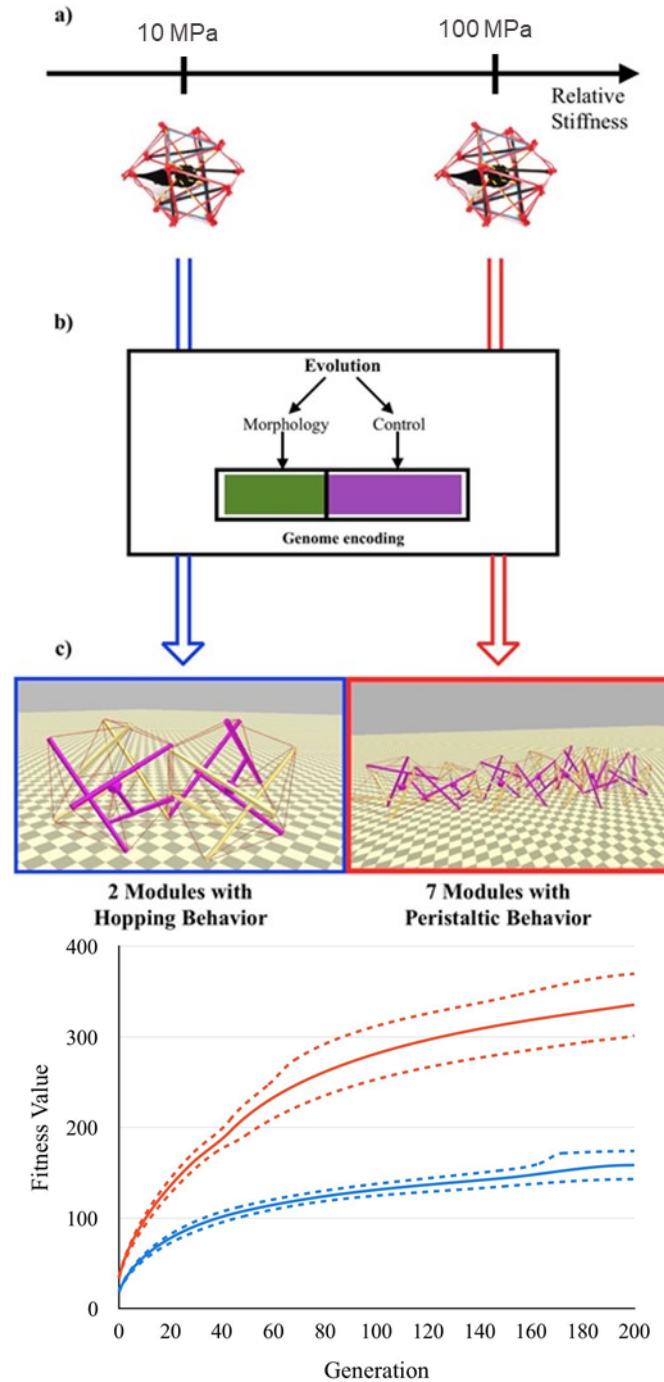


Figure 49. Co-evolution results with two different modules' stiffness.

(a) Stiffness scale of the module. (b) Co-evolution of morphology and control with a sequential genome. (c) Different module stiffnesses (Blue soft and red ten times stiffer) lead to different average fitness, morphology, control, and locomotion strategy.

Table 2 is a summary of all different evolution conditions and results.

The evolution with only stiffer modules favored long robots of 6-8 modules and evolved locomotion strategies similar to that of a caterpillar (CAT) (e.g. activation in longitudinal sequence observed like in peristaltic locomotion). See an attached movie for reference [140]. The evolution with lower stiffness modules consistently selects robots composed of only 2-3 modules and evolves a hopping behavior (Hop) or a rolling on its side behavior (Rol). In the Hop/Rol behavior, one module is compressed to store energy like a spring and one-two additional modules are used to orient the re-expansion of it to propel the robot forward or sideward. See the attached movie for reference [141].

The different evolutions gave consistently similar results for the same stiffness in both design and control strategies. Our hypothesis to explain the drastic difference in results between the two sets of experiments is that peristaltic locomotion requires a specific stiffness and length of the robot for a certain scale of the tensegrity modular robot, and friction of the ground [142]. This could mean that in the low stiffness experiment it is not optimal to evolve a caterpillar structure and behavior. While other approaches like rolling or hopping are more efficient locomotion strategies at lower stiffnesses. This demonstrates how the stiffness of a tensegrity robot is an important design parameter.

## 6.3 Co-evolution of body, brain, and stiffness of tensegrity modular robots

In the previous section, we have discussed how the stiffness of tensegrity robots is important in determining task-optimal morphology and control strategy. In soft robotics, it has been shown that is possible to exploit the dynamics of the soft system to perform more efficiently in locomotion, much like animals and natural systems do [75]. Indeed, the behavior of robotic systems is not due to their control structure and morphology only but is also affected by the material properties of the elements composing the morphology. However, only a few cases exist in literature where morphology, control, and stiffness are co-optimized [143]. Moreover, they are demonstrated only in simulation. In this work, we use our modular soft tensegrity hardware platform coupled with an evolutionary and simulation software platform to design soft tensegrity modular robots and investigate the importance of optimizing the cable's stiffness along with their morphology and control. Moreover, we present first insights and preliminary results on a data-driven technique to improve the sim-to-real problem and transfer to reality tensegrity modular robots optimized in terms of morphology, stiffness, and control.

### 6.3.1 Method

In this project, the morphology encoding includes an additional global property affecting the entire robot: the stiffness. As in the previous study, the second global property is the number of modules, and the local ones, specific to each module, are: the number  $\rho$ , which identifies the triangular face that is connected to the next module in the chain, and the three control parameters: frequency, amplitude and offset.

The allowed mutations by the genetic algorithm include the addition of changing the stiffness of the entire robot. The other mutations like in the previous project are the addition of a new module in a random position; the deletion of a random module in the chain; the change of the connection face to the next module (local mutation). For the control, a mutation is applied to each module to the frequency, amplitude, and phase.

In this project, two genetic algorithms are used: ViE and MapElite.

ViE is an algorithm that adopts a different selection method. It does not choose the fittest individuals, but one that removes from the population all the individuals that do not comply with specific requirements. To accomplish this, ViE uses a viability boundary, which is a dynamic region of the solution space. At each algorithm step, the boundaries are updated to converge towards either the optimal or a known a-priori target value. To further maintain the population size, at each algorithm step the population is split into families according to their lineage. Then the selection process randomly draws one family at a time, based on its size with respect to the whole population, and from it one individual is sampled to be reproduced, repeating the process until a maximum population size is reached again [144]. This algorithm allows to more efficiently explore the design space without sacrificing the quality of the found solutions [144].

MAP-Elites algorithm [132], differently from the other optimization algorithms uses the Multidimensional Archive of Phenotypic Elites as an illumination technique to provide a global view of high-performing solutions throughout a feature space. In this manner, it is possible to uncover information on specific interested solution properties that highly influence the resulting fitness. This algorithm allows to better explore the design space at the expense of the quality of solutions.

### 6.3.2 The sim-to-real problem

A major challenge for evolved robots is the accurate reproduction of simulated robotic results in reality: namely the *sim-to-real problem*. To solve this problem the simulation must be as close as possible to the real physical system. We individuated that the main discrepancy between the simulated module and the real one is in the kinematics of the actuation system. In the real hardware, a servomotor rotates to pull six cables which in turn compress the module by moving six

vertices of two opposite faces of the tensegrity module Figure 50. In the previous project, we applied the same pulling load and contraction to each of these six cables, however, due to manufacturing asymmetries the loads and kinematics of the six vertices are different.

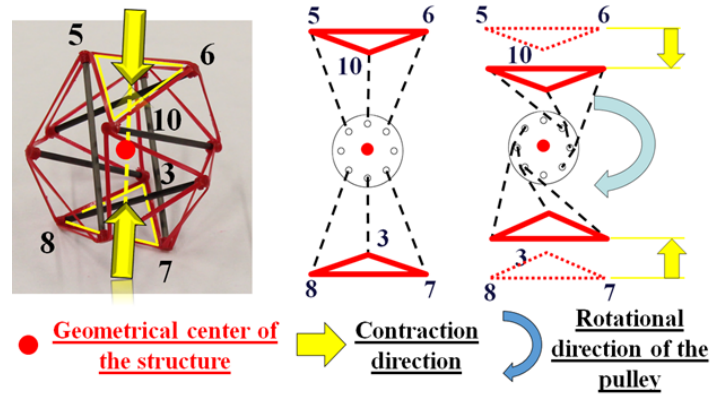


Figure 50. The actuation system of the module.  
In dashed lines are highlighted the six cables used for compressing the module.

We approached this problem similarly to recent works [145], where Artificial Neural Networks (ANNs)—trained on real data—were used to approximate the output kinematics in simulation. Our approach consists of recording the kinematics of the six actuated vertices during a complete cycle of servomotor (i.e., from 0 to 180 degrees) using an Optitrack motion capture system. We then used these recorded data to train an ANN to approximate the vertices motions in the Tensoft simulated environment.

Specifically, we recorded the motion of each of the six vertices of nine Tensegrity modules with three relative stiffness values (0.1, 0.5, 1 - where 0.1 and 1 are the two extremes of the stiffness range considered). By recording multiple modules with the same stiffness, we allowed the ANN to generalize over the inevitable differences caused by manufacturing. While, by recording different stiffnesses, we allowed the ANN to generalize over the kinematic differences caused by the different modules' stiffness. Figure 51 shows an example of a comparison of data recorded from hardware (Figure 51a) and calculated by the model in the simulation (Figure 51b). The relative cable length represents how much the cable is shortened by the servomotor which can assume an angle between 0 and 180 degrees. The results for different modules and different stiffness show an average error of 5 % of the ANN in predicting lengths of the actuated cables.

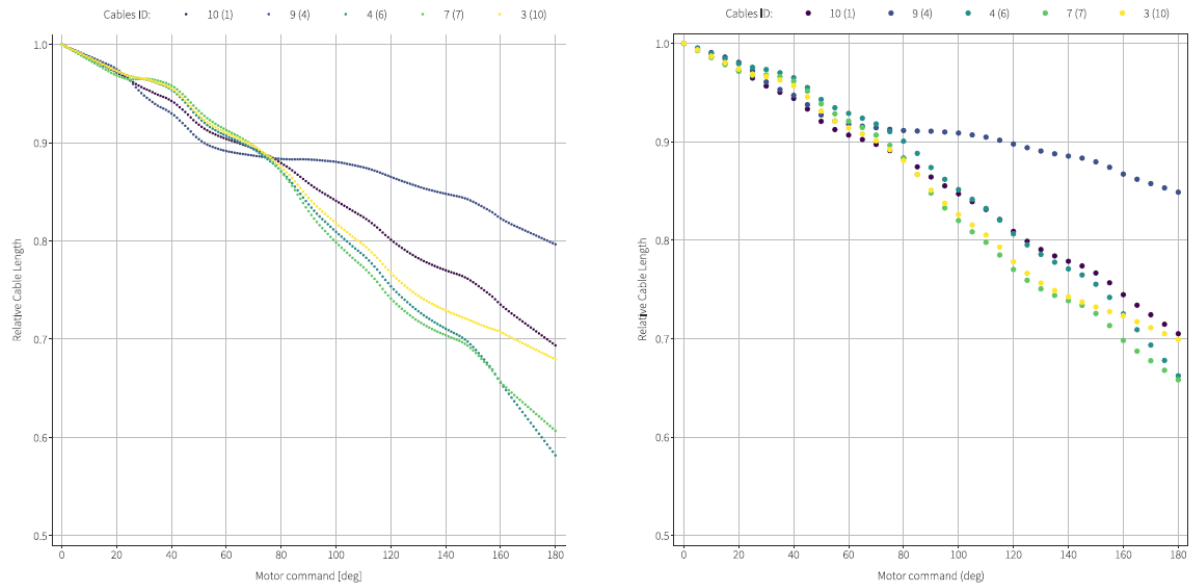


Figure 51. The ANN model prediction of actuated cable lengths.

(a) Real hardware data for a module of stiffness 0.1, each color is one of the six different cables. (b) Data in simulation for the same module predicted by the ANN model.

### 6.3.3 Results

We ran two sets of experiments to compare results from the two different algorithms and assess the impact of including the stiffness parameter in the evolutions. The two sets were composed of five experiments each for a total of ten experiments. These were all initialized with different random seeds. The fitness and task are the same as the previous project. The following ranges were applied for the evolved parameters.

- Range of number of modules: 2-9
- The frequency range of module actuators: 0-1 Hz
- Amplitude range of module actuators: 0-1
- Offset range of module actuator: 0, 1.57, 3.14, 4.71
- Stiffness of the robot: 0.1, 0.2, 0.3, 0.4, 0.5, 0.6, 0.7, 0.8, 0.9, 1. Where the values are relative values of 100Mpa

The results in Figure 53 and Table 3 show that the ViE algorithm can find unique solutions with higher fitness. However not a clear trend is observed on the relationship between stiffness and fitness. Isolated good solutions can be found with different stiffness values in the design space. However, worse solutions (stiffness lower than 70% fitness of the best solutions) are found with stiffness values above 0.6, suggesting that these algorithms can allow finding areas in the design space where more high-quality solutions can be found.

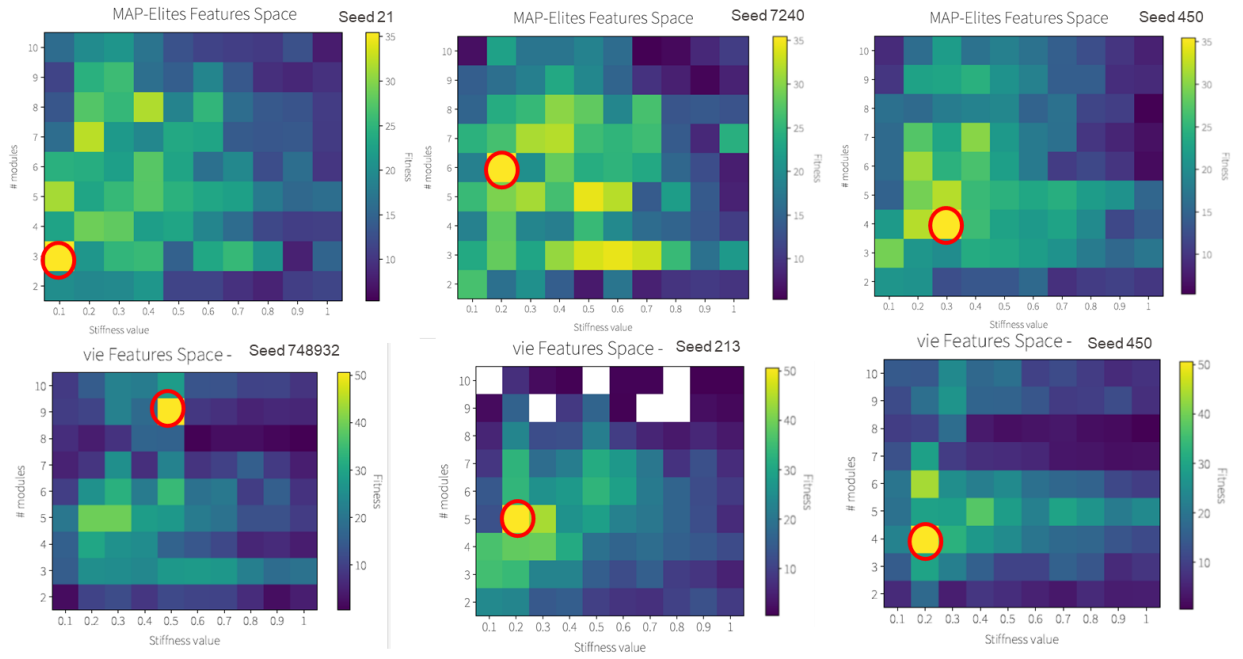


Figure 52. Evolutionary runs feature spaces results. The red circles highlight the best unique solution per run.

Table 3. Aggregated results of the evolutionary experiments.

Algorithm	Fitness best mean	STD	Stiffness average best
Map-Elite	31	3.51	0.2
ViE	46	5.10	0.3

To assess the “sim-to-real” performances of such a method we manufactured in hardware one of the best robots from the previous experiment (i.e. ViE seed 748932). For simplicity, we built the robot with the least number of modules and with a novel locomotion behavior that we named sidewalk (Figure 53 right). The sidewalk locomotion consists of moving in a direction transversal to the chain length direction. The robot consists of three modules and uses the two external modules as wheels to push its body forward in the transversal direction. A sequence of images of such locomotion is presented in Figure 54. A comparison of the trajectories is presented in Figure 53 showing a good match of the direction but almost half the speed of the simulated robot. This may be due to the modeling of the friction in the simulation or inertia of the electric cables in the real hardware that -even if very lightweight- may slow down the robot. These results suggest that these algorithms can be exploited to find novel locomotion behaviors not intuitively imagined by human designers.

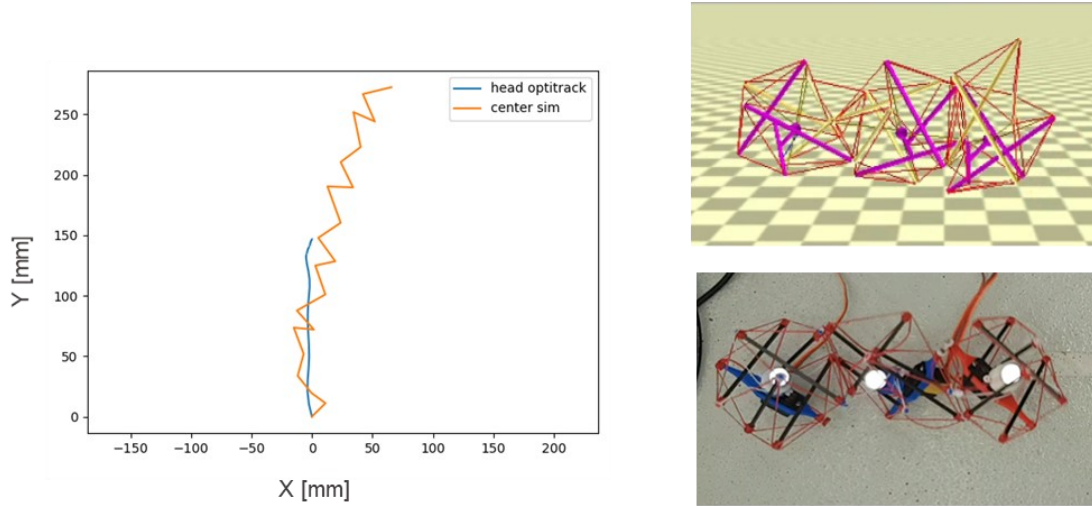


Figure 53. Simulated and real robot trajectory comparison.

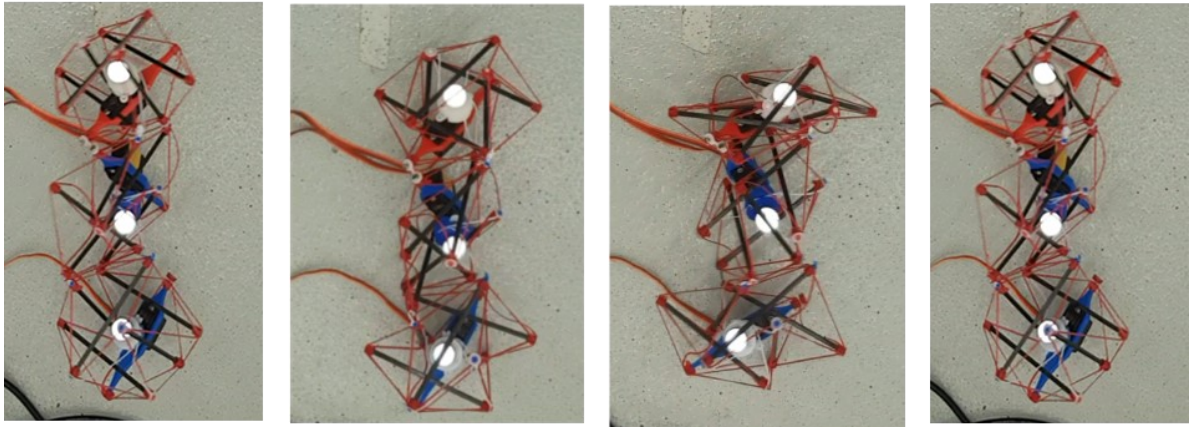


Figure 54. A sequence of images of an evolved robot locomotion in hardware.

## 6.4 Discussion

In this work, we presented our modular strategy to develop soft tensegrity robots and we showed that co-evolution of body and brain is an effective design strategy. Moreover, we showed the importance of co-optimizing body stiffness by demonstrating the emergence of novel different locomotion strategies and higher quality of the solutions for the same task. Moreover, by applying a data-driven approach we improved the sim-to-real problem and we presented preliminary results on transferring to reality modular tensegrity robot co-optimized in terms of morphology, stiffness, and control. Although the sim-to-real problem is not fully solved our preliminary results suggest that evolutionary algorithms can be exploited to find novel locomotion behaviors not intuitively imagined by human designers.

At the moment the “TensSoft” platform allows only co-evolution of chain-like structures. However, in the future, the implementation of tree-structures and lattices may further expand the ability to find task-optimal morphologies. Future work will also investigate the possibility of evolving modules with different morphologies including the bending modules presented in chapter 3 of this thesis. Moreover, further co-evolution should allow programming and modulating the local stiffness of each module to expand the set of possible tasks performed by the designed modular tensegrity robots. Finally, the future co-evolutionary platform for modular tensegrity robots should include a closed-loop controller for designing fully autonomous robots.

In conclusion, we believe that the use of heuristic algorithms and a co-evolutionary approach has great potential as an effective design method for successfully design future tensegrity modular robots.

# Chapter 7 Conclusions

In this thesis, we investigated tensegrity modular structures as a new approach to develop soft robots with variable stiffness capabilities. This investigation led to a set of design strategies to manufacture and actuate tensegrity modules with programmable stiffness and deformation, to connect mechanically and electrically tensegrity modules without hindering deformability, and to implement variable-stiffness capabilities in the modules for active and passive stiffness change. Finally, we presented preliminary results and insights on using heuristic algorithms to design task-optimal morphology, stiffness, and control of modular tensegrity robots; and on a data-driven approach to improve transfer to the reality of such designs.

## 7.1 Summary

After we reviewed and discussed the state of the art of tensegrity robotics, we individuated state of the art limitations to develop modular variable-stiffness tensegrity robots. Due to difficulties in designing and manufacturing tensegrity structures, designers still use simple and hand-picked morphologies with the intuitive placement of actuators. A modular approach that can lead to diverse morphologies and increased robustness has been investigated only for simple chain structures of artistic inspiration and is still limited by tethered technological solutions. Moreover, the great potential of implementing variable-stiffness capabilities into tensegrity robots is still not expressed and only a few studies exist in this direction with implementations that exhibit limited stiffness change. Comprehensive simulators such as the NASA NTTR and promising control strategies such as data-driven bio-inspired strategies are promising for designing also modular robots. However, the co-optimization of morphology, control, and stiffness has still not been attempted. Moreover, finding an appropriate compromise between design parameters while ensuring that the corresponding robot is physically realizable is still challenging due to the reality-gap between tensegrity models and hardware prototypes.

To overcome state-of-the-art limitations, we first introduced a novel manufacturing strategy to facilitate the realization of tensegrity structures using planar manufacturing techniques, such as 3D printing. We used this strategy to develop most of the tensegrity structures manufactured in this thesis. The first type of module developed for the modular robotic kit was the icosahedron tensegrity module that can deform in a three-dimensional space with programmable stiffness.

We also introduced the concept of modular actuation strategy consisting of developing modules with 1DOF (i.e. one degree of freedom) actuation along a specific axis. The actuated modules can then be assembled into multi-DOF actuated robotic structures. We initially demonstrated this strategy by developing icosahedron tensegrity modules with pre-programmed linear actuation and we assembled multiple of these modules into a modular crawling robot biomimicking peristaltic locomotion. In chapter three we expand the current kit adding modules that have bending actuation, computation, and energy storage capabilities completing a full kit to develop untethered modular tensegrity robots. Moreover, in chapter three we also introduced a novel bio-inspired connection strategy to connect the tensegrity modules mechanically and electrically without hindering their individual deformability. We demonstrate the connection strategy and the modular tensegrity kit by assembling two proofs-of-concept untethered soft robots: a gripper and a crawler.

In chapters four and five, we introduced design strategies to implement variable-stiffness capabilities into the tensegrity modules. In chapter four we focused on two novel design strategies to implement active stiffness-change capability to tensegrity modules. The first relied on the use of variable-stiffness cables (VSCs) manufactured with the LMPA smart material. We showed the tensegrity structures capabilities of the implemented proposed strategy in three validation scenarios with different tensegrity structures: 1) a two-modules tensegrity beam with tuneable load-bearing capability, 2) a tensegrity module that can self-deploy and lock its shape in both deployed and undeployed states, and 3) an actuated tensegrity joint module with underactuated shape deformations. The second active variable-stiffness design strategy was based on type-changing tensegrity structures. We investigated the strategy on a proof-of-concept tensegrity module which uses an active mechanism to add or remove a ball-joint constraint among its rigid components, allowing transition among different

tensegrity types and stiffness modes. We demonstrated the variable-stiffness strategy by developing a variable-stiffness robotic spine that can operate in different stiffness modes.

In chapter five we introduced a novel design strategy to develop modular tensegrity structures able to passively change-stiffness during collisions. We named such structures dual-stiffness tensegrity structures. The dual-stiffness allows tensegrity modular robots to be rigid during tasks such as navigation and to soften during collisions to absorb energy, and avoid damage. We demonstrated the strategy by developing two modular frames for a quadcopter drone and a wheeled rover exhibiting dual-stiffness capabilities.

Finally, in the last chapter, we presented preliminary results and insights on using heuristic algorithms to design task-optimal morphology, stiffness, and control of modular tensegrity robots. Moreover, we presented preliminary results on how to perform the sim-to-real transfer of modular tensegrity robots evolved with the presented design method and we transferred to reality the first modular tensegrity robot with co-optimized morphology, stiffness, and control.

## 7.2 Future work and possible research directions

In this thesis, we presented a modular bio-inspired strategy to design tensegrity robots with variable-stiffness capabilities. Although the proposed design in the first chapter with an individual module displays many desirable features that could lead to the assembly of a variety of robots with a diverse set of behaviors. Other tensegrity modules with different morphologies and actuation were included for developing the robots in chapter four and to demonstrate the variable stiffness strategies in chapters four and five. Future directions of research may improve the modular strategy in two ways. Firstly, by individuating the minimum amount of passive and actuated modules needed in a heterogeneous modular kit to cover the most diverse and large morpho-functional space. Secondly by individuating the best tensegrity module for a certain function and according to certain requirements, such as energy consumption, range of deformation, load transmission, or achievable stiffness change. For instance, the bending module presented in chapter three may not be the best solution in terms of reachable bending angle, or the variable-stiffness module demonstrated in chapter four may not be the best solution in terms of the amount of stiffness change achieved. In the future, form-finding techniques and heuristic algorithms may be used in tandem to individuate the optimal modules to perform a certain function.

In this thesis, we demonstrated the possibility of developing untethered soft modular tensegrity robots thanks to our novel connection-strategy. However, our connection strategy has been applied only on a tensegrity soft modular system of type two [13]. In the robots developed here, the junction connector connected vertices of rigid struts from neighboring modules together. However, if tensegrity soft modular systems are developed as type-one structures, there may be no adjacent vertices where to attach the female parts of the connectors. In these cases, in future investigations, the female parts of the junction connectors could be incorporated into membranes or attached to elastic cables with 3d-printed housings on the external surface. Of great interest for future work on connection strategies will be exploitation of multi-material 3D printing [101] to manufacture the stiff cable, conductive cables, and the plug system at the same time in a unique component, making faster the manufacturing and more consistent the contact resistances given by manual soldering.

In this thesis, we have presented two different active stiffness-change design strategies for tensegrity modules: through activation of smart materials or with bio-inspired type-changing tensegrity structures. While the first strategy can be implemented in any type of tensegrity module morphology including structures with no actuators. The second needs a more advanced form-finding technique to design compatible morphologies and seems to be of more difficult application. However, smart materials existing in the current state of the art are still prone to some disadvantages like high energy consumption or low speed. We believe that the two strategies are complementary and that in some applications type-changing tensegrity variable stiffness may be a preferable strategy to include variable stiffness capabilities in tensegrity modular robots. However, future work will need to individuate type-changing tensegrity structures compatible with tensegrity modules to allow their implementation in a modular robotic kit.

The dual-stiffness tensegrity modules and assemblies described in this thesis offered collision resilience capability. While the dual-stiffness struts described in this project were based on Ninja flex elastic hollow tubes, extended literature on materials and metamaterials that make use of elastic instabilities exists. Future work may investigate other techniques to implement dual-stiffness in tensegrity struts possibly improving its dual-stiffness properties such as initial stiffness and buckling load or reducing its weight even further [123] [124] [125]. Moreover, we implemented the dual-stiffness strategy

in rigid frames, but future work may investigate their use in any type of tensegrity module to include a safety failure mechanism in case of higher actuation loads or even to store energy for other types of behaviors, such as jumping.

An important limitation of the current tensegrity modular kit is the lack of sensing capabilities. In living soft animals, tension components like muscles, tendons, and fascia are integrated by stretch receptors that detect their stress change while going through large deformations. This functionalization of the tensile components is essential for the proprioceptive and self-sensing abilities [13]. Future research will need to investigate the implementation of sensing capabilities in passive and/or active modules. Such modules could sense mechanical perturbances from the environment or from within the robot, like an actuator malfunction. Moreover, self-sensing could lead to mechanical communication between modules, a phenomenon known as mechanotransduction in biology [13]. In living tissues, mechanical perturbances transmitted to cells can activate biochemical processes or gene expression. In an artificial modular system, this form of communication could enhance or replace digital electrical communication by propagating mechanical disturbances that control or alter the behavior of the modules. Different strategies and technologies already exist and may be further explored to implement sensor capabilities in tensegrity modules. Some work on optimization of sensor placement has been already investigated in simulation [146] while possible implementation strategies with smart cables [147], membranes [148] and others [149], have been proposed in some preliminary results by our group and others.

One of the main advantages of using tensegrity structures is their low weight. Extensive research in civil engineering has proved that the tensegrity paradigm offers minimum mass-to stiffness solutions for a variety of load conditions [11]. Most of the modules and robots developed in this thesis exhibit very low weight. However future work should systematically investigate how much is the weight reduction compared to existing other robotic solutions and evaluate advantages in terms of safety thanks to low inertia, energy efficiency, transportability, and COT (Cost of Transportation) for the locomoting robots.

In this thesis, we presented a modular strategy to develop tensegrity robots and we showed that co-evolution of morphology, stiffness, and control is an effective design strategy. However, now the “TensSoft” platform allows only co-evolution of chain-like structures and the use of icosahedron modules. Future research should aim at implementing the evolution of tree-structures and lattice-structures, as well as, the use of heterogeneous modular kits to further expand the ability to find task-optimal designs. Moreover, further co-evolution should allow programming and modulating the local stiffness of each module to possibly improve performances and expand the set of possible tasks performed by the designed modular tensegrity robots. Finally, the future co-evolutionary platform for modular tensegrity robots should include sensors and a closed-loop controller for designing fully autonomous robots. In a work recently submitted by our group [150], we started to investigate such possibility and we demonstrated how implementing simulated sensors and a Neural Network controller we were able to successfully co-evolve morphology and control of modular tensegrity robots able to squeeze throughout narrow passages (Videos are available at [151]) and steer to reach a goal in the simulated arena (Videos are available at [152]). However, no stiffness optimization was implemented.

In the last chapter of this thesis, we showed how with a data-driven approach we improved the sim-to-real problem and we presented preliminary results on transferring to reality modular tensegrity robots co-optimized in terms of morphology, stiffness, and control. Although the sim-to-real problem is not fully solved, our preliminary results suggest that evolutionary algorithms can be exploited to find novel locomotion behaviors not intuitively imagined by human designers. Two possible research directions may be pursued to further improve transferring to reality. Firstly, the importance of exploring the design space to find novel high-quality solutions should be investigated further and techniques able to improve the quality of the exploration may help in finding designs transferable to reality. Following this research direction, in recent work, we presented a novel algorithm named Double Map MAP-Elites that outperformed both MapElite and ViE at illuminating the search space in both squeezing and goal-reaching tasks [152]. A second research direction as suggested in the literature [153] may involve improving the data-driven technique by extending the amount of data collected in real hardware not only with experiments performed on individual modules but also on evolved assembled robots. Similar approaches in the literature demonstrated to further reduce the sim-to-real gap and make it possible to further reduce the sim-to-real gap of performances [73] [59]. Finally, other possible future directions may include alternative approaches such as using differentiable physics engines, that can further reduce the reality-gap by learning a physical model directly from data [74].

### 7.3 Opportunities

Although in this thesis modular tensegrity robots have been developed only for locomotion and grasping tasks, their use can potentially bring benefits into several robotic fields where being lightweight and having variable-stiffness capabilities are of primary importance. When considering the potential of a modular tensegrity approach in robotics, another important advantage has to be taken into account: scalability. Tensegrity structures are stable at every scale [11]. Although the technology used for the hardware implementation and the type of actuators may change according to the scale, most of the design strategies proposed in this thesis, such as the modular tensegrity strategy and modular actuation strategy along with the connection strategy and the variable stiffness active and passive strategies, are applicable at different scales. In the future, we can envision large-scale tensegrity modular robots with variable-stiffness capabilities used to develop lightweight active robotic architectures, giant robots for constructions and field application [103]. At the human scale, tensegrity modular robots with mechanical adaptability are promising for exploration, monitoring, and even for working safely in collaboration with humans. The bio-inspiration and bio-mimicking of the tensegrity approach can lead to more human-like prostheses and safer human-robot interaction interfaces [8]. Moreover, micro tensegrity modular robots may be used for minimally invasive surgery devices where mechanical adaptability is crucial for safely interact with the soft tissues [105].

In this thesis we have often used biological models as inspiration to develop artificial tensegrity robots, however, tensegrity robotic structures can also provide the opportunity to test biomechanical theories. Variable stiffness tensegrity robots can be developed to test theories of vertebrates' locomotion, stability and other dynamic behaviours. These investigations could lead in the future to have a better understanding of the human body mechanics and improve physical therapy, ergonomics and human-machine interactions.

In conclusion, we believe that the work presented and discussed in this thesis will pave the way to future research on lightweight and variable-stiffness tensegrity robots for a great variety of robotics tasks and applications.

# Chapter 8 Annex A – Supporting information on LMPA-based VSC and VSTS manufacturing

## Manufacturing and characterization of variable-stiffness cables (VSCs)

VSCs are made by filling silicone tubing (Platinum cured silicone tubing, Silex, LTD, UK) 2 mm inner diameter and 3 mm outer diameter, with LMPA (Cerrolow 147, Rotometal, Tm 47 °C). The technique is inspired by previous work from Tonazzini et al. [154]. Figure 55 presents an overview of all VSCs manufacturing steps and VSCs characterization. LMPA was melted in an aluminum foil cup on a hot plate at 55 °C and was sucked into the silicone tubing using a syringe. The tube and LMPA were then cooled, solidifying the LMPA (Figure 55a). The LMPA-filled tubing was cut into 40 mm length. The solidified LMPA in the tubing was cut into 30 mm length by partly removing the silicone tubing to one end of the LMPA rod. Then, silicone tubing was pre-stretched by 10% by pulling the tubing toward both ends (Figure 55a). Connectors are composed of hook-shaped threads (SpiderWire, ultracast invisi-braid 29.4 kg maximum load) and insulated copper wire (100  $\mu$ m diameter, SX0090S-D160, Scientific Wire Company) for heating the LMPA. The two components, thread, and copper wire are held together with metallic crimps (Figure 55b). To assemble connectors and LMPA-filled silicone tubes together, both ends of LMPA were partially melted with a heat gun (JTE-2D 173764, JBC) in order to insert the connectors in both ends (Figure 55c). After natural cooling of the LMPA with the connectors inside, both ends of the tube were encapsulated with silicone glue (Dow Corning) at room temperature for 2 hrs (Figure 55c).

In Figure 55d final VSC and mechanical characterization in the soft and rigid state are shown.

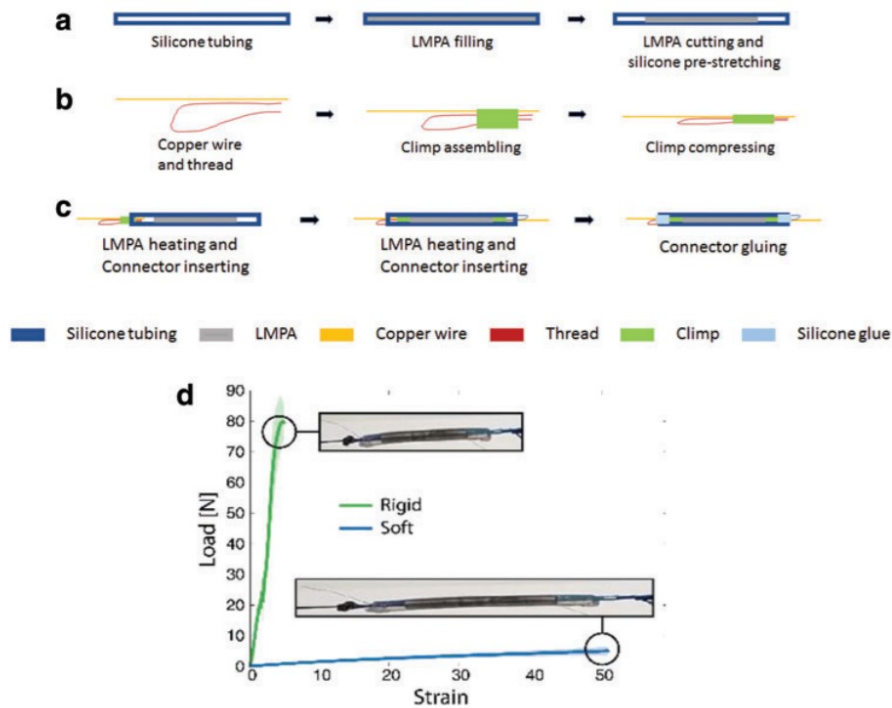


Figure 55. VSCs manufacturing steps.

(a-c) Detailed scheme of VSCs manufacturing steps divided into three groups: (a) manufacturing of the LMPA-filled tube, (b) manufacturing of the connector to transmit both mechanical loads and electrical currents (c) assembling of the tube and connectors (d) VSCs characterization with an Instron machine. Curves show average measures of 3 fibers and standard deviation in a lighter color. While in the soft state

the behavior is almost linear, in the stiff state the fibers seem to have lower stiffness in the first part of the curve. This may explain the difference between experimental and simulation results in stiff state.

### 3-strut Variable-stiffness tensegrity structure (VSTS)

3-strut VSTSs modules are composed of 3D printed rigid cables (3D printer FlashForge Dreamer) made of 3D printable nylon material (Taulman 618, taulman3D), VSCs described in Figure 55, and carbon composite struts with an inner diameter of 2mm and external diameter of 3mm (200.3020, SwissComposites). At both struts ends two 3D printed flexible hollow connectors are attached and threaded rods (M3 standard) were inserted through. Once a rigid cable or a VSC is attached to the screwed rods, a nut is attached to fix them in position.

#### VSTS beam

The VSTS beam is a two modules 3-strut tensegrity structure with VSCs replacing the cables at the junction of the two stages. The two 3-strut stages have their struts ends screwed together at the junction allowing respective rotations.

### Underactuated VSTS joint

The VSTS joint is obtained with a modified VSTS beam. Two rigid triangular faces are 3D printed in nylon, as it was done for the VSTS rigid cables, and are attached to the beam extremities. The actuation was obtained by using a 100:1 Micro Metal Gearmotor from Pololu (maximum torque 1.7 kg·cm (24 oz·in), at 1.6 A and 6V), inserted in a 3D printed PLA case placed at the bottom of the VSTS joint. The motor shaft is connected to the top vertices of the structure throughout tendon cables (SpiderSilk, ultracast invisi-braid 29.4 kg maximum load). To control the phase change of LMPA, 3As were applied to the copper wires by a power supply (72-8350A, TENMA).

### Kinematic experiments

The stiffness in both compression and bending of VSCs and VSTSs were characterized with a Universal Instron Machine series 5800R. A power supply was connected to the samples for controlling the stiffness of the VSCs. 1.5 A at 12V is applied for 3 minutes for changing the stiffness of VSCs, while 1.5 A for 1 minute is applied for one VSC. In all experiments, VSCs were allowed to cool for 5 minutes after interrupting the heating current.

Motion capturing (OptiTrack) was used for recording deformations of the underactuated VSTS joint.

# References

- [1] K. Sangbae, C. Laschi and B. Trimmer, "Soft Robotics: A Bioinspired Evolution in Robotics," *Trends in Biotechnology*, vol. 31, no. 5, p. 287–94, 2013.
- [2] G. Bao, H. Fang, L. Chen, Y. Wan, F. Xu, Q. Yang and L. Zhang, "Soft Robotics: Academic Insights and Perspectives Through Bibliometric Analysis," *Soft Robotics*, vol. 5, no. 3, pp. 229-41, 2018.
- [3] M. Tolley and D. Rus, "Design, fabrication and control of soft robots," *Nature*, vol. 521, no. 7553, pp. 467-75, 2015.
- [4] Y. Zhang and M. Lee, "A review of recent advancements in soft and flexible robots for medical applications," *The international Journal of Medical Robotics and Computer Assisted Surgery*, vol. 16, no. 3, pp. 1-13, 2020.
- [5] C. Majidi, "Soft Robotics: A Perspective—Current Trends and Prospects for the Future," *Soft Robotics*, vol. 1, no. 1, pp. 5-11, 2014.
- [6] S. R. Ward and R. L. Lieber, "Density and hydration of fresh and fixed human skeletal muscle," *Journal of Biomechanics*, vol. 38, no. 11, pp. 2317-20, 2005.
- [7] C. Laschi, B. Mazzolai and M. Cianchetti, "Soft Robotics: Technologies and Systems Pushing the Boundaries of Robot Abilities," *Science Robotics*, vol. 1, no. 1, p. eaah3690, 2016.
- [8] S. M. Levin, *Tensegrity: The New Biomechanics*, Oxford: Oxford University Press, 2006.
- [9] M. S. Levin, "The Tensegrity-Truss as a Model for Spine Mechanics: Biotensegrity," *Journal of Mechanics in Medicine and Biology*, vol. 2, no. 03n04, pp. 375-88, 2002.
- [10] E. D. Ingber, "The Architecture of Life," *Scientific American*, vol. 278, no. 1, p. 48–57, 1998.
- [11] M. Oliveira and R. E. Skelton, *Tensegrity Systems*, New York: Springer, 2009.
- [12] R. Goyal, R. E. Skelton and E. A. P. Hernandez, "Design of minimal mass load-bearing tensegrity lattices," *Mechanics Research Communications*, vol. 103, no. 103477, pp. 1-8, 2020.
- [13] D. E. Ingber, N. Wang and D. Stamenovic, "Tensegrity, cellular biophysics, and the mechanics of living systems," *Report on Progress in Physics*, vol. 77, no. 4, p. 046603, 2014.
- [14] M. Benjamin, "The Fascia of the Limbs and Back – a Review," *Journal of Anatomy*, vol. 214, no. 1, pp. 1-18, 2009.
- [15] T. R. Souza, S. T. Fonseca, G. G. Gonçalves, J. M. Ocarino and M. C. Mancini, "Prestress Revealed by Passive Co-Tension at the Ankle Joint," *Journal of Biomechanics*, vol. 42, no. 14, p. 2374–80, 2009.
- [16] K. Koohestani, "On the Analytical Form-Finding of Tensegrities," *Composite Structures*, vol. 166, p. 114–19, 2017.
- [17] J. Rieffel, B. Trimmer and H. Lipson, "Mechanism as mind - what tensegrities and caterpillars can teach us about soft robotics," in *Proceedings of the Eleventh International Conference on the Simulation and Synthesis of Living Systems*, Cambridge, 2008.

- 
- [18] C. Paul, J. W. Roberts, H. Lipson and F. J. V. Cuevas, "Gait Production in a Tensegrity Based Robot," in *Proceedings of the International Conference on Advanced Robotics*, Ithaca, 2015.
- [19] M. Shibata, F. Saijyo and S. Hirai, "Crawling by body deformation of tensegrity structure robots," in *Proceedings of the IEEE International Conference on Robotics and Automation*, Kobe, 2009.
- [20] R. Motro, "Structural Morphology of Tensegrity Systems," *Meccanica*, vol. 46, p. 27–40, 2011.
- [21] R. Baines, J. Booth and R. Kramer-Bottiglio, "A design methodology for rolling soft membrane-driven tensegrity robots," *Robotics and Automation Letters*, vol. 5, no. 4, pp. 6567–74, 2020.
- [22] V. Boehm, T. Kaufhold, I. Zeidis and K. Zimmermann, "Dynamic analysis of a spherical mobile robot based on a tensegrity structure with two curved compressed members," *Archive of Applied Mechanics*, vol. 87, p. 853–864, 2017.
- [23] P. Schorr, V. Bohm, K. Zimmermann and L. Zentner, "An approach to the estimation of the actuation parameters for mobile tensegrity robots with tilting movement sequences," in *Proceedings of the IEEE International Conference on Reconfigurable Mechanisms and Robots*, Delft, 2018.
- [24] V. Bouehm, T. Kaufhold, F. Schale and K. Zimmermann, "Spherical mobile robot based on a tensegrity structure with curved compressed members," in *Proceedings of the IEEE International Conference on Advanced Intelligent Mechatronics*, Banff, 2016.
- [25] T. Kaufhold, F. Schale, V. Boehm and K. Zimmermann, "Indoor locomotion experiments of a spherical mobile robot based on a tensegrity structure with curved compressed members," in *Proceedings of the IEEE International Conference on Advanced Intelligent Mechatronics*, Munich, 2017.
- [26] M. Vespignani, J. M. Friesen, V. SunSpiral and J. Bruce, "Design of SUPERball v2, a Compliant Tensegrity Robot for Absorbing Large Impacts," in *Proceedings of the IEEE/RSJ International Conference on Intelligent Robots and Systems*, Madrid, 2018.
- [27] Y. S. Chung, J.-H. Lee, J. H. Jang, H. R. Choi and H. Rodrigue, "Jumping Tensegrity Robot Based on Torsionally Prestrained SMA Springs," *ACS Appl Mater Interfaces*, vol. 11, no. 43, p. 40793–99, 2019.
- [28] L. Wu, M. J. de Andrade, T. Brahme, Y. Tadesse and R. H. Baughman, "A reconfigurable robot with tensegrity structure using nylon artificial muscle," in *Proceedings of Active and Passive Smart Structures and Integrated Systems*, Las Vegas, 2016.
- [29] Z. Wang, K. Li, Q. He and S. Cai, "A Light-Powered Ultralight Tensegrity Robot with High Deformability and Load Capacity," *Advanced Materials*, vol. 31, no. 7, pp. 1–8, 2019.
- [30] Y. Koizumi, M. Shibata and S. Hirai, "Rolling tensegrity driven by pneumatic soft actuators," in *Proceedings of the IEEE International Conference on Robotics and Automation*, Saint Paul, 2012.
- [31] K. Kim, A. K. Agogino and A. M. Agogino, "Rolling Locomotion of Cable-Driven Soft Spherical Tensegrity Robots," *Soft Robotics*, vol. 7, no. 3, pp. 346–61, 2020.
- [32] J. Bruce, K. Caluwaerts, A. Iscen, A. P. Sabelhaus and V. SunSpiral, "Design and evolution of a modular tensegrity robot platform," in *Proceedings of the IEEE International Conference on Robotics and Automation*, Hong Kong, 2014.
- [33] D. Surovik, J. Bruce, K. Wang, M. Vespignani and K. Bekris, "Any-Axis Tensegrity Rolling via Symmetry-Reduced Reinforcement," in *Proceedings of the 2018 International Symposium on Experimental Robotics*, Buenos Aires, 2018.

- 
- [34] K. Zhao, J. Chang, B. Li and W. Du, "Rolling direction prediction of tensegrity robot on the slope based on FEM and GA," *Journal of Mechanical Engineering Science*, vol. 234, no. 18, pp. 3846-58, 2020.
- [35] L.-H. Chen, K. Kim, E. Tang, K. Li, R. House, E. L. Zhu, K. Fountain, A. M. Agogino and al., "Soft Spherical Tensegrity Robot Design Using Rod-Centered Actuation and Control," *Journal of Mechanisms and Robotics*, vol. 9, no. 2, pp. 025001-9, 2017.
- [36] T. Rhodes, C. Gotberg and V. Vikas, "Compact Tensegrity Robots Capable of Locomotion Through Mass Shifting," *Frontiers in Robotics and AI*, vol. 6, p. 111, 2019.
- [37] V. Boehm and K. Zimmermann, "Vibration driven mobile robots based on single actuated tensegrity structures," in *Proceedings of the IEEE International Conference on Robotics and Automation*, Karlsruhe, 2013.
- [38] J. Rieffel and J.-B. Mouret, "Adaptive and Resilient Soft Tensegrity Robots," *Soft Robotics*, vol. 5, no. 3, pp. 318-29, 2018.
- [39] J. Rieffel, R. Stuk, F. J. Valero-Cuevas and H. Lipson, "Locomotion of a tensegrity robot via dynamically coupled modules," in *Proceedings of the IEEE International Conference on Morphological Computation*, Venice, 2007.
- [40] J. Friesen, A. Pogue, T. Bewley, M. d. Oliveira, R. Skelton and V. Sunspiral, "DuCTT: A tensegrity robot for exploring duct systems," in *Proceedings of the IEEE International Conference on Robotics and Automation*, Hong Kong, 2014.
- [41] J. M. Friesen, P. Glick, M. Fanton, P. Manovi, A. Xydes, T. Bewley and V. Sunspiral, "The second generation prototype of a Duct Climbing Tensegrity robot, DuCTTv2," in *Proceedings of the IEEE International Conference on Robotics and Automation*, Stockholm, 2016.
- [42] P. Schorr, L. Zentner, K. Zimmermann and V. Böhm, "Jumping locomotion system based on a multistable tensegrity structure," *Mechanical Systems and Signal Processing*, vol. 152, p. 107384, 2021.
- [43] S. Mintchev, D. Zappetti, J. Willemin and D. Floreano, "A Soft Robot for Random Exploration of Terrestrial Environments," in *Proceedings of the IEEE International Conference on Robotics and Automation*, Brisbane, 2019.
- [44] J. Zha, X. Wu, J. Kroeger, N. Perez and M. W. Mueller, "A collision-resilient aerial vehicle with icosahedron tensegrity structure," arXiv, 2020.
- [45] D. Hustig-Schultz, V. SunSpiral and M. Teodorescu, "Morphological Design for Controlled Tensegrity Quadruped Locomotion," in *Proceedings of the IEEE/RSJ International Conference on Intelligent Robots and Systems*, Vancouver, 2017.
- [46] E. Jung, V. Ly, N. Cessna, M. L. Ngo, D. Castro, V. SunSpiral and M. Teodorescu, "Bio-inspired tensegrity flexural joints," in *Proceedings of the IEEE International Conference on Robotics and Automation*, Brisbane, 2018.
- [47] S. Lessard, J. Bruce, E. Jung, M. Teodorescu, V. SunSpiral and A. Agogino, "A lightweight, multi-axis compliant tensegrity joint," in *Proceedings of the IEEE International Conference on Robotics and Automation*, Stockholm, 2016.
- [48] W. Li, H. Nabae, G. Endo and K. Suzumori, "New Soft Robot Hand Configuration With Combined Biotensegrity and Thin Artificial Muscle," *Robotics and Automation Letters*, vol. 5, no. 3, p. 4345-51, 2020.
- [49] J. Sun, G. Song, J. Chu and L. Ren, "An Adaptive Bioinspired Foot Mechanism Based on Tensegrity Structures," *Soft Robotics*, vol. 6, no. 6, p. 778-89, 2019.

- 
- [50] S. Lessard, D. Castro, W. Asper, S. D. Chopra, L. B. Baltaxe-Admony, M. Teodorescu, V. SunSpiral and A. Agogino, "Bio-inspired tensegrity manipulator with multi-DOF, structurally compliant joints," in *Proceedings of the IEEE/RSJ International Conference on Intelligent Robots and Systems*, Daejeon, 2016.
- [51] D. Gauge, S. Coros, S. Mani and B. Thomaszewski, "Interactive Design of Modular Tensegrity Characters," in *Proceedings of the Eurographics Symposium on Computer Animation*, Copenhagen, 2014.
- [52] J. Rimoli and K. R. Pal, "Mechanical Response of 3-Dimensional Tensegrity Lattices," *Composites Part B: Engineering, Composite lattices and multiscale innovative materials and structures*, vol. 115, p. 30–42, 2017.
- [53] A. Micheletti, A. F. dos Santos and P. Sittner, "Superelastic tensegrities: matrix formulation and antagonistic actuation," *Smart Materials and Structures*, vol. 27, no. 10, pp. 1-29, 2018.
- [54] A. Sabouni-Zawadzka and W. Gilewski, "Towards unusual mechanical properties of tensegrity lattice metamaterial," in *Proceedings of the MATEC Web of Conferences*, 2018.
- [55] J. Bauer, J. A. Kraus, C. Crook, J. Rimoli and L. Valdevit, "Tensegrity Metamaterials: Toward Failure-Resistant Engineering Systems through Delocalized Deformation," *Advanced Materials*, vol. 33, no. 10, pp. 1-9, 2020.
- [56] L. Y. Zhang, S. X. Li, S. Zhu, B. Zhang and G. Xu, "Automatically assembled large-scale tensegrities by truncated regular polyhedral and prismatic elementary cells," *Composite Structures*, vol. 184, pp. 30-40, 2017.
- [57] B. T. Mirletz, P. Bhandal, R. D. Adams, A. K. Agogino, R. D. Quinn and V. Sunspiral, "Goal-Directed CPG-Based Control for Tensegrity Spines with Many Degrees of Freedom Traversing Irregular Terrain," *Soft Robotis*, vol. 2, no. 4, p. 165–176, 2015.
- [58] B. R. Tietz, R. W. Carnahan, R. J. Bachmann, R. D. Quinn and V. SunSpiral, "Tetraspine: Robust terrain handling on a tensegrity robot using central pattern generators," in *International Conference on Advanced Intelligent Mechatronics*, Wollongong, 2013.
- [59] B. T. Mirletz, I. Park, R. D. Quinn and V. SunSpiral, "Towards bridging the reality gap between tensegrity simulation and robotic hardware," in *Proceedings of the IEEE/RSJ International Conference on Intelligent Robots and Systems*, Hamburg, 2015.
- [60] B. T. Mirletz, I.-W. Park, T. E. Flemons, A. K. Agogino, R. D. Quinn and V. SunSpiral, "Design and Control of Modular Spine-Like Tensegrity Structures," in *Proceedings of the IEEE International Conference on Robotics and Automation*, Barcelona, 2014.
- [61] A. P. Sabelhaus, J. Friesen, V. SunSpiral, H. Ji, P. Hylton, Y. Madaan, C. Yang and A. M. Agogino, "Mechanism design and simulation of the UltraSpine, a Tensegrity Robot," in *Proceedings of the ASME 2015 International Design Engineering Technical Conferences and Computers and Information in Engineering Conference. Volume 5A: 39th Mechanisms and Robotics Conference*, Boston, 2015.
- [62] H. Lee, Y. Jang, J. K. Choe, S. Lee and H. Song, "3D-printed programmable tensegrity for soft robotics," *Science Robotics*, vol. 5, no. 45, p. eaay9024, 2020.
- [63] Q. Boehler, S. Abdelaziz, M. Vedrines and al., "From modeling to control of a variable stiffness device based on a cable-driven tensegrity mechanism," *Mechanical Machine Theory*, vol. 107, pp. 1-12, 2017.
- [64] M. Azadi, S. Behzadipour and G. Faulkner, "Variable stiffness spring using tensegrity prisms," *Journal Mech Robot*, vol. 2, no. 4, pp. 1-13, 2010.

- 
- [65] J. M. Friesen, J. L. Dean, T. Bewley and al, "A tensegrity-inspired compliant 3-DOF compliant joint," in *Proceedings of the IEEE International Conference on Robotics and Automation*, Brisbane, 2018.
- [66] C. Sultan, M. Corless and R. E. Skelton, "Tensegrity flight simulator," *Journal of Guidance, Control, and Dynamics*, vol. 23, no. 6, p. 1055–106, 2000.
- [67] A. G. Rovira and J. M. M. Tur, "Control and Simulation of a Tensegrity-based Mobile Robots," *Robotics and Autonomous Systems*, vol. 57, no. 5, p. 526–535, 2009.
- [68] E. Todorov, T. Erez and Y. Tassa, "Mujoco: A physics engine for model-based control," in *Proceedings of the IEEE/RSJ International Conference on Intelligent Robots and Systems*, Algarve, 2012.
- [69] "Tensegrity matlab objects," [Online]. Available: [https://github.com/Jfriesen222/Tensegrity\\_MATLAB\\_Objects](https://github.com/Jfriesen222/Tensegrity_MATLAB_Objects).
- [70] R. Smith, "Ode: Open dynamics engine," [Online]. Available: <http://www.ode.org>.
- [71] E. Coumans, "Bullet physics engine," [Online]. Available: <http://bulletphysics.org>.
- [72] NASA, "NASA Tensegrity Robotics Toolkit," [Online]. Available: <https://github.com/NASA-Tensegrity-Robotics-Toolkit/NTRTsim>.
- [73] K. Caluwaerts, J. Despraz, A. Işçen, A. P. Sabelhaus, J. Bruce, B. Schrauwen and V. SunSpiral, "Design and control of compliant tensegrity robots through simulation and hardware validation," *Journal of The Royal Society Interface*, vol. 11, no. 20140520, 2014.
- [74] K. Wang, M. Aanjaneya and K. Bekris, "A first principles approach for data-efficient system identification of spring-rod systems via differentiable physics engines," arXiv, 2020.
- [75] D. Howard, E. A. Eiben, F. D. Kennedy, J.-B. Mouret, P. Valencia and D. Winkler, "Evolving embodied intelligence from materials to machines," *Nature Machine Intelligence*, vol. 1, no. 1, p. 12–19, 2019.
- [76] T. Bliss, T. Iwasaki and H. Bart-Smith, "Central Pattern Generator Control of a Tensegrity Swimmer," *IEEE/ASME Transactions on Mechatronics*, vol. 18, no. 2, pp. 586–97, 2013.
- [77] A. Iscen, A. Agogino, V. SunSpiral and K. Tumer, "Controlling Tensegrity Robots through Evolution," in *Proceedings of the Genetic and Evolutionary Computation Conference*, Amsterdam, 2013.
- [78] V. Mnih, K. Kavukcuoglu, D. Silver and al, "Human-level control through deep reinforcement learning," *Nature*, vol. 518, p. 529–533, 2015.
- [79] M. Zhang, X. Geng, J. Bruce, K. Caluwaerts, M. Vespignani, V. SunSpiral, P. Abbeel and S. Levine, "Deep reinforcement learning for tensegrity robot locomotion," in *Proceedings of the IEEE International Conference on Robotics and Automation*, Singapore, 2017.
- [80] B. Alberts, D. Bray, J. Lewis, M. Raff, K. Roberts and J. D. Watson, *Molecular biology of the cell*, New York: Garland Publishing, 1983.
- [81] O. Foucher, "Polyèdres et tensegrité," Université Montpellier II, Montpellier, 2001.
- [82] J. Bruce, K. Caluwaerts, A. Iscen, A. P. Sabelhaus and V. SunSpiral, "Design and evolution of a modular tensegrity platform," in *Proceedings of the IEEE International Conference on Robotics and Automation*, Hong Kong, 2014.

- 
- [83] M. Shibata, F. Saijyo and S. Hirai, "Crawling by body deformation of tensegrity structure robots," in *Proceeding of the IEEE International Conference on Robotics and Automation*, Kobe, 2009.
  - [84] E. N. Kanu, K. A. Daltorio, R. D. Quinn and H. J. Chiel, "Correlating kinetics and kinematics of earthworm peristaltic locomotion," in *Proceedings of the International Conference of Living Machines*, Barcelona, 2015.
  - [85] T. Fukuda, S. Nakagawa, Y. Kawauchi and M. Buss, "Self organizing robots based on cell structures – CEBOT," in *Proceedings of the IEEE International Conference on Robotics and Automation*, Scottsdale, 1989.
  - [86] P. Moubarak and P. Ben-Tzvi, "Modular and reconfigurable mobile robotics," *Robotics & Autonomous Systems*, vol. 60, no. 12, p. 1648–1663, 2012.
  - [87] M. B. Yim, W.-M. Shen, B. Salemi, D. Rus, M. Moll, H. Lipson, E. Klavins and S. G. Chirikjian, "Modular self-reconfigurable robot systems [Challenges and opportunities for the future]," *IEEE Robotics & Automation Magazine*, vol. 14, no. 1, p. 43–52, 2007.
  - [88] S. Hauser, M. Mutlu, P.-A. Léziart, H. Khodr, A. Bernardino and A. J. Ijspeert, "Roombots extended: Challenges in the next generation of self-reconfigurable modular robots and their application in adaptive and assistive furniture," *Robotics and Autonomous Systems*, vol. 127, no. 103467, 2020.
  - [89] Y. Suzuki, Y. Tsutsui, M. Yaegashi and S. Kobayashi, "Modular robot using helical magnet for bonding and transformation," in *Proceedings of the IEEE International Conference on Robotics and Automation*, Singapore, 2017.
  - [90] S. Coyle, C. Majidi, P. LeDuc and J. K. Hsia, "Bio-inspired soft robotics: Material selection, actuation, and design," *Extreme Mechanics Letters*, vol. 22, pp. 51-59, 2018.
  - [91] J. Germann, M. Dommer, R. Pericet-Camara and D. Floreano, "Active Connection Mechanism for Soft Modular Robots," *Advanced Robotics*, vol. 26, no. 7, p. 785–798, 2012.
  - [92] C. H. Belke and J. Paik, "Automatic Couplings With Mechanical Overload Protection for Modular Robots," *Transactions on Mechatronics*, vol. 24, no. 3, p. 1420–1426, 2019.
  - [93] A. Vergara, Y. Lau, R.-F. Mendoza-Garcia and J. Zagal, "Soft modular robotic cubes: toward replicating morphogenetic movements of the embryo," *PLOS ONE*, vol. 12, no. 1, pp. 1-17, 2017.
  - [94] C. D. Onal and D. Rus, "A modular approach to soft robotics," in *Proceedings of the IEEE RAS/EMBS International Conference on Biomedical Robotics and Biomechatronics*, Rome, 2012.
  - [95] D. Zappetti, S. Mintchev, J. Shintake and D. Floreano, "Bio-Inspired Tensegrity Soft Modular Robots," in *Proceedings of the Conference on Biomimetic and Biohybrid Systems*, Palo Alto, 2017.
  - [96] Y. A. Tse, S. Liu, Y. Yang and M. Y. Wang, "A Flexible Connector for Soft Modular Robots Based on Micropatterned Intersurface Jamming," arXiv, 2020.
  - [97] J. Y. Lee, B. W. Kim, Y. W. Choi and J. K. Cho, "Soft robotic blocks: introducing SoBL, a fast-build modularized design block," *IEEE Robotics and Automation Letters*, vol. 23, no. 3, p. 30–41, 2016.
  - [98] A. S. Morin and al., "Elastomeric tiles for the fabrication of inflatable structures," *Advanced Functional Materials*, vol. 24, no. 35, p. 5541–5549, 2014.
  - [99] J. Guo, C. Xiang and J. Rossiter, "Electrically controllable connection and power transfer by electroadhesion," *Smart Mater. Struct.*, vol. 28, p. 105012, 2019.

- 
- [100] M. E. Karagozler, J. D. Campbell, G. K. Fedder, S. C. Goldstein, M. P. Weller and B. W. Yoon, "Electrostatic latching for inter-module adhesion, power transfer, and communication in modular robots," in *Proceedings of the IEEE/RSJ International Conference on Intelligent Robots and Systems*, San Diego, 2007.
  - [101] S. I. Rich, R. J. Wood and C. Majidi, "Untethered soft robotics," *Nature Electronics*, vol. 1, no. 2, p. 102–112, 2018.
  - [102] J. Kimber and al., "Low-Cost Wireless Modular Soft Tensegrity Robots," in *Proceedings of the IEEE International Conference on Soft Robotics*, Seoul, 2019.
  - [103] E. Fuchs and W. J. Nelson, *Cell-Cell Junctions*, Brisbane: Cold Spring Harbor Press, 2010.
  - [104] A. Hartsock and W. J. Nelson, "Adherens and Tight Junctions: Structure, Function and Connections to the Actin Cytoskeleton," *Biochim. Biophys. Acta*, vol. 1778, no. 3, p. 660–669, 2008.
  - [105] R. C. Hibbeler, *Engineering Mechanics: Dynamics*, New York: Prentice Hall, 2010.
  - [106] Y. Fang and L.-W. Tsai, "Enumeration of a class of overconstrained mechanisms using the theory of reciprocal screws," *Mechanism and Machine Theory*, vol. 39, no. 11, p. 1175–1187, 2004.
  - [107] J. Choi, O.-C. Kwon, W. Jo, H. J. Lee and M.-W. Moon, "4D Printing Technology: A Review," *3D Printing and Additive Manufacturing*, vol. 2, no. 4, p. 159–167, 2015.
  - [108] K. Nagase, T. Yamashita and N. Kawabata, "On a connectivity matrix formula for tensegrity prism plates," *Mechanics Research Communications*, vol. 77, pp. 29-43, 2016.
  - [109] E. G. Fenci and G. N. Currie, "Deployable structures classification: a review," *International Journal of Space Structures*, vol. 32, no. 2, p. 112–130, 2017.
  - [110] S. Mintchev and D. Floreano, "Adaptive morphology: a design principle for multimodal and multifunctional robots," *IEEE Robotic Automation Magazine*, vol. 23, no. 3, p. 42–54, 2016.
  - [111] C. Chautems, A. Tonazzini, D. Floreano and al., "A variable stiffness catheter controlled with an external magnetic field," in *Proceedings of the IEEE/RSJ International Conference on Intelligent Robots and Systems*, Vancouver, 2017.
  - [112] J. R. Potvin, S. M. McGill and R. W. Norman, "Trunk muscle and lumbar ligament contributions to dynamic lifts with varying degrees of trunk flexion," *Spine*, vol. 16, no. 9, pp. 1099-1107, 1991.
  - [113] J. R. Kowalski, L. A. Ferrara and E. C. Benzol, "Biomechanics of the spine," *Neurosurgery Quarterly*, vol. 15, no. 1, p. 42–59, 2005.
  - [114] W. K. Moored and H. Bart-Smith, "Investigation of clustered actuation in tensegrity structures," *International Journal of Solide Structures*, vol. 46, no. 17, pp. 3272-81, 2009.
  - [115] I. De Falco, M. Cianchetti and A. Menciassi, "A soft multi-module manipulator with variable stiffness for minnimally invasive surgery," *Bioinspired & Biomimetics*, vol. 12, no. 5, pp. 1-16, 2017.
  - [116] A. Jiang, G. Xynogalas, P. Dasgupta, K. Althoefer and T. Nanayakkara, "Design of a variable stiffness flexible manipulator with composite granular jamming and membrane coupling," in *Proceedings of the IEEE/RSJ International Conference on Intelligent Robots and Systems*, Algarve, 2012.
  - [117] S. Coyle, C. Majidi, P. LeDuc and K. J. Hsia, "Bio-inspired soft robotics: material selection, actuation, and design," *Extreme Mech. Lett.*, vol. 22, pp. 51-59, 2018.

- [118] brunoip, "Simple 3d printed 9g servo gripper," [Online]. Available: <https://www.thingiverse.com/thing:2302957>.
- [119] M. Manti, V. Cacucciolo and M. Cianchetti, "Stiffening in Soft Robotics: A Review of the State of the Art," *Robotic and Automation Magazine*, vol. 23, no. 3, pp. 93 - 106, 2016.
- [120] D. Zappetti, S. H. Jeong, J. Shintake and D. Floreano, "Phase Changing Materials-Based Variable-Stiffness Tensegrity Structure," *Soft Robotics*, vol. 7, no. 3, pp. 362-369, 2019.
- [121] D. Zappetti, R. Arandes, E. Ajanic and D. Floreano, "Variable-stiffness tensegrity spine," *Smart Mater. Struct.*, vol. 29, no. 7, pp. 1-10, 2020.
- [122] D. González, J. Pérez, V. Milanés and F. Nashashibi, "A Review of Motion Planning Techniques for Automated Vehicles," *IEEE Transactions on Intelligent Transportation Systems*, vol. 17, no. 4, p. 1135–1145, 2016.
- [123] I. K. Kuder, U. Fasel, P. Ermanni and A. F. Arrieta, "Concurrent design of a morphing aerofoil with variable stiffness bi-stable laminates," *Smart Mater. Struct.*, vol. 25, no. 11, p. 115001, 2016.
- [124] J. Paulose, A. S. Meeussen and V. Vitelli, "Selective buckling via states of self-stress in topological metamaterials," *PNAS*, vol. 112, no. 25, p. 7639–7644, 2015.
- [125] H. V. Phan and H. C. Park, "Mechanisms of collision recovery in flying beetles and flapping-wing robots," *Science*, vol. 370, no. 6521, pp. 1214-1219, 2020.
- [126] S. Mintchev, J. Shintake and D. Floreano, "Bioinspired dual-stiffness origami," *Science Robotics*, vol. 3, no. 20, p. eaau0275, 2018.
- [127] S. Mintchev, S. de Rivaz and D. Floreano, "Insect-Inspired Mechanical Resilience for Multicopters," *IEEE Robotics and automation letters*, vol. 2, no. 3, pp. 1248-55, 2017.
- [128] N. Hu and R. Burgueño, "Buckling-induced smart applications: recent advances and trends," *Smart Mater. Struct.*, vol. 24, no. 6, p. 063001, 2015.
- [129] Y. -J. Park and al., "Dual-stiffness structures with reconfiguring mechanism: Design and investigation," *Journal of Intelligent Material Systems and Structures*, vol. 27, no. 8, p. 995–1010, 2016.
- [130] K. Bertoldi, V. Vitelli, J. Christensen and M. van Hecke, "Flexible mechanical metamaterials," *Nature Reviews Materials*, vol. 2, no. 17066, 2017.
- [131] J. Rimoli, "On the impact tolerance of tensegrity-based planetary landers," in *Proceedings of the 57th AIAA/ASCE/AHS/ASC Structures, Structural Dynamics, and Materials Conference*, San Diego, 2016.
- [132] J.-B. Mouret and J. Clune, "Illuminating search spaces by mapping elites," ArXiv, 2015.
- [133] N. Cheney, R. MacCurdy, J. Clune and H. Lipson, "Unshackling Evolution: Evolving Soft Robots with Multiple Materials and a Powerful Generative Encoding," in *Proceedings of the Genetic and Evolutionary Computation Conference*, Amsterdam, 2013.
- [134] M. Joachimczak, R. Suzuki and T. Arita, "Artificial Metamorphosis: Evolutionary Design of Transforming, Soft-Bodied Robots," *Artificial Life*, vol. 22, p. 271–298 , 2016.
- [135] N. Cheney, J. Bongard and H. Lipson, "Evolving Soft Robots in TightSpaces," in *Proceedings of the Genetic and Evolutionary Computation Conference*, Washington, 2015.

- 
- [136] P. Chandana, H. Lipson and F. Cuevas, "Evolutionary form-finding of tensegrity structures," in *Proceedings of the Genetic and Evolutionary Computation Conference*, Washington, 2005.
  - [137] H. E. Cheng-yu, "Viability of Tensegrity Robots in Space Exploration," University of California at Berkeley, San Francisco, 2014.
  - [138] C. Paul, F. Valero-Cuevas and H. Lipson, "Design and control of tensegrity robots for locomotion," *IEEE Transactions on Robotics*, vol. 22, no. 5, pp. 944-957, 2006.
  - [139] H. -G. Beyer and H. -P. Schwefel, "Evolution strategies—a comprehensive introduction," *Natural computing*, vol. 1, no. 1, p. 3–52, 2002.
  - [140] J. M. Bejjani and D. Zappetti, "HIGH Stiffness Result," [Online]. Available: [https://youtu.be/rhPljQPLO\\_w](https://youtu.be/rhPljQPLO_w).
  - [141] D. Zappetti and J. Bejjani, "LOW Stiffness Result," [Online]. Available: [https://youtu.be/Y8\\_a2DRWBfE](https://youtu.be/Y8_a2DRWBfE).
  - [142] A. Kakogawa and S. Ma, "Stiffness Design of Springs for a Screw Drive In-Pipe Robot to Pass through Curved Pipes and Vertical Straight Pipes," *Advanced Robotics*, vol. 26, no. 3-4, pp. 253-276, 2012.
  - [143] J. Bongard, C. Laschi, H. Lipson, N. Cheney and F. Corucci, "Material properties affect evolutions ability to exploit morphological computation in growing soft-bodied creatures," in *Proceedings of the Fifteenth International Conference on the Synthesis and Simulation of Living Systems*, Cancun, 2016.
  - [144] A. Maesani, P. R. Fernando and D. Floreano, "Artificial evolution by viability rather than competition," *PLOS ONE*, vol. 9, no. 1, pp. 1-12, 2014.
  - [145] J. Hwangbo and al, "Learning agile and dynamic motor skills for legged robots," *Science Robotics*, vol. 4, no. 26, p. eaau5872, 2019.
  - [146] O. Aloui, J. Lin and L. Rhode-Barbarigos, "A theoretical framework for sensor placement, structural identification and damage detection in tensegrity structures," *Smart Materials and Structures*, vol. 28, no. 12, pp. 1-11, 2019.
  - [147] L. Campanaro, D. Zappetti, J. Shintake, Y. Ikemoto, M. Chiaberge and D. Floreano, "Sensor Integration and Controller Design for a Tensegrity-Modular Robot," Polito, Turin, 2017.
  - [148] J. W. Booth, O. Cyr-Choinière, J. C. Case, D. Shah, M. C. Yuen and R. Kramer-Bottiglio, "Surface Actuation and Sensing of a Tensegrity Structure Using Robotic Skins," *Soft Robotics*, 2020.
  - [149] K. Caluwaerts, J., J. M. Bruce, Friesen and V. SunSpiral, "State Estimation for Tensegrity Robots," in *Proceedings of the IEEE International Conference on Robotics and Automation*, Paris, 2016.
  - [150] E. Zardini, D. Zappetti, D. Zambrano, G. Iacca and D. Floreano, "Seeking Quality Diversity in Evolutionary Co-design of Morphology and Control of Soft Tensegrity Modular Robots," in *Proceedings of the Genetic and Evolutionary Computation Conference*, Lille, 2021.
  - [151] E. Zardini and al, "Squeezing task - Best evolved modular tensegrity robots," [Online]. Available: <https://www.youtube.com/playlist?list=PLtSGcQw3Wpzaoa3nev1RUmMGRSFb18jFf>.
  - [152] E. Zardini and al, "Goal-reaching task - Best evolved modular tensegrity robots," [Online]. Available: <https://www.youtube.com/playlist?list=PLtSGcQw3Wpzti9pgGVgk0F5fH9cPZlvm>.

- [153] T. Howison, S. Hauser, J. Hughes and F. Iida, "Reality-Assisted Evolution of Soft Robots through Large-Scale Physical Experimentation: A Review," *Artificial Life*, vol. 26, no. 4, pp. 484-506, 2021.
- [154] A. Tonazzini, S. Mintchev, B. Schubert, B. Mazzolai, J. Shintake and D. Floreano, "Variable Stiffness Fiber with Self-Healing Capability," *Advanced Materials*, vol. 28, no. 46, p. 10142–48, 2016.
- [155] D. Zappetti, J. M. Bejjani and D. Floreano, "Evolutionary Co-Design of Morphology and Control of Soft Tensegrity Modular Robots with Programmable Stiffness," arXiv, 2021.

## Curriculum Vitae

# Davide Zappetti

Rue Edouard-Payot, 10  
Lausanne, 1005, Switzerland  
+41 763222837  
✉ [d.zappetti@gmail.com](mailto:d.zappetti@gmail.com)  
Skype id: d.zappetti



## WORK EXPERIENCES

Aug 2016 –  
present

**Ph.D. candidate at Laboratory of Intelligent Systems - Lausanne, Vaud Canton, Switzerland.**

Main responsibilities:

- Investigated tensegrity modular robots, soft robotic technologies including smart materials, and design optimization.  
Thesis title: Variable-Stiffness Tensegrity Robots
- Supervision of seventeen student projects and teaching assistant coordinator of the Evolutionary Robotics course for three semesters
- Co-organized and participated in two international tensegrity robotics workshops and multiple conferences

Jan 2016 –  
Jul 2016

**Intern at Laboratory of Intelligent Systems - Lausanne, Vaud Canton, Switzerland.**

Main responsibilities:

- Investigation of soft modular robots
- Helping with teaching activities

Jan 2015 –  
Jul 2015

**Intern at Sensirion AG - Stäfa, Zürich Canton, Switzerland.**

Main responsibilities:

- MEMS Sensors characterization, calibration, and qualification.
- MEMS research and development
- Data Analysis with data analysis software or programming languages
- Engineering reports.

## PUBLICATIONS

- Phase changing materials-based variable-stiffness tensegrity structures. *D. Zappetti, S.H. Jeong, J. Shintake, D. Floreano*. Soft robotics 7 (3), 362-369, 2020.
- Variable-stiffness tensegrity spine. *D. Zappetti, R. Arandes, E. Ajanic, D. Floreano*. Smart Materials and Structures 29 (7), 2020.
- Bio-inspired tensegrity soft modular robots. *D. Zappetti, S. Mintchev, J. Shintake, D. Floreano*. Conference on Biomimetic and Biohybrid Systems, 497-508 21, 2017.
- Evolutionary Co-Design of Morphology and Control of Soft Tensegrity Modular Robots with Programmable Stiffness. *D. Zappetti, J.M. Bejjani, D. Floreano*. arXiv preprint arXiv:2101.11772, 2021.
- A soft robot for random exploration of terrestrial environments. *S. Mintchev, D. Zappetti, J. Willemin, D. Floreano*. 2018 IEEE International Conference on Robotics and Automation (ICRA), 7492-7497, 2018.
- Bio-inspired Tensegrity Fish Robot. *J. Shintake, D. Zappetti, T. Peter, Y. Ikemoto, D. Floreano*. 2020 IEEE International Conference on Robotics and Automation (ICRA), 2887-2892, 2020.

## EDUCATION

2011-2014

**Masters in Material and Nanotechnologies Engineering**

*La Sapienza - University of Rome, Italy*

*Mark: 110 /110 cum laude*

*Average courses mark: 29.1/30*

- Project thesis: Design and manufacturing with MEMS-based technologies of a microgripper.

2008 - 2011	<b>Bachelor's in Mechanical Engineering</b> Polytechnic of Bari, Italy Mark: 110/110 <ul style="list-style-type: none"> <li>• <u>Project thesis</u>: Measurement of common rail injector valve displacement.</li> </ul>
	<b>AWARDS &amp; SCHOLARSHIPS</b>
2014	<ul style="list-style-type: none"> <li>• Won the “<b>Progetto Concreto</b>” contest, where winners are supported by a mentor chosen amongst major Italian company managers, winners are recognized for their outstanding performances during their academic careers, abroad studying experiences and extra-academic experiences.</li> </ul>
2011-2012	<ul style="list-style-type: none"> <li>• Won “<b>Wanted the Best</b>” scholarship from Università La Sapienza Roma, where winners are recognized for their outstanding performances during their Bachelor's degree, including a 110/110 mark.</li> </ul>
2011	<ul style="list-style-type: none"> <li>• Winner of a <b>merit scholarship</b> that recognizes outstanding performance for the undergraduate career.</li> </ul>
<b>INFORMATIC SKILLS</b>	
Languages	<ul style="list-style-type: none"> <li>• <u>Python</u> for data analysis and experimental set-up controlling, <u>C</u>, <u>C++</u>, <u>Matlab</u> &amp; <u>Simulink</u> for modeling and data analysis, mechanical design, electrical design, multiphysics design, atomistic simulations: Molecular Dynamics and Monte Carlo methods. <u>LabVIEW</u> for data acquisition.</li> </ul>
CAD Software	<ul style="list-style-type: none"> <li>• 2D and 3D models: <u>Autocad</u>, <u>Solid Works</u>, <u>Solid Edge</u>.</li> </ul>
FEM Software	<ul style="list-style-type: none"> <li>• FEM simulations: <u>Ansys</u>, <u>Abaqus</u>, and <u>Comsol</u> for mechanical analysis and Coupled-field analysis as electromechanical analysis, <u>CST</u> e <u>Ansoft</u> for 3D and 2D electromagnetic analysis.</li> </ul>
<b>SOFT SKILLS</b>	
	<ul style="list-style-type: none"> <li>• Creative thinking, innovation, open-mindedness</li> <li>• Professional written and oral communication in Italian, English, and basic French</li> <li>• Leadership and management</li> </ul>
<b>VOLUNTEERING</b>	
September 2011	<ul style="list-style-type: none"> <li>• <b>India.</b> Went with a missionary group to India in the states of Kerala, Tamil Nadu, and Karnataka, for one month.  <u>Responsibilities</u>: To watch and organize educational games for children, accomplished different tasks like the animation for children and orphan children, and handyman in a mental institution.</li> </ul>
August 2010	<ul style="list-style-type: none"> <li>• <b>Guinea Bissau.</b> Volunteered for an Italian Association “Solidaunia” which helps the local community of missionaries in Guinea Bissau in many tasks.  <u>Responsibilities</u>: Organizing educational games for children at the summer camp of a local school, to attract children from different tribes to attend schools.</li> </ul>
<b>HOBBIES</b>	
	<p>Interested in Open source electronics, 3D printing, Arduino, history, economy, videogames, miniatures creation and painting, traveling.</p> <p>Team sports, such as soccer and basketball.</p>